

**NOVEL BIO-INSPIRED STRUCTURES AND SAMPLE TRANSLATION APPROACHES FOR
THE RAMAN DETECTION OF PHARMACEUTICAL AGENTS IN WATER**

by

Héctor I. Areizaga Martínez

A dissertation submitted in partial fulfillment of the requirements for the degree of

**DOCTOR OF PHILOSOPHY
in
Applied Chemistry**

**UNIVERSITY OF PUERTO RICO
MAYAGUEZ CAMPUS
June 2016**

Approved by:

Oscar Perales, PhD

Member Graduate Committee

Date

Nilka Rivera, PhD

Member Graduate Committee

Date

Felix Román, PhD

Member Graduate Committee

Date

Marco A. De Jesús Ruíz, PhD

President, Graduate Committee

Date

Silvina Cancelos, PhD

Representative of Graduate Studies

Date

Enrique Meléndez, PhD

Chairperson, Department of Chemistry

Date

ABSTRACT

Over the years the widespread use of pharmaceuticals and personal care products (PPCPs) has become an emerging environmental problem affecting agriculture, ecological systems, and water quality as well. Surface Enhanced Raman Scattering (SERS) is emerging as a practical alternative for the detection and characterization of pharmaceuticals and bioactive compounds. This process demands the construction of new high performance substrates, with improved plasmonic responses to ensure sensitive and reproducible trace analysis determination. This research focused: (1) on the development of bio-inspired nanocomposite structures, which offer the opportunity to develop nanostructures with higher and more reproducible plasmonic fields. (2) The fabrication of an economical sample translational portable device (STPD), which could be used for on-site screening and real time analysis. The fabrication, characterization and evaluation of nine bio-inspired nano plasmonic substrates was achieved with two of the arrays; the sunflower and the orchid. Both of these designs are the most promising patterns as SERS substrates with enhancement factor (EF) on the $10^8 - 10^9$ range. This fact along with the development of a STPD have become an innovative tool for the Raman analysis of chemical agents such as Rhodamine 6G, 4-carboxybenzene sulfonamide and fluoroquinolones. The analytical capabilities to perform qualitative and quantitative analysis of such compounds will be discussed. Finally, the removal of PPCPs using transitions metals nanoparticles including cerium oxide was tested. The results show a promising potential for the fluoroquinolone and sulfonamide removal. This results promote the synthesis of zinc sulfide nanoparticles using an economical method involving the Stokes' law for their future evaluation as a new tool for the removal of antimicrobial drugs.

RESUMEN

A través de los años, el uso generalizado de productos farmacéuticos y de higiene personal (PPCPs) se ha convertido en un nuevo problema medioambiental que afecta a la agricultura, los sistemas ecológicos, y la calidad del agua también. La técnica de dispersión Raman de superficie está emergiendo como una alternativa práctica para la detección y caracterización de los productos farmacéuticos y compuestos bioactivos. Este proceso exige la construcción de nuevos sustratos q de alto rendimiento, con una mejor respuesta plasmónicas. Esto con el fin de realizar de forma más sensitiva y reproducible el análisis a nivel trazas de contaminantes ambientales. Esta investigación se enfoca: (1) en el desarrollo de nano compuestos estructuras inspiradas en la biología, que ofrecen la oportunidad de desarrollar nano estructuras con campos plasmónicos más altos y más reproducibles y (2) en la fabricación de un dispositivo de traslación portátil (STPD) de bajo costo, que podría ser utilizado para la detección in situ y análisis en tiempo real. La fabricación, caracterización y evaluación de nueve nano sustratos plasmónicas bio-inspiradas se logró con dos de las matrices (girasol y de la Orquídea); como los patrones más prometedores como sustratos SERS con un factor de intensificación (EF) en el 108 - 109 rango. Este hecho, junto con el desarrollo de un STPD se ha convertido en herramientas innovadoras para el análisis Raman de agentes químicos como la Rodamina 6G, la sulfonamida de benceno 4-carboxy y dos tipos de fluoroquinolonas. Las capacidades de análisis para llevar a cabo análisis cualitativo y cuantitativo de tales compuestos será discutido. Por último, se probó la eliminación de metales PPCP utilizando nanopartículas de óxido de cerio. Los resultados muestran un potencial prometedor para la eliminación de las fluoroquinolonas y sulfonamidas. Estos hallazgos impulsaron la síntesis de nanopartículas de sulfuro de zinc utilizando un método económico que implica la ley de Stokes

para su evaluación en el futuro como una nueva herramienta para la eliminación de drogas antimicrobiales.

Copyright ©2016

by

Héctor I. Areizaga Martínez

Dedication
To God and Mom

Acknowledgements

The moment has arrived, maybe I am worthy of it or maybe not. But to be honest, I need another dissertation to say thank you to all the people that helped me along this years. It is not easy to write this lines when I am tired of writing, making corrections and changes and all of the common stuff of this process. If for any reason when you read this document someday your name is not included, that does not mean you are not part of this. If that happen I really apologize.

First of all I want to say thank you to my mom. Thanks for your support, for always being aware of me. I'm sorry for every night that you lost waiting for me to come home and for all the hard time I gave to you. To my father thank you. To my brothers Luis and Carlos thank you for all their support and for always be aware of how I was. To my nephews Walby (Ivelisse and Marideliz, Zuhey (Vicky), Yesenia, José Luis and Ariana Carolina I wish they take this achievement as an example that you can achieve what you intend. You need only need to believe in yourself. I would like to thank my aunts Celia and Sita for their support every time they could.

I would like to express my gratitude to my graduate committee. To my advisor Dr. Marco De Jesús, thank you for always believe in me, for all patience, for never losses the confidence in myself, hints, ideas. For all hard tests that you put in my way just to try to prepare me for the future as a complete professional. Thanks for being really a friend. I want to say thank you to Dra. Nilka Rivera for her advice about the will that you need to finish a PhD. My recognition to Dr. Félix R. Román and Dr. Oscar Perales for all their disposition to help me no matter how late I request their help. My special gratitude to Dr. Michael Sepaniak whose invaluable cooperation during my internship made possible part of this work. Also I acknowledge the Center for Nanophase Materials

Sciences in Oak Ridge and Center for Education and Training in Agriculture and Related Sciences (CETARS) for support part of this research.

I want to thanks to Ms. Nayda Menéndez for always be present, for your help at all times, for your support and for all the patience all these time. Thanks for always have the time to heard my frustrations and for always be concern of how I was after the long days at the laboratory.

To my lab partners Jennifer, Elena, Grecia, Katy, Francisco Queziel and José Carmona, Raymond thank you for all the good memories and times I spent with you at the Q-031. Thanks for let me help you at the different moments, because you help me keep myself. I want to express my gratitude to the several undergraduate students that along the years help me in my research. Special thanks to Francisco Negrón, Natalie Martínez, Katherine Rivera, Legna Figueroa Edna Vargas, Stephanie Hall and Stephanie Benítez for all their support, time and persistence in the different projects and assigned tasks.

I would like to express my eternal gratitude Dr. Carmen A. Vega, for all the unconditional help that she always gave to me. This moment is possible thanks to your help. For let me use her research laboratory as my shelter during this writing process. At the same time I would like to say thank to Dr. Samuel Hernández for let me use facilities and instrumentations during all this years and for all the support and for always be open to help me.

I also want to say a special thanks to Ms. Marielys Crespo for always be there in the good and bad times. For always have a smile, a helpful attitude, for taking your time to help me. Because you always put me first before anything. Thanks for be an angel taking care of me. Also thanks, for support me when my frustrations take on me and I lost my maturity.

I also want to thank Dr. Nairmen Mina for always been aware of how everything is going. To Dr. Aidalu Joubert for all the support and for the chance to be part of the Analytical Chemistry TA's and one time Faculty member of the Department of Chemistry. Also thanks to Francheska for always be willing to help me.

A special thanks to my godchildren (and parents) José Luis, Derek (Felix and Marylee), Andrea Vimar (Violeta) and Yelianis (Carlos and Yairi) for believe in me.

To all the other persons involved in this project or in the different aspects of my life Thank You.

Table of Contents

Introduction.....	2
Chapter #1: Basic Principles of Raman Effect, SERS Spectroscopy and their effect on Plasmonic Substrates	4
1.1. Raman Effect.....	4
1.2. Surface enhanced Raman Spectroscopy (SERS)	11
1.2.1. SERS Mechanisms	14
1.2.2. Enhancement factor	15
1.3. SERS Substrates.....	16
1.3.1. Immobilized metallic nanoparticles.....	16
1.3.2. Physical Vapor Deposition	18
1.4. Lithography Methods	21
Chapter #2: Antimicrobial and Antibacterial Drugs and problem statement	26
2.1. Fluoroquinolones.....	26
2.1.1.1. Ciprofloxacin	27
2.1.1.2. Levofloxacin	28
2.2. Sulfonamides.....	29
2.2.1.1. 4-Carboxybenzene sulfonamide.....	30
2.2.1.2. Sulfadiazine.....	30

2.3. Statement of the problem	32
Chapter #3: Performance Characteristics of Bio-inspired Metal Nanostructures as Surface Enhanced Raman Substrates	35
3.1. Introduction	35
3.2. Experimental	41
3.2.1. Fabrication of the Bio-Inspired Designs:.....	41
3.2.2. Substrate Application	45
3.3. Results and discussion:.....	46
3.3.1. Initial Studies	46
Initial Studies	46
3.3.2. Substrate Characterization.....	48
3.3.3. SERS Studies:.....	53
3.3.4. Pillar height Study	64
3.3.5. Detection of Fluoroquinolones and Sulfonamide:.....	69
3.3.6. Substrate working life and cleaning procedure.	70
3.3.7. Hyphenated Bio Inspired arrays with a sample translational device.....	70
Chapter #4: USB sample translation probe to enable the reproducible detection of photo-labile drugs by Surface Enhanced Raman Scattering (SERS).....	74
4.1. Introduction	74
4.2. Initial Studies and Justification	78

4.3. Experimental	84
Chapter 5: Remediation alternatives for the fluoroquinolones and Sulfonamides Removal.....	121
5.1. Introduction:	121
5.2. Method Chromatographic Method evaluation	124
5.3. Method Validation for the Pharmaceutical Products Separation	128
5.3.1. Experimental.....	128
5.3.2. Results and Discussion	129
5.4. 4-carboxybenzene sulfonamide HPLC determination	140
5.5. Cerium Oxide nanoparticles for PPCPs remediation	142
5.5.1. Experimental.....	143
5.5.2. Results	146
5.6. New economical alternative for a nanoparticle synthesis	153
5.6.1. Introduction	154
5.6.2. Materials and Experimental.....	155
5.6.3. Optical Properties:	157
5.6.4. X-Ray Analysis:	159
Chapter #6: Concluding Remarks and Future Works.....	162
References.....	165
Appendix 1.....	177
Appendix 2.....	184

Table of Figures

Figure 1: Scattering process represented by this version of the Jablonski diagrams showing the elastic Rayleigh (b) and inelastic Raman scattering(anti-Stokes(a) and Stokes and (c)).*	6
Figure 2: Difference between stokes and the anti-stokes vibrations compared to the excitation energy*	8
Figure 3: Classical description of Raman Effect for diatomic molecule. ⁴ *	10
Figure 4: Schematic representation of a physical vapor deposition (PVD) chamber.*	20
Figure 5: Simplified scheme of electron beam lithography tool.....	23
Figure 6: General Structure of a Fluoroquinolone	26
Figure 7: Ciprofloxacin chemical structure	28
Figure 8: Levofloxacin chemical structure	29
Figure 9: General Structure of a Sulfonamide	30
Figure 10: Chemical Structures of: a. 4-carboxybenzene sulfonamide and b. 4-aminobenzoic acid	30
Figure 11: Sulfadiazine chemical structure. This pharmaceutical agent was analyzed to demonstrate method roughness and capability.	31
Figure 12: Benchmark biomimetic patterns: A). asymmetric patterns; b). radially symmetric c). bilaterally symmetric patterns.....	40
Figure 13: SEM micrograph for the four doses experiments performed. Circle shows over exposure of those areas led to incomplete development and poor liftoff efficiency for the most patterns..	47
Figure 14: Bio Inspired arrays micrographs obtained with a Ziess Scanning electron microscope (SEM); Power = 3.0 kV; Magnification = 90.00 K X Tilted at 30 degrees; Detector Mode = InLens. Characterization of the nano composite substrates after the etching step was done to evaluate the	

efficiency of the nanofabrication process. Patterns are presented following the order defined on

Figure 12. 51

Figure 15: BT SERS spectra using the Sunflower array as substrate. This was collected using a 632.8 nm excitation source for 1 s with a 2.30 mW laser power..... 56

Figure 16: 4-ABT SERS spectra over the Sunflower Bio Inspired array. The acquisition was performed using a 632.8 nm excitation source for 1 s with a 2.30 mW laser power..... 57

Figure 17: Enhancement Factor evaluation for the nine Bio Inspired arrays analyzed using excitation sources of 532, 632.8 and 785 nm..... 61

Figure 18: Long range view SEM micrograph using a Ziess Scanning electron microscope (SEM); Power = 3.0 kV; Magnification = 19 X Tilted at 30 degrees; Detector Mode = InLens, of the Acacia(1),Asian Liliium(2) Sunflower (3) and Orchid (4) arrays for one of the Bio-inspired chips etched at 45 seconds. (B) Micrographs were acquire with a magnification of 315Kx, Orchid arrays (clockwise direction) images after 30, 60, 120 and 150 seconds of etching. Pillar heights differences are clearly observed. Images for the four arrays selected using a 30 seconds (C) and 120 seconds (D) etching time. (E) Pillar Heights measurements results for the 4 selected Bio-Inspired arrays..... 66

Figure 19: Benzenethiol EF plots of the average and the high intensity point for the (a) Acacia leaf, (b) Asian liliium, (c) Sunflower and (d) Orchid Bio Inspired arrays. Optimum pillars heights are between 105-189 nm for all of the patterns except the Acacia..... 68

Figure 20: Levofloxacin analysis with the Bio-inspired arrays. (a.) overlay (b) stacked..... 72

Figure 21: 4-Carboxybenzene sulfonamide analysis with the Bio-inspired arrays. (a.) overlay (b) stacked..... 73

Figure 22: Setup designs for the evaluation of bimetallic substrates..... 79

Figure 23: PABA SERS spectra for the bimetallic substrates evaluation	80
Figure 24: PABA SERS spectras showing the reproducibility issues with the use of an immobilized substrate	82
Figure 25: Calibration Curve for the analysis of levo using a PDMS slide.....	83
Figure 26: (A, B) Schematic of the PSSTD using both power options. (C) Photo of the designed device (D) Image of the Ag-PDMS substrate to be analyzed.....	85
Figure 27: Revolutions per minute correlation chart revolutions per minute correlation chart for the evaluation of the PSTTD using a DC and USB power	91
Figure 28: SERS spectra for 4-carboxy. Acquisitions was made using a 638 nm emission line for 10s acquisition using 3.00 mW laser power.	95
Figure 29: SERS spectra for Cipro. Acquisitions was made using a 638 nm emission line for 10s acquisition using 3.00 mW laser power.....	96
Figure 30: SERS spectra for levo. Acquisitions was made using a 638 nm emission line for 10s acquisition using 3.00 mW laser power.....	97
Figure 31: Effect of pH on the intensity of each pharmaceutical drug	100
Figure 32: Spinning rate effect on the analyte signal for PSTTD.....	102
Figure 33: Time adsorption study for the 4-carboxy analysis. Reproducible measurements can be observed over the seventeen minutes analysis over the rotational mode.....	105
Figure 34: R6G adsorption study. The maximum intensity was achieved in a short time analysis over the static mode	106
Figure 35: Levo adsorption study for a 30 minutes analysis. The rotational analysis show a constant response over the entire analysis.....	107
Figure 36: Levo adsorption study for a 30 minutes analysis.	108

Figure 37: R6G SERS spectra for the 1.00×10^{-05} M solution for the raster acquisition of 1s and 3 acquisition from -600 μm to 600 μm	111
Figure 38: 4-carboxybenzenesulfonamide Calibration Curve using PDMS wells analyzing the 830 cm^{-1} band using 10 s acq at 638 nm.....	113
Figure 39: Rhodamine 6G Calibration Curve using the 770 cm^{-1} Band using 2 sec acquisition at 638.....	114
Figure 40: SERS Spectra Region for R6G for Partial Least Squares for R6G.....	116
Figure 41: Partial Least Squares results for the analysis of 4-carboxy.....	119
Figure 42: Partial Least Squares results for the analysis of Rhodamine 6G.....	120
Figure 43: Ultraviolet spectra for the four pharmaceutical drugs to determine their maximum absorption wavelength	125
Figure 44: Chromatogram for the separation of the antimicrobial drugs	127
Figure 45: Calibration curve for the linearity evaluation of Ciprofloxacin.....	134
Figure 46: Calibration curve for the linearity evaluation of Levofloxacin.....	134
Figure 47: Calibration curve for the linearity evaluation of Sulfadiazine	135
Figure 48: Acid Base Equilibria for: a. Levofloxacin and b. Ciprofloxacin.....	139
Figure 49: Antimicrobial standard mixture containing: 4-Carboxy, Sulfa, Levo and Cipro at 10^{-6} M range	141
Figure 50: CeO_2 filter setup containing 0.01 g for antimicrobial removal evaluation	145
Figure 51: Loading plot for the 1.00×10^{-4} M sulfa standard solution	147
Figure 52: Sulfa chromatogram for the loading experiment.....	148
Figure 53: Loading plot for the 1.00×10^{-4} M sulfa standard solution.....	149
Figure 54: Levo chromatogram for the loading experiment.....	150

Figure 55: CeO ₂ filter removal effect against laboratory and surface water samples.....	152
Figure 56: Schematic illustration of controlled IR assisted chemical precipitation method based on Stokes' law for a free body falling in a quiescent and viscous fluid as used for synthesis of ZnS nanoparticles.	156
Figure 57: Absorption spectra of as-prepared ZnS nanocrystals.....	158
Figure 58: Diamond Micrograph	178
Figure 59: Honeycombs Micrograph	180
Figure 60: Wings Micrograph.....	182

List of Tables

Table 1: Comparison of the mentioned electron beam resists and the smallest structures investigated with these mediums. ³⁵	24
Table 2: Bio-Inspired nanoarrays patterns and dimensions.....	44
Table 3: Dimensions for the fabricated Bio Inspired arrays:	52
Table 4: Characteristic Raman spectra and band for assignments for 4-AminoBenzenethiol and Benzenethiol	55
Table 5: Enhancement Factors for the fabricated Bio Inspired arrays.....	62
Table 6: Correlation of the normalized surface area vs. EF for the different Bio Inspired arrays at the different power source evaluated.	63
Table 7: Experimental Heights for the Pillar Height study of Bio Inspired arrays.....	67
Table 8: SERS characterization of pharmaceutical drugs under Static and rotational mode	94
Table 9: Precision study results for the PSTTD.....	110
Table 10: PLS regression results for the PSTTD.....	118
Table 11: Suitability results for the method validation of the sulfonamide and fluoroquinolones	130
Table 12: Linearity and Accuracy results for each compound	132
Table 13: Suspended Solids results for the analysis of “Quebrada Oro” sample	138
Table 14: Experimental conditions for the initial percent removal determination	144
Table 15: Lattice constants as-prepared ZnS nanocrystals	160
Table 16: Diamond particles dimension characterization.....	179
Table 17: New Honeycombs particles dimensions characterization	181
Table 18: Wings particles dimensions Characterization.....	183

Table 19: Resolutions results for the HPLC Analysis	185
Table 20: Results of the Validation process for HPLC Analysis for 4-Carboxy.....	185
Table 21: Results of the Validation process for HPLC Analysis for Sulfadiazine.....	186
Table 22: Results of the Validation process for HPLC Analysis for Levofloxacin.....	186
Table 23: Results of the Validation process for HPLC Analysis for Ciprofloxacin.....	187
Table 24: Results of the Regression Analysis.....	187

LIST OF ABBREVIATIONS

4-ABT	4-aminobenzenethiol
4-carboxy	4-carboxybenzene sulfonamide
A.U.	arbitrary units
CE	Chemical Enhancement
CeO ₂	Cerium Oxide
Cipro	Ciprofloxacin
CV	coefficient of variation
DAD	Diode Array Detector
DW	deionized water
EM	Electromagnetic
EMF	electromagnetic fields
EBL	electron beam lithography
EPL	electron beam projection lithography
EF	Enhancement factor
H	Height

HPLC-UV	High Performance Liquid Chromatography with Ultraviolet Detector
HOMO	highest occupied molecular orbital
IPA	isopropyl alcohol
L	Length
LC-MS	Liquid Chromatography with Mass Spectrometry (LC-MS)
Levo	Levofloxacin
LSPs	localized surface plasmons
LUMO	lowest unoccupied molecular orbital
NIL	nanoimprint lithography
NSL	nanosphere lithography
nTP	nanotransfer printing
PLS	Partial Least Squares
% RSD	Percent Relative Standard Deviation
PPCPs	pharmaceuticals and personal care products
PVD	physical vapor deposition

PDMS	polydimethylsiloxane
PSTTD	Portable sample translational technique device
RIE	reactive ion etching
R6G	Rhodamine 6G
SEM	scanning electron microscope
SAM	self-assembled monolayer
SiO ₂	silicon dioxide
Ag	Silver
Ag-PDMS	silver-polydimethylsiloxane
SERS	surface enhanced Raman scattering
SPR	Surface Plasmon Resonance
W	Width

Introduction

In recent years, the disposal of pharmaceutical and personal care products (PPCPs) had represented a major problematic due to the impact on water systems quality. The fluoroquinolones and sulfonamides are two examples of those compounds which are commonly acquired by patients on any drugstore without medical prescription. For that reason there is a constant need to develop new alternatives on the detection, and reproducible quantification and remediation of those products. This research focuses on the development of new analytical tools that will improve the analytical application and use of surface enhanced Raman spectroscopy (SERS) in the detection and quantification of pharmaceutical products. The use of advanced lithographic methods, provide new insight into the design and construct of analytical grade SERS substrates. In addition this work also focuses on development of new portable instrumentation devices that will enhance Raman technique in field applications for screening and monitoring analysis. This, will result on the generation of fast, accurate, precise and reliable data. This will result on the development of new assays to monitor environmental pollutants. In addition, this research provide remediation alternatives using transition metal nanoparticles to minimize its impact on the ecological systems. The description of the different sub projects are provided on the following section

The work presented here starts with an introductory chapter that discusses the basics of the Raman effect, SERS technique, and the instrumentation used. The chapter continues with an analysis of the techniques employed for the fabrication of advanced SERS substrates, like electron beam lithography (EBL) and reactive ion etching (RIE). The statement of the problem and target system under study will be discussed on Chapter #2. Chapter #3 focuses on the development, process used and fabrication of novel bio-inspired substrates by means of electron beam

lithography (EBL) technique and their plasmonic activity evaluation. As an alternative for field analysis, the construction, test and assessment of a Portable sample translational technique device (PSTTD) with model SERS compounds and pharmaceutical agents is looked at in Chapter #4. The development and validation of a chromatographic method for the detection of a series of drugs active agents will be discussed in Chapter #5. Also the use of novel alternatives that involves the use of cerium oxide nanoparticles for the rapid and effective remediation of these pollutants from environmental matrices are tested and discussed. The simple and economic synthesis of zinc sulfide nanoparticles that could be used as a separate alternative or in combination with the cerium oxide nanoparticles for enhanced removal of the fluoroquinolones and sulfonamides are also presented. Finally, closing statements, conclusions and future works based on the findings of this project are presented in Chapter #6.

Chapter #1: Basic Principles of Raman Effect, SERS Spectroscopy and their effect on Plasmonic Substrates

1.1. Raman Effect

Raman spectroscopy refers to the vibrational spectroscopy technique that is used to identify solid, liquid, and gas matter. It is similar to infrared (IR) spectroscopy and is a technique that is widely used to study molecular vibrations.¹ The Raman based methods can provide IR complementary information with excellent fingerprint information and reasonable resolution. The formation of polarizability tensor rather than the dipole changes makes this technique a complementary option to the IR technique. This polarizability parameter makes that several substances exhibits low analytical responses, like water for example, making Raman spectroscopy an attractive alternative for the analysis of several types of compounds in aqueous media.² Raman vibrational spectroscopy technique uses vibrational modes with bands that are too narrow compared to other spectral analysis. This means that there is a possibility of taking advantages of this feature to maximize output and accuracy.

The Raman Effect basically consists of two simultaneous processes happening at the same time. As it will be discussed latter in the document, only a minuscule fraction of the photons are able to exhibit Raman scattering. Therefore highly monochromatic laser sources are employed to produce a virtual state normally way below any naturally occurring electronic state of the molecule. The state enable transitions from the various vibrational states according to the Raman selection rules. This state is a short live state which is not quantum favored and it's a function of

the frequency of the light source. After the relaxation process most of the electrons return to the same energy level, this is most of the photons are deflected with the same energy of the radiation source. This phenomenon is known as elastic scattering. However, a small number of photons exhibit an absorption process and the emission of a new photon called scattered photon is observed. In other words, this scattered radiation has either higher or lower energy than the incident photons (inelastic scattering) and is known as Raman scattering. Due to light-matter interactions, energy is either gained or lost by the molecule during Raman scattering. As such, the conservation of energy states:

$$h\nu + E = h\nu' + E' \quad (1)$$

where ν and ν' are incident and scattered frequencies while E and E' are the initial and final energy of a molecule, respectively. The energy change for the molecule could be written as:

$$\Delta E = h(\nu' - \nu) \quad (2)$$

Using the above equation the different scattering observed could be classified as follows:

Rayleigh scattering: In this type of interaction there is no energy changes between the incident photon and the emitted photon. The net change in energy described on equation 2 is zero.

This is also known as elastic scattering.

Stokes Scattering: In this process the electron that was promoted to a virtual scatter photon has less energy than the incident photon. For this reason the electron will be in a vibrational state of high energy and ΔE will be less than zero. For that reason is considered as inelastic scattering.

Anti-Stokes Scattering: This is considered another type of inelastic scattering, the incoming photon with the excitation of an electron, when this excited electron lose energy it will be on a vibrational level of lower energy. As consequence, the resulting photon has more energy than the incident one. Thus, ΔE will be higher than zero.

Figure1 presents the possible scattering process that a molecule can undergo.

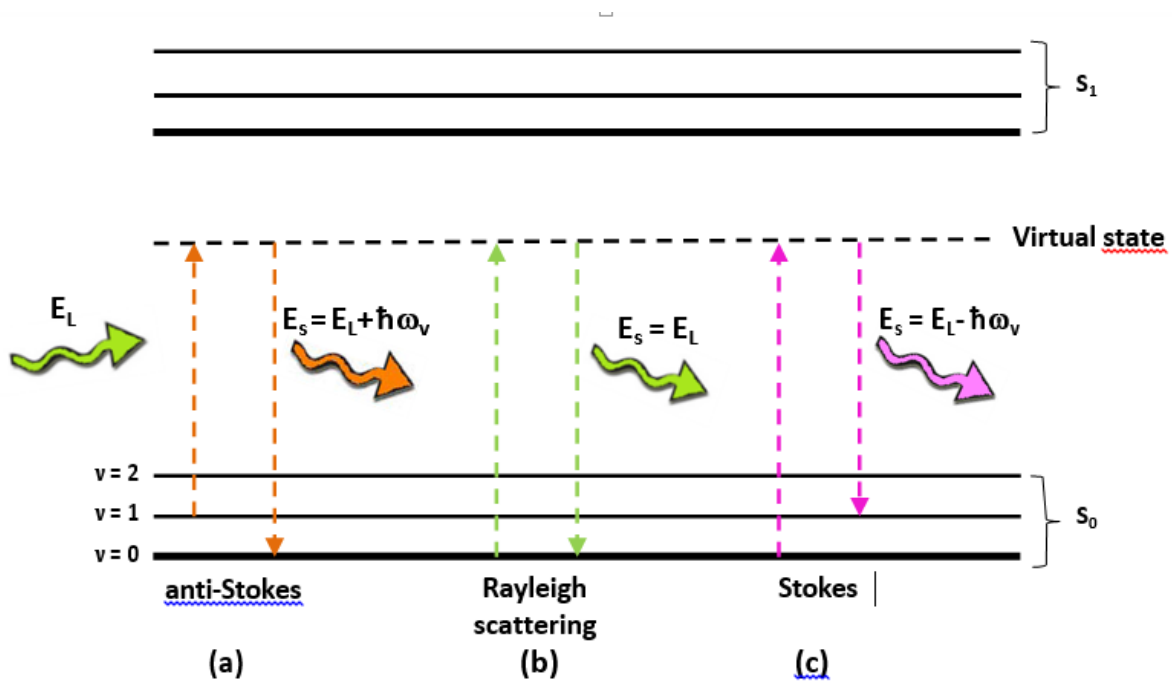


Figure 1: Scattering process represented by this version of the Jablonski diagrams showing the elastic Rayleigh (b) and inelastic Raman scattering(anti-Stokes(a) and Stokes and (c)).*

* (Copy with permission of Olavarría Fullerton, J. from the dissertation work “Development of Plasmonic Nanostructures as Raman Sensors for the Detection of Arsenic Antimicrobials”)

According to Maxwell-Boltzmann distribution of energy, a large amount of molecules will be in the fundamental vibrational state ($\nu = 0$) at room temperature, therefore the Anti-stokes shifts are much less common than the Stokes shift unless a population inversion is induced. This could happen by increase in temperature or other factors. As a consequence, the anti-stokes side of Raman spectrum is much weaker than Stokes side (Figure 2). Although both phenomenon leads to an observable Raman response, a net change in polarizability is required for it to show Raman Effect.

The dipole moment (μ) is related to the energy as:

$$\mu = \alpha E \quad (3)$$

where α is the polarizability of the molecule and E is strength of the applied electric field. "Polarizability is a tensor quantity, that describes the extent to which the molecular orbitals are deformed by the presence of an external field".³ The magnitude vector of the electric field in an electromagnetic wave is described by:

$$E = E_0 \cos(2\pi\nu_0 t) \quad (4)$$

In this relation ν_0 corresponds to the frequency of the incident radiation in Hertz (Hz).

The physical displacement due to a particular vibration is expressed as:

$$q = q_0 \cos(2\pi\nu_m t) \quad (5)$$

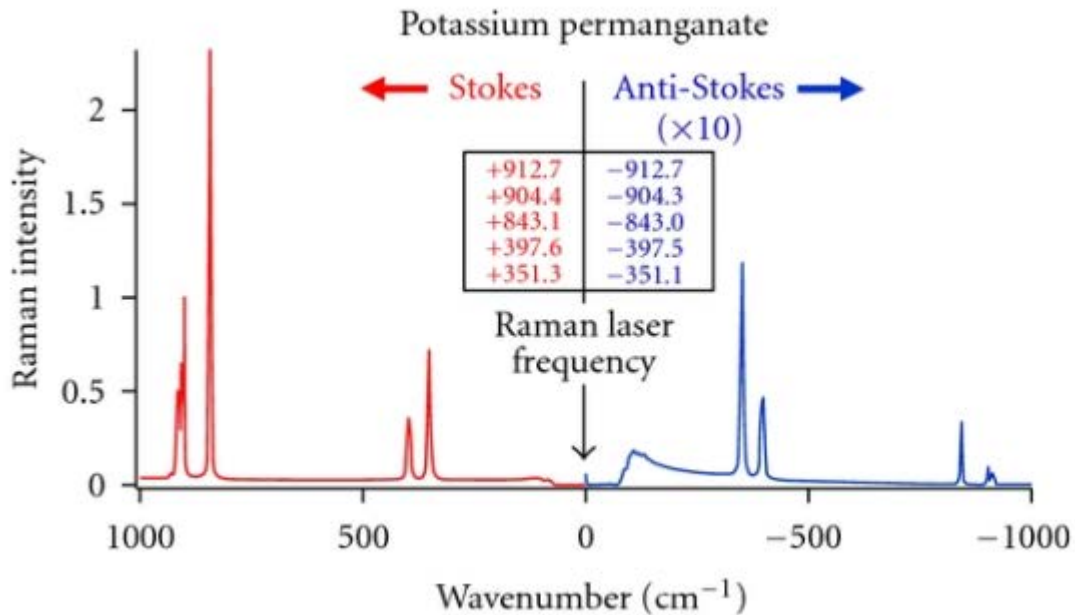


Figure 2: Difference between stokes and the anti-stokes vibrations compared to the excitation energy*

*Taken from Johnson, Timothy J., et al. "Demonstrated wavelength portability of Raman reference data for explosives and chemical detection." *International Journal of Spectroscopy* 2012 (2012). Copyright © 2012 Timothy J. Johnson et al. "This is an open access article distributed under the Creative Commons Attribution License, which permits unrestricted use, distribution, and reproduction in any medium, provided the original work is properly cited."

where q_0 is the maximum displacement about the equilibrium position. If the amplitude of the vibration is small the polarizability is linear to q and may be approximated by a Taylor series expansion:

$$\alpha = \alpha_0 + \left(\frac{\partial \alpha}{\partial q}\right)_{q=0} q + \dots \quad (6)$$

Considering the atom displacement in equation (5) μ may be expressed as:

$$\alpha = \alpha_0 + \left(\frac{\partial \alpha}{\partial q}\right)_{q=0} q_0 \cos(2\pi \nu_m t) \quad (7)$$

Substituting equation (5) within equation (1) yields:

$$P = \alpha_0 E_0 \cos(2\pi \nu_0 t) + \left(\frac{\partial \alpha}{\partial q}\right)_{q=0} q_0 \cos(2\pi \nu_m t) E_0 \cos(2\pi \nu_0 t) \quad (8)$$

Employing the trigonometric identity $\cos \alpha \cos \beta = \frac{1}{2} \{ \cos(\alpha + \beta) + \cos(\alpha - \beta) \}$ ⁴ equation 8

can be simplified as

$$P = \alpha_0 E_0 \cos(2\pi \nu_0 t) + \frac{1}{2} \left(\frac{\partial \alpha}{\partial q}\right)_{q=0} q_0 E_0 [\cos(2\pi \{ \nu_0 - \nu_m \} \cdot t) + \cos(2\pi \{ \nu_0 + \nu_m \} \cdot t)] \quad (9)$$

As noted on this classical treatment, the induced dipole moment results in radiation in three distinct frequencies, ν_0 , $\nu_0 - \nu_{\text{vib}}$ and $\nu_0 + \nu_{\text{vib}}$. The first term, ν_0 , represents the Rayleigh scattering which represents the elastic scattering where the frequency is the same as the incident light. The latter two terms refer to inelastic processes: $\nu_0 - \nu_{\text{vib}}$ is the frequency that was down-shifted known as Stokes Raman scattering and $\nu_0 + \nu_{\text{vib}}$ is the frequency that is up-shifted referred to as anti-Stokes Raman scattering (figure 3). “In order to Raman scattering to take place the external field must induce a net change in polarizability along the nuclear mode where $\left(\frac{\partial\alpha}{\partial q}\right)$ must be non-zero, and can be regarded as the Raman selection rule.”⁴

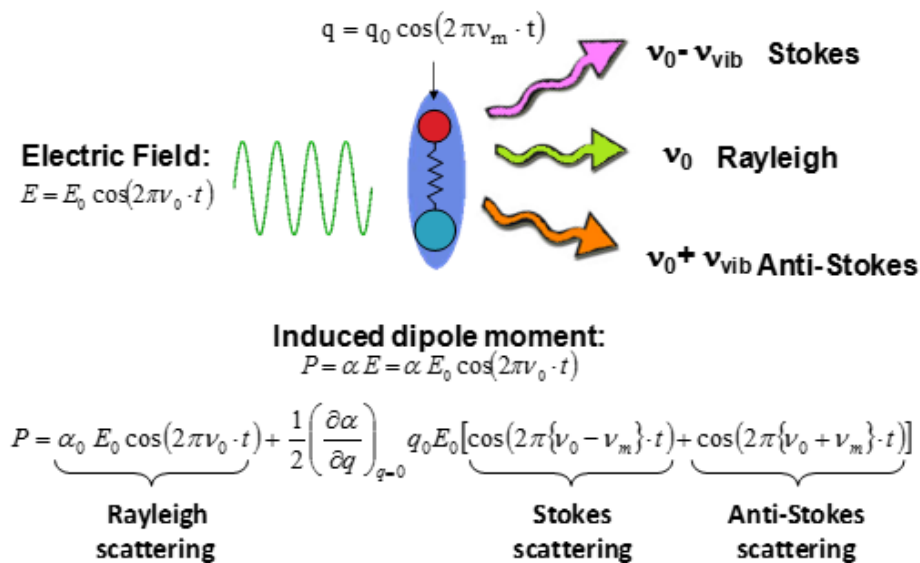


Figure 3: Classical description of Raman Effect for diatomic molecule.⁴*

(Copy with permission of Olavarría Fullerton, J. from the dissertation work “Development of Plasmonic Nanostructures as Raman Sensors for the Detection of Arsenic Antimicrobials”)

Figure 3 presents the classic mechanic interpretation of the effect of an electric field in a diatomic molecule. One of the misinterpretations of this approach is the consideration of stokes and anti-stokes scattering equals in magnitude.

The use of Raman as an alternative analytical work has compromised by its low sensitivity due to weakness of the occurrence of scattering process, where only one photon will be scattered out of 1×10^{10} incident photons.

1.2. Surface enhanced Raman Spectroscopy (SERS)

Despite of the several advantages that Raman offers one of the most important limitations is the reduce ability of molecules to show Raman scattering. Traditionally this fact had been identified as small cross section. The normal cross section for a single molecule is found to be close to 10^{-30} cm^2 . This inherent variable has a significant impact on the possible applications the technique could have because the low sensitivity and possible high detection limits it has. In fact, the applicability of the technique is focused mainly to pure samples or solutions with concentrations greater than 0.1 M.⁵ These drawbacks are overcome with the use of Surface Enhanced Raman Spectroscopy.

By the middle of the 70 Fleishman et al. observed an increase in the signal of pyridine adsorbed in a roughed piece of silver (Ag) used as an electrode.⁶ Later that decade several research groups observed that the enhancement in signal was not only related with the surface area available for the analyte.⁷⁻⁸ Since then, the technique has evolved as the principal type of Raman.

There are a number of advantages of using SERS over the traditional Raman spectroscopy. SERS increase the small cross section area, which basically is that the number of molecules showing Raman Effect. The concentration of the analyte could be at the 10^{-4} M and it would show a significant response. Therefore, this implies that SERS can be used as an enhancement mechanism so that we can detect the compound elements that is in concentrations to be extremely too small to detect with traditional Raman spectroscopy. The possibility of interferences due to fluorescence induced by the irradiation source are decreased significantly because the use of a metallized substrate quenches the emission of light. This advantages combined with the structural information and high specificity that conventional Raman shows makes SERS a more attractive option to study a broader spectrum of molecules.

The use of SERS as an analytical tool had expanded the field of analysis to several areas like polymer science, biochemistry, sensors development and electrochemistry among others.⁹ This increase in SERS applications were benefit by the development in the late 90's of new nano structured substrates which brought the fabrication of reproducible substrates. This new generation of substrates and the development of portable instrumentation led to the exploration of environmental, forensic and biomedical applications as well.¹⁰⁻¹²

The nature of the SERS effect and how the effect is produced depends on several variables that need to be discussed in detail. Generally, the SERS effect needs the use of an excitation source that will induce an electromagnetic field (EMF) by means of the oscillation of the electrons on a surface of a roughed or structured metal. The resulting EMF complements the first EMF resulting in the amplification of the Raman signal. This phenomenon is identified as Surface Plasmon

Resonance (SPR). Typically silver or Gold in a colloidal¹³⁻¹⁴ or nanoparticles¹⁵ forms are being used in SERS active substrates due to their strong capacities of generate SPR that results in the SERS enhancement created by their characteristic and uniqueness. However, the use of some metal oxides such as ZnO and CaO had also been employed as SERS substrates with acceptable success.¹⁶ The process that lead to the success of this oxide compounds is based on the enhancement that is not strictly related with the electronic environment of the particles. Which does not overcome the success of the noble metals mentioned.

Several theories and possible explanations had been develop to explain the SERS effect, two had reach the scientific maturity and acceptance, namely electromagnetic and chemical enhancements. Since all the SPR properties depends on the metallic nature such as dielectric environment, particle size, shape, orientation properties surrounding the metal structures, then most important key to a wider application of SERS mechanism is to develop an efficient and strong Plasmon resonant.¹⁷⁻¹⁸ This is achieved with the use of structures with unique geometries so as to enhance Raman signals and also to control the number and periodicity of the arrays of the structures over an enormous area which results on a reproducible Raman enhancement.

1.2.1. SERS Mechanisms

Since the discovery of SERS, a lot of work and research has been put forward and theories formulated on the effect. After a lot debate, a general consensus was arrived at which stated that there are two mechanisms which are very important in SERS. The mechanisms include Electromagnetic mechanism (EM)¹⁹ and a chemical mechanism (CM)²⁰. Each of them has their impact on SERS Enhancement and is EM the preferred mechanism over Chemical mechanism.

Electromagnetic Enhancement

The EM Enhancement Mechanism basically is more general in nature and it typically does not depend of the analyte used. It can be seen in SERS when substrates are made of roughened metal surfaces or nanoparticles that have features smaller than the wavelength of light being used. The incident light promotes that the electron of the metal surface starts to oscillate producing and induced EMF which is responsible for the enhancement in the signal. If the surface of the metal is separated by more of 5nm, each surface began to behave as an individual surface. And it produces a Localized Surface Plasmon. To produce a large enhancement in the signal of a single molecule it is necessary that the resonance of the surface plasmon correspond with the frequency of the incident radiation.

CM Enhancement Mechanism:

CM causes an increase in Raman cross section area of the adsorbed molecular elements. The evidence for its presence was documented in the past studies which was first observed that enhancement varied depending on the potential applied in the electrochemical experiments. The chemical enhancement is usually well-thought-out to be more relative to the direct relationship

with the adsorbed molecular element and the metallic surface, and that the most striking deliberation is the charge transfer in between the adsorbed molecule and the metallic surface. The mechanism involves the transfer of an electron from the Highest Occupied Molecular Orbital (HOMO) to the Lowest Unoccupied Molecular Orbital (LUMO) of the molecule by means of the metal Fermi levels.²¹⁻²² This is the most preferred mode due to the chemisorption of analyte metal substrates molecules, the electronic state of the molecules is either moved or extended as a result of either the interaction with the metal or the origin of new electronic states

1.2.2. Enhancement factor

One of the key parameters to describe SERS substrates solutions is the enhancement factor (EF) which is a general figure of merit to assess SERS performance (equation 10).

$$EF(\bar{\nu} \text{ cm}^{-1}) = \frac{N_{vol} I_{surf}}{N_{surf} I_{vol}} \quad (10)$$

The enhancement Factor (EF) is averaged over all the likely positions of the metallic surface and also the molecules which are arbitrarily adsorbed on the surface of the metal as compared to a similar value and number of non-adsorbed molecules denoted by N_{vol} and N_{surf} . The standard operating procedure for signal normalization and EF calculation, particularly the number of molecules present at the sample volume (N_{vol}), is readily available on the literature.²³ The terms I_{vol} and I_{surf} represent the analytical signal of the neat and a SAM of the reference material on the different surfaces. Limitations arise that the formula does not account for the

nanometric properties and dimensions of the substrate, as consequence it represents a broad guideline than an accurate one.

1.3. SERS Substrates

There are several methods associated with the fabrication of SERS substrates. Early substrates were created by the formation of silver colloidal suspensions. These type of substrates present several advantages, such as the simple fabrication and low cost. The disadvantages of this fabrication process is based on the low reproducibility of the measurements because of the low control in particle size and morphology. This inherent disadvantage of this process had led the development of new alternatives for substrates fabrication. These techniques are based on the formation of immobilized substrates methods and lithographic methods. Description of the mentioned methodologies in terms of the advantages equipment and applications are described in the following sections.

1.3.1. Immobilized metallic nanoparticles

The use of metal nanoparticles has grown greatly over the past years. Immobilized metallic particles are much easier to fabricate via normal wet chemistry, giving various choices with regard to shape and size.²⁴ Furthermore, SERS hotspots can be cheaply formed through the aggregation of immobilized metallic particles from their suspensions through the use of salts or any analyte of interest. Nevertheless, the use of aggregated and dispersed immobilized metallic particles as SERS

substrates within real analytical complications is limited as a result of the poor reproducibility. The issue of reproducibility could be solved through advanced metallic nanoparticles immobilization together with some solid support²⁵.

The simple SERS experiments are achieved with metallic nanoparticles under the presence of particular analyte concentration. However, suspension of metallic nanoparticles should be mixed with the SERS analyte solution, a sampling demand that may be hampering some applications.²⁶ Regardless, of the reproducibility low cost and possible sampling shortcomings, metallic nanoparticles are widely used as SERS substrate because of their good stability, high SERS performance and easy fabrication.

Another methodology comprises the generation of some SERS substrates through immobilization of the metallic nanoparticles under a planar foundation. The metallic nanoparticles adhered to solid supports is so poor that particular immobilization methodologies have to be devised to retain the performance and integrity of SERS substrate over time.²⁷ For example the permanent immobilization of silver or glass particles on glass might be undertaken through former glass surface modification through derivatized silanes.²⁸

SERS substrates could also be achieved through fabricated biochips by soft lithography which are discussed on the next section. Other substrates can be fabricated using polydimethylsiloxane (PDMS). PDMS is an off the-shelf available chemically and physically stable silicone rubber. It contains some unique properties that includes sorptive capacity, ability to trap the analytes, its able decrease oxidation of the metal. It is also used for fabrication of substrates use in printing technology as well. Due to its clean process ability, the high flexibility and low temperature, the chances of change to any of its functional components as well as property drift

over temperature and time, as opposed to glass, PDMS is suitable for chemical and mechanical sensors as it has many desirable features than can be found in glass when producing SERS signals and further helps in making the SERS signal stronger. Furthermore, the di-electric properties of PDMS are an advantage to Surface Plasmon generated on metal nanoparticles which is much greater than the di-electric properties of glass.

1.3.2. Physical Vapor Deposition

Physical vapor deposition is a term commonly used to elucidate a set of coating procedures. This art of vaporization is obviously very high as opposed to other vaporization techniques. The substrates are mounted within some distance from the source of evaporation so as to minimize substrate radiant heating through the vaporization source. All these procedures come through vacuum under working pressure and often integrate substrate bombardment to be coated using positively charged energetic ions within the coating procedure to foster high density.

Furthermore, reactive gases emitted like nitrogen, oxygen or acetylene might be brought into the vacuum chamber in the metal deposition process to establish several compound coating compositions. The outcome is a formidable bond between the tooling and coating substrate with structural properties of the film.

The main difference is based on the source of evaporation employed by each mode. Those methods include: Chemical evaporation, Laser evaporation, Electron beam evaporation, and Physical vapor methods which include sputtering and thermal evaporation.

The use of Physical Vapor Deposition (sometimes called vacuum deposition) has the following advantages: first, the multitude of substrate materials which can be coated: metals,

alloys, ceramics, glass, polymers etc. In addition, it has an unlimited choice of coating materials: metals, alloys, semiconductors, metal oxides, carbides, nitrides, cermet, sulfides, selenides, tellurides etc. Finally, it has an easy tuning of the microstructure by the choice of the coating parameters.²⁹ There are also some disadvantages like relatively low deposition rates and film thicknesses compared to other modes, technologically demanding processes (vacuum based) which requires high power vacuum systems and the coating of geometrically complex patterns could be difficult.

Silver/polydimethylsiloxane (Ag/PDMS) nanocomposites are an example of the substrates with immobilized nano particles. These are simple, low cost metal/polymer nanocomposites that are metalized by physical vapor deposition (Figure 4). Rendered nanoparticles are distributed just below the surface as embedded clusters or isolated nanoparticles resulting in fractal-like surface morphologies. Their optical and sorptive properties make them a broad spectrum SERS substrate for the detection of small aromatic molecules particularly aromatic acids.⁸ The immobilization of the silver particles within the PDMS matrix inhibit the rapid oxidation of nanometallic silver and reduces the number of experimental variables facilitating the study of metal adsorbate interactions. Films from a few nm to thousands of angstroms can be obtained with higher reproducibility.

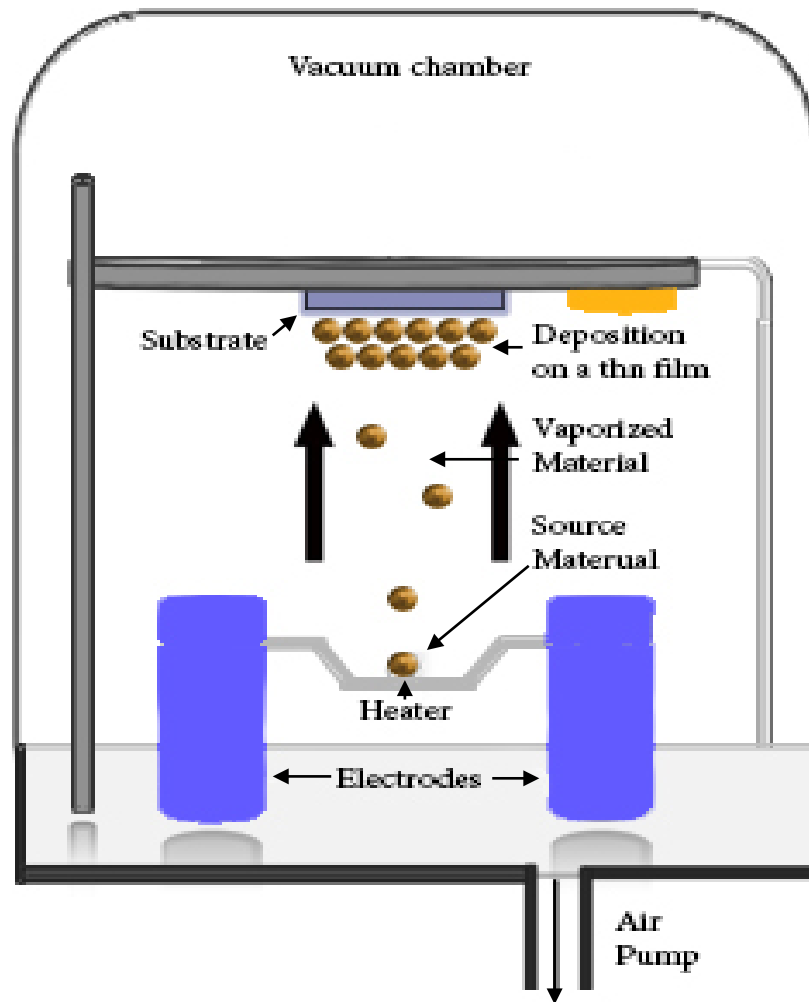


Figure 4: Schematic representation of a physical vapor deposition (PVD) chamber.*

(Modified with permission of Olavarría Fullerton, J. from the dissertation work “Development of Plasmonic Nanostructures as Raman Sensors for the Detection of Arsenic Antimicrobials”)

1.4. Lithography Methods

Over the last decade lots of investigations have been aimed on the development of sensitive, fast and low cost method of detecting chemical and biological compounds on nanolevel. This set of methods is called surface (nano-) lithography. A few methods were develop here: optical lithography, nanoimprint lithography and nanosphere lithography.³⁰

Optical lithography is based upon the principle of substrate irradiation with the photons of a spin-coated resin through the mask. As optical lithography implies irradiation with photons, the best achievable resolution is only 100nm (generated with Fluor based laser), whereas applying electron radiation (which have higher energy and thus lower wavelength) allows to achieve higher resolution up to 20 nm. Nanoimprint lithography (NIL) is a completely different approach compared to conventional photon and electron based lithography's. NIL implies direct contact between a template and a thermoplastic to imprint the pattern. Thus, one of the advantages of NIL is that it does not require high-cost optics nor a light source to create an image. In addition it is possible to produce sub-10nm images with NIL. The drawback is that quality of image depends namely on mechanical behavior of the stamp and resist. Also the technique has a restrictive elements like pattern designs, reproducibility and low resolution. The nanosphere lithography (NSL) implies self-organization of a nanoparticles monolayer on a surface. This monolayer, when used as a mask gives rise to metal nanoparticles (MNPs) arrays when the monolayer is removed from the surface. The limitation of image quality in NSL depends greatly on self-assembly step and restrictive morphology. Here various defects such as holes or dislocations on a monolayer appear.

Due to the mentioned limitations, there is a need for technology that lead to the construction of substrates with tailored patterns and unique morphologies over extended areas. These group of techniques and there advantages are discussed on the following section.

1.4.1. Electron Beam lithography (EBL)

Due to the small probe size and small wavelength electron beam lithography (EBL) provides a great resolution of investigated sample. In addition, EBL is a flexible method that can operate with variety of materials. The main drawback of EBL is that it is slow (generally 10^7 pixels per second) and expensive for volume manufacturing. Electron beam is used to irradiate (thus, chemically modifying) a suitable resist, applied to coat the substrate.

An important factor that governs the minimum feature size is resist material used in the EBL. Photoresist technology can be divided in two main groups of polymers: at electron beam irradiation the polymeric architecture is either cross-linked (negative resists) or broken (positive resist). The main advantage of positive photoresists in front of negative ones is that in case polymer backbone is broken, another soluble molecular fragments, but of smaller size are formed. In contrast when polymer system is cross-linked, insoluble material which demands further processing is formed. However, in both cases (of application positive and negative resists) the smallest recognizable pattern is approx. several nanometers for the most polymeric materials (as large as molecular area of polymer molecule on the substrate). Lots of different materials have been studied to reduce resist molecule surface to as low as practicable. In this perspective organic

molecules of low molecular weight³¹, metal fluorides (as well as other inorganic materials), fullerenes³² and their derivatives³³ were investigated. However, in order to achieve sub 20-nm resolution, various extra steps before, during and after irradiation are often required³⁴. A brief comparison of the best resolution (both: isolated and dense structures) as well as respective electron dose of all mentioned electron beams is shown in the Table 1.

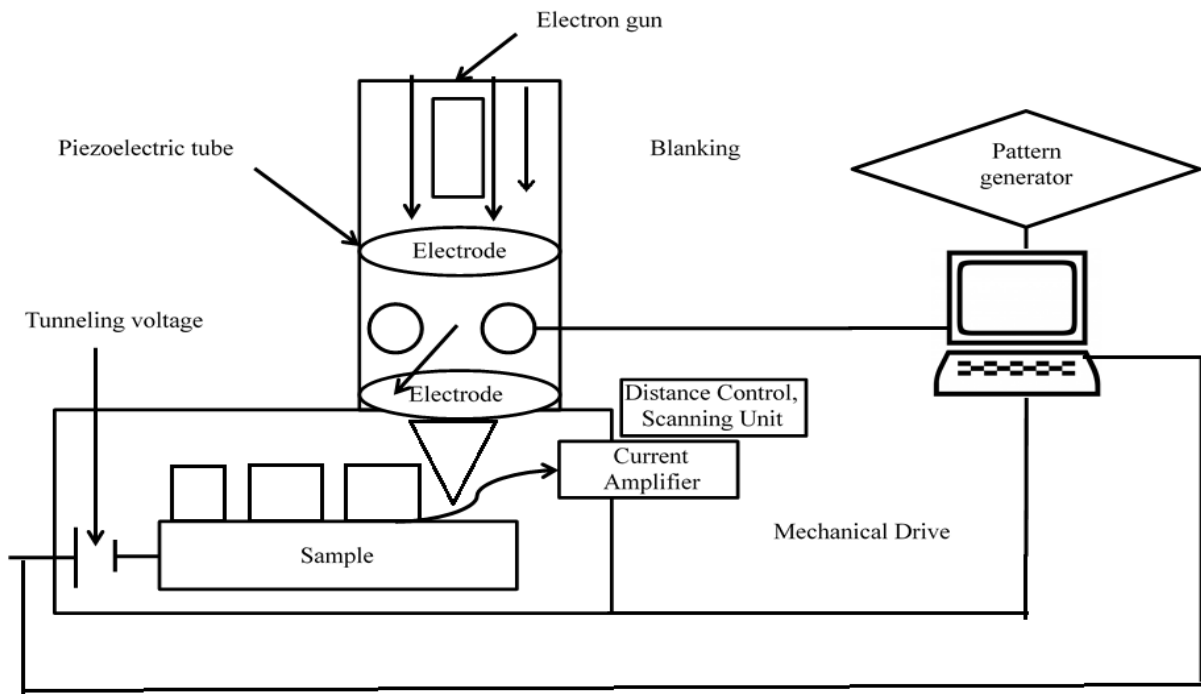


Figure 5: Simplified scheme of electron beam lithography tool.

(Inspired from the design published at this location: [www. ieeexplore.ieee.org](http://www.ieeexplore.ieee.org); presented from the work: EBES, a practical electron lithographic system ; D. R. Herriott, et al. IEEE Trans. Electron Devices, vol. 21, p. 385–392, 1975-07)

Table 1: Comparison of the mentioned electron beam resists and the smallest structures investigated with these mediums.³⁵

Resist name	Resist type	Resolution	Disadvantages
PMMA, (polymethylmethacrylate),	Negative	10 nm	Problems related with the destruction of the design, low etch resistance
SAMs (self-assembled monolayers),	Positive	25 nm	Complicated etching process
CARs (chemically amplified resists)	Positive	40 nm	Developing complications caused by complex chemical structure
Fullerene	Positive	250 nm	Low sensitivity, difficulties in fabricating thin, defect free film
Metal halides	Positive	30 nm	High doses, spin coating problems
Metal oxide	Positive	30 nm	Low sensitivity, instability of pattern
Nanocomposite	Negative	100 nm	Lack of knowledge of the process of incorporating nanoparticles to the resist layer

The mask is then formed on irradiated surface after removing resin by the chemical treatment (usually by reactive ion etching), thus producing holes of desired size and shape. The following step include deposition of the desired metal that covers the whole surface and also fill the holes

that were formed after chemical treatment. Finally, the last step is separating the resin and metal layers by applying the lift – off method. In this way in EBL study fabrication of a large set of 2D – nanoparticle geometries (arrays of non-coupled nanoshapes) are being created.

1.4.2. Reactive Ion Etching (RIE)

Reactive Ion Etching is an etching technology that is often used in microelectronics. Chemically active plasma is used to remove material from the basement. Plasma is obtained at low pressure by virtue of gas discharge. Ions in the plasma are being accelerated by difference in potentials between plasma itself and proceeding surface. Coaction of chemical reaction, ion dispersing and ionic activation lead to destruction of the basement, forming volatile compounds which are desorbed from the surface on the final stage³⁶.

Content and pressure of substrate applied depends on the material that have to be etched as well as requirements of the shape of etching. For example, for anisotropic silicon etching through the mask of silicon dioxide, a mixture of $\text{SF}_6 + \text{O}_2$ is used. To obtain reverse selectivity (silicon dioxide etching), CF_4 is used.

In modern RIE systems separated plasma generator is applied to increase the density of current. Plasma is created by inductor with high frequency, and ions are being extracted from it by creating high-frequency shift on the treating surface. As well as voltage of ionic current saturation in plasma do not exceed a few dozen Volts, a combination of high current density with relatively low ion energy at pressure of 0.1-1 Pascal can be obtained.

Chapter #2: Antimicrobial and Antibacterial Drugs and problem statement

The following section presents the analytes selected to carry out this work. To do this, two fluoroquinolones have been selected and a sulfonamide, this selection was made taking into account the ease of acquisition of them in drugstores by patients and their high use for the treatment of specific medical conditions. The chemical structures, uses, treatment will be presented. To end the state of problem and the objectives of this research to help solve this problem are discussed.

2.1. Fluoroquinolones

Fluoroquinolones are an essential class of antibacterial, and widely used in clinical application. Fluoroquinolones are antibacterial agents that have been used widely in the treatment of respiratory and urinary tract infections. The widespread use of fluoroquinolones in clinical practice is because antibiotics that are broad spectrum activity against Gram -negative microorganisms, Gram positive, anaerobes and mycobacteria.³⁷ Quinolones consist of bicyclic ring structure and different functional groups are substituted at position: 1, 2, 7 and 8. The addition of a fluorine at position 6 atom gives the characteristic name of the pharmaceutical compound. The figure 6 present the general structure of a fluoroquinolones.

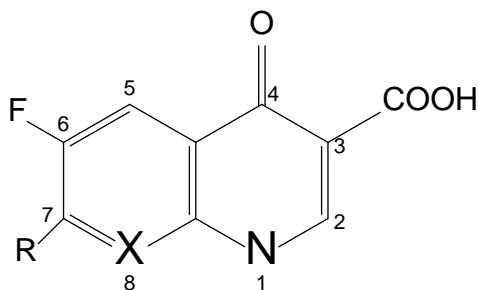


Figure 6: General Structure of a Fluoroquinolone

The position of the different functional groups leads to specific clinical effects as discussed in several reviews. The Carboxyl group is substituted at position 3, a ketone functional group at position 4, fluorine atom at 6 positions, and while at position 7 can be a piperazinyl group or a methyl piperazinyl. The derivatives of second and third generation arise from making small changes in their structure and the introduction of any atom. For example, the introduction of a fluorine in the carbon position 6 (C-6) and piperazine in the C-7, gives rise to second generation fluoroquinolones, such as Ciprofloxacin and Norfloxacin.³⁸ Further development of second generation derivatives with the introduction of new C-7 rings or chiral resolution of existing agents lead to third generation derivatives, such as levofloxacin. Presences of different functional group at N-1 or at C-7 positions influence both microbiological and pharmacokinetic properties. In this study two fluoroquinolones derivatives have been used for the Raman spectroscopic.

2.1.1.1. Ciprofloxacin

Ciprofloxacin chemical name is 1-cyclopropyl-6-fluoro-1, 4-dihydro-4-oxo-7-(1-piperazinyl)-3-quinoline carboxylic acid, is a second generation fluoroquinolone. It is an antibiotic which is an important antibacterial drug that have been widely used for treatment of many bacterial infections such as urinary tract, typhoid, tuberculosis, diarrhea, sinusitis, prostatitis, pneumonia and many others.³⁷

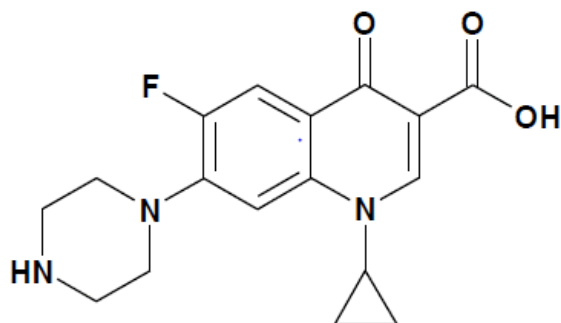


Figure 7: Ciprofloxacin chemical structure

2.1.1.2. Levofloxacin

Levofloxacin chemical name (-)-(S)-9-fluoro-2,3-dihydro-3-methyl-10-(4-methyl-1-piperazinyl)-7-oxo-7H pyrido [1,2,3-de]-1,4-benzoxazine-6-carboxylic acid hemihydrate is a third generation of fluoroquinolones.³⁹ This drug is the pure enantiomer (-)-(S)-enantiomer of the racemic drug Ofloxacin. Levofloxacin is an antibiotic for oral and intravenous administration, with broad spectrum drug of activity against various bacteria, including gram-positive and gram-negative (anaerobic and aerobic). This medicine is most commonly used to treat diseases such as chronic bronchitis, pneumonia, urinary tract infections, among others.⁴⁰ Levofloxacin is rapidly absorbed after oral administration. Has been found in recent studies that Levofloxacin has a limited metabolism and approximately 87% of an administered dose was recovered as unchanged drug in urine and less than 4% of the dose was recovered in feces.⁴¹

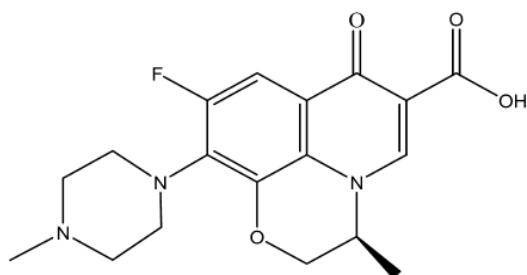


Figure 8: Levofloxacin chemical structure

2.2. Sulfonamides

The sulfonamides or sulfa drugs, one type of the most group of broad-spectrum antibiotics, have been mostly used for clinical and veterinary purposes because of their efficacy and low cost. This drug competitively inhibits folic acid synthesis in microorganisms and were formerly used as bacteriostatic against a wide variety of bacteria gram positive and gram negative, and some protozoa. These type of drugs serves as an alternative to the use of fluoroquinolones in people who suffers from allergy reactions or the use of fluoroquinolones does not result in an improvement of the patient condition. Sulfonamide are used in the treatment of numerous infectious diseases; it is mostly used in the treatment of AIDS.⁴² This drug is readily absorbed orally and topically. Sulfonamides are distributed throughout the body and they are metabolized by the liver and excreted by the kidneys.⁴³ The metabolism of Sulfonamides usually is not complete, thus a large amount could be excreted through urine and feces.⁴⁴

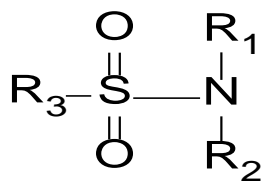


Figure 9: General Structure of a Sulfonamide

2.2.1.1. 4-Carboxybenzene sulfonamide

This compound also known as Carzenide and as 4-Sulfamylbenzoic acid is a compound that had been related as a Carbonic Anhydrase inhibitor.⁴⁵ This enzyme is responsible for the conversion of carbon dioxide to other ionic forms and also is responsible for the reverse effect of converting the ions to carbon dioxide. In addition the chemical structure of this compound is quite similar to the 4-aminobenzoic acid also known as PABA, which is known to be a model Raman compound. This situation suggest that the study of the 4-carboxybenzene sulfonamide by means of SERS could be achieved.

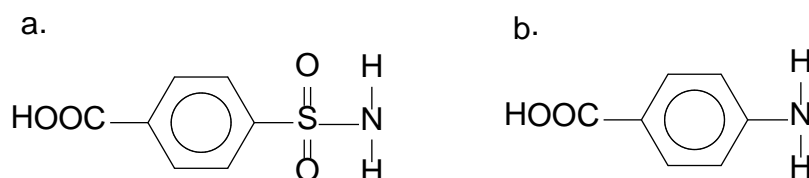


Figure 10: Chemical Structures of: a. 4-carboxybenzene sulfonamide and b. 4-aminobenzoic acid

2.2.1.2. Sulfadiazine

Sulfadiazine (Sulfa) also known as 4-amino-N-(2-pyrimidinyl)benzene sulfonamide is a second generation of sulfonamide known for the treatment of several bacteriological infections.⁴⁶

It's considered a broad spectrum drug based on their activity on Grams positive and Grams negative bacteria. Sulfa is also considered as primarily option in the veterinary medicine.⁴⁷⁻⁴⁸ The drug is eliminated from the human and or animals body in the urine as original compound or as the acetylated form. As for 4-carboxy their structure resembles to the p-aminobenzoic acid (PABA). In this project their study will be focus on Chapter #4 as one of the analyte to be considered as a pollutant in surface waters.

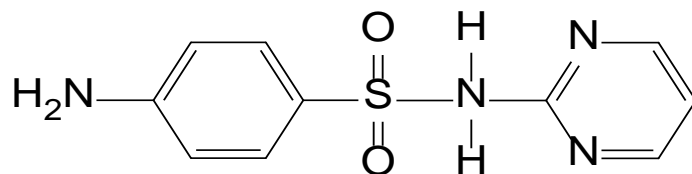


Figure 11: Sulfadiazine chemical structure. This pharmaceutical agent was analyzed to demonstrate method roughness and capability.

2.3. Statement of the problem

Pharmaceuticals and Personal Care Products as Pollutants (PPCPs) are an emerging class of pollutant that are rising serious concerns among regulatory agencies due to their lack of regulation, widespread use and potential toxicological effects. PPCPs comprise a diverse collection of thousands of chemical substances, including prescription, over-the-counter, and veterinary drugs, as well as fragrances, and cosmetics.⁴⁹ Upon ingestion, drugs are not entirely absorbed by the organism. Then a portion of the drug is excreted and subsequently passed to the environment representing a potential source of contamination or detrimental conditions of nutrient source on some natural resources.⁵⁰ Studies confirm that pharmaceuticals are present in trace amounts in surface waters on the United States,⁵¹⁻⁵² in other countries⁵³⁻⁵⁴ and in wastewaters.⁵⁵⁻⁵⁸

Antibacterial and antimicrobial agents are a particular class of PPCPs of significant importance environmental research since trace amounts of these drugs can promote the growth of resistant pathogens and bacteria. Sulfonamides and fluoroquinolones are two examples of these types of drugs and the possible routes of introduction of these compounds in the environment include litter leachate, wastewater, runoff water and leakage from manure storage tanks. This situation had been recorded on recent studies that had detected the presence of sulfa in systems composed of soil and manure,⁴⁸ and their persistence lasted for several months.⁴⁷ Cipro and Levo also had been detected on several of the sources previously described.⁵⁹⁻⁶⁰ The information on their bioavailability and chemical decomposition in water and soil is relative unknown. Some methods that have been employed for the detection and study of these pollutants are: Liquid Chromatography with Mass Spectrometry (LC-MS) or traditional High Performance Liquid Chromatography with ultraviolet

detection (HPLC-UV) or with diode array detection (DAD) as detection alternatives for other antimicrobials. These techniques, although effective, are expensive to perform as well as they are destructive.⁶¹⁻⁶²

As explained on the previous sections the use of Surface enhanced Raman spectroscopy (SERS) with the development of metallic nanostructures generates a secondary electric field with significant enhancement of the signal produced by the analyte. But, this technique faces two problems: a) in recent years there is a constant need for the development of new and more effective plasmonic substrates. b) Lack of reproducible results that could consider it as an analytical tool for the detection and quantification of several environmental pollutants.

The first problem can be overcome with the development of a new type of substrates based on natural patterns. This type of bio-inspired material had become an attractive alternative for the development of new substrates based on their unique features, morphology and design as a result of constant evolution. The second problematic had been explored using the option of rotating the sample to get more reproducible results.

This work aims at the design, development and application of a series of bio-inspired plasmonic nanoarrays for the detection, characterization and quantification of antimicrobial drugs in aqueous media. The development of a Sample translational technique portable device (PSTTD) used with low cost Ag/PDMS nanocomposites to improve the figures of merit of traditional static analysis and their capabilities to be considered an alternative for field analysis are also presented. Finally, the development of remediation alternatives which consider the use of transition metal and internal transition metal oxides for the removal of the studied compounds is considered. At

the same time the development and validation of a chromatographic method to quantify the selected fluoroquinolones and sulfonamides as a detection tool.

Chapter #3: Performance Characteristics of Bio-inspired Metal Nanostructures as Surface Enhanced Raman Substrates

This chapter is a revised version of an article under the same name published in Applied Spectroscopy by Héctor Areizaga, Ivan Kravchenko, Nikolai Lavrik, Michael J. Sepaniak and Marco A. De Jesús:

Areizaga-Martinez, H. I.; Kravchenko, I.; Lavrik, N.V.; Sepaniak, M. J.; Hernández-Rivera, S.P. Marco A. De Jesús; “**Performance Characteristics of Bio-inspired Metal Nanostructures as Surface Enhanced Raman Substrates**” To be published in September 2016.

My primary contributions to this article included: (A) design and fabrication of the Bio-Inspired nanocomposites, (B) Validate the substrates plasmonic properties (C) collection and interpretation of the most of the analytical data, (E) collection and interpretation of cited data, and (F) most of the writing.

3.1.Introduction

Nanoparticle plasmonic is a rapidly emerging research field that deals with the fabrication and optical characterization of noble metal nanoparticles for chemical sensing applications. The increased demand for ultra-trace detection and the need to monitor and control bioactive species and emerging pollutants using plasmonic sensor development is of significant importance. Consequently, there is a continuous demand to manufacture new more sophisticated plasmonic nanostructures whose responses exceeds those of traditional substrates. Over the years there has been a growing scientific consensus on the figures of merit to assess the substrate viability for

surface enhanced Raman scattering (SERS) applications.⁶³⁻⁶⁷ From a substrate perspective, performance of nanostructured systems is highly dependent on inter-particle properties: morphology,⁶⁸⁻⁷³ aspect ratio,⁷⁴⁻⁷⁷ height⁷⁸⁻⁷⁹ and gap.⁸⁰⁻⁸¹ While from a physico-chemical perspective, plasmonic signal depends on the dielectric properties at the sample/metal interface.⁸² Studies on nanolithographically constructed metal dimers have shown that the localized surface plasmons (LSPs) of particles smaller than the excitation wavelength red shifts exponentially with decreasing inter-particle separation.⁸³ Research conducted by Jain and El Sayed⁸³ has recently led to the proposition that the fractional shift of the plasmon wavelength decrease with interparticle separation. Their research also revealed that for simple dielectric systems, the sensitivity can be adjusted by size scaling the corresponding size/length ratios. However, the available information for more complex systems with such dense metal nanoarrays is rather limited. Dense nanoarrays enhance the substrate surface area resulting in an increase loading capacity suitable for quantitative applications. Moreover, adjustments on inter-particle separation can lead to a collective coupling of the LSPs which once optimized can argument SERS performance and reproducibility. Coupling metal nanostructures LSPs can result in large field enhancement at the interparticle junction, which has the ability to amplify Raman scattering from molecules within close proximity to the metal surface by up to 14-15 orders of magnitude.^{2, 84} Morphological effects on substrate performance has been studied using arrays of simple geometrical shapes such as ellipses, cubes, cylinders and triangular prisms.⁸² Nanostructured arrays based on the abovementioned geometries had successfully enabled the SERS detection of drugs such as Mitoxantrone and dyes such as Crystal Violet down to nano-molar amounts.⁸² All the mentioned variables can be adjusted during the design or fabrication of substrates to fine tuning effective conditions.

Considerable strides have been made to improve SERS performance resulting in an evolution from conventional, randomly distributed nanostructures like those from silver islands on glass³, colloidal silver solutions⁸⁵, silver coated microspheres⁸⁶, and Ag/PDMS⁸⁷ to more uniform, sensitive and highly reproducible metallized-nanostructures (MNs). MNs are fabricated either by random metallization of a bulk surface or the metallization of nanolithographically constructed arrays, like those created by electron beam lithography (EBL).⁸⁸⁻⁸⁹ Some benefits of bulk MNs are their relatively low fabrication costs, tunability by either changes in substrate composition or by adjusting simple deposition parameters such as deposition rate, temperature and pressure. Conversely, the combination of EBL-engineered substrates with existing electro-thermal and chemical vapor deposition methods provides a rapid, more sensitive, easily controlled and reproducible route to reproducibly create SERS active MNs with virtually unlimited geometries, sizes, and packing densities. This enables tailoring the substrate performance and their optical properties. In addition, a number of high throughput EBL systems are currently under development⁹⁰⁻⁹², which would allow the rapid commercialization and mass scale production of nanolithographic-MNs, thus considerably lowering fabrication time and costs. The ability to tailor MNs morphology through either controlling the deposition parameters, EBL or a combination of both offers two major opportunities: (1) enable the optimization of the Raman excitation frequency without other spectral interferences such as background fluorescence; (2) nanostructuring of the polymeric surface to improve selectivity toward a specific target or class of compounds (e.g., antimicrobials, peptides, proteins, etc.) Nanocomposite SERS sensors are an emerging piece of technology that is important in biophysics⁹³⁻⁹⁴, environmental⁹⁵⁻⁹⁷ and soft material⁹⁸ studies due

to their unique capabilities for gathering large amounts of both structural and conformational information on drugs⁹⁹ and bioactive systems¹⁰⁰⁻¹⁰¹ in quasi-real-time. MNs also provide connectivity sites due to the extended areas of its nano-scale components, which is particularly useful to monitor bioactive processes.

Nature offers a diverse number of functional surfaces which are the end result of millions of years of evolutionary adaptation to extreme conditions and whose properties are unrivaled by most modern synthetic materials. The capabilities and use of Bio inspired materials in several areas like medical,¹⁰²⁻¹⁰³ drug delivery¹⁰⁴, environmental remediation¹⁰⁵ and as alternative for catalysis remediation¹⁰⁶ has been studied over the past decade. From the scientific point of view, systems that follow natural arrays associated with the Fibonacci sequences and golden ratio has been studied as suitable prospects for plasmonic applications.¹⁰⁷⁻¹¹⁰ In its early stages, such bio-inspired designs has set the mathematical basis for the engineering of more sophisticated sequences but without directly measuring their spectroscopic responses.¹¹¹ Research conducted by Dal Negro et. Al., provided computational evidence that support the occurrence of suitable plasmonic responses over Fibonacci designs and quasi-periodical nano arrays are possible.¹¹²⁻¹¹⁵ The information and results supports the idea that complex periodical systems can lead to improved plasmonic responses can be influenced by properties of the noble metal, the density of the array, and interparticle density¹¹⁶⁻¹¹⁸. Use of bio-inspired designs can potentially reduce search for viable plasmonic morphologies. This work uses biomimetic techniques for the nanolithographic construction, characterization and performance testing of nanostructures inspired on evolutionary successful patterns of fractals of spirals

(sunflower seeds and romanesco broccoli); bilaterally symmetric (acacia leaves, and honeycombs) and radially symmetric (orchids and lilies flowers) with the potential to exhibit highly intense and reproducible plasmonic fields over extended areas of complex-periodicity. The developed designs consists of $40 \times 40 \mu\text{m}^2$ nanoarrays with 150-120 nm particle size and 50 nm minimum inter-particle gap. These benchmark dimensions are based on previous studies performed by our group which showed improved SERS responses for that metal nanoparticles (MNPs) with an aspect ratio of 2.5.^{88, 119} For instance, this first generation arrays elliptical prisms, 150 long to 50 nm ratio in which the longest axis aligned with the polarization vector of laser source produces the most intense radiation scattering.^{23, 88} Likewise, larger particle sizes and densities have been explored;²³ and although proven to be SERS active, their enhancement are yet far from that suggested for denser arrays with potential interparticle coupling.^{88, 120} Finally, ZEP-520 was selected as the standard EBL photoresist since it was currently validated at the EBL facility to enable reproducible nanofabrication at the 50 nm threshold of LSPs responses. Fabrication was focused toward constructing a unit cell of each bio-inspired design, for whom its plasmonic responses can be replicated over an extended area of $40 \times 40 \mu\text{m}$. This allows for a suitable and cost-effective dimensionality for this proof of concept design. It also provide enough surface area to test and validate the SERS responses and quantitative loading of each arrays. The patterns, were selected to address an intriguing area of SERS research that can lead to empirically answer if either local asymmetry or quasi-periodic nanoparticle distribution is required to construct high performance SERS substrates. The driving hypothesis of this work is that MNs of bio-inspired morphologies has the potential to more effectively explore plasmonic morphological space, thus raising a faster, more effective creation of substrates with tailored plasmonic responses. As a result, nine Bio-

inspired patterns were chosen and classified as: bilaterally symmetric, radially symmetric and asymmetric according to the periodicity and symmetries of their arrays (figure 12).

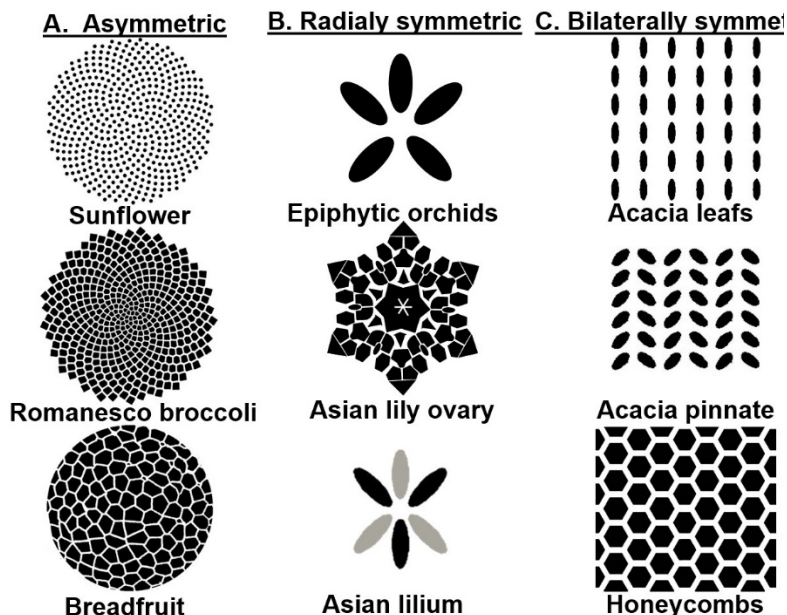


Figure 12: Benchmark biomimetic patterns: A). asymmetric patterns; b). radially symmetric c). bilaterally symmetric patterns

Characterization of the array fabrication process was conducted via scanning electron microscopy (SEM), while an assessment of the plasmonic capabilities of each pattern was determined based on an analysis of the EF at different excitation wavelengths. Studies conducted at 632.8 nm shows Raman enhancements factors greater than 10^7 for the acacia leaf, sunflower and lilies patterns. The substrate characterization and SERS performance of the developed substrates as the strategies to improve the design performance are presented. The applicability of the developed substrates for routine trace analysis of bioactive agents is discussed.

3.2. Experimental

3.2.1. Fabrication of the Bio-Inspired Designs:

All bio-inspired nanoparticles, dimensions and inter-particle gaps per array, were designed using Auto CAD® version 2005 (Table 2). Each array had dimensions of 40 μm by 40 μm with 100 μm separation from each particular design. Conversion of each file to GDSII format was necessary before files were transferred to the EBL instrument.

All patterns were made on 4 inch silicon wafers that were spun coated with ZEP-520A photoresist at 6,000 r/s for 45 seconds to obtain an estimated 300 nm thick coat. All wafers were soft-baked at 180 °C for 2 minutes. The nanofabrication step was conducted on a JEOL JBX-9300 EBL system equipped with a field emission gun that applied a base dose of 275 $\mu\text{C}/\text{cm}$. The proximity correction method was used to avoid possible electron scattering due the close gap between particles. Once exposed, patterns were developed by immersing the wafer in xylene for 30 s and then rinsing with isopropyl alcohol (IPA).

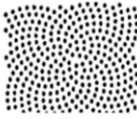
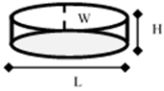
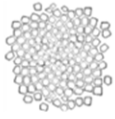
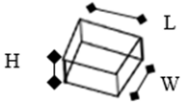
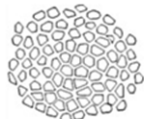
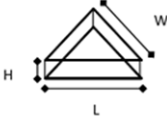
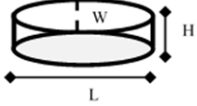
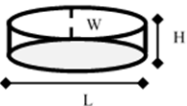
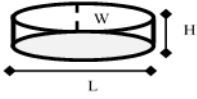
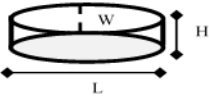
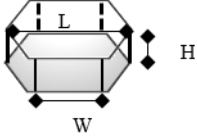
Developed wafers were de-scummed and coated with a 10 nm chromium layer prior been etched in an Oxford RIE system. Pattern liftoff was performed using the NMP-1165® as stripping solvent since it showed an adequate chromium removal for all patterns. Wafers were rinsed with acetone and IPA and then etched for 75 s. After the etching process was completed each wafer was coated with a 10 nm silicon dioxide (SiO_2) layer using a plasma enhanced vapor deposition system.

Characterization was made using a Zeiss SEM, model Merlin using a field emission gun at 3.0 kVA, and 20-315 k magnification. All micrographs were collected in lens mode at 30° tilt angle for more efficient measurement of pattern dimensions.

Fabricated substrates were rendered SERS active by applying a 20 nm of silver (99.999% Alfa Aesar) using a physical vapor deposition system at a 3.7 Å/s rate and pressure of 1×10^{-6} torr. Once coated, substrates were stored under vacuum until analysis. Substrate performance was assessed using benzenethiol (BT) and 4-aminobenzenethiol (4-ABT) as Raman reference materials. To accomplish this, substrates were immersed for 5 min in a 1.00×10^{-4} M aqueous solutions of the corresponding Raman reference material in order to form a self-assembled monolayer (SAM). Coated substrates were subsequently rinsed to remove any excess (unbound) standard and dried with nitrogen (99.99%, Linde Co.). Raman spectral acquisitions were made at 3 excitation wavelengths, 532, 632.8, and 785 nm. The 632.8 nm studies were made on a confocal Raman microscope (Lab-RAM, Horiba Co.). Spectra were also collected using an infinity corrected 50X objective and a spectral window from 100 cm^{-1} – 3000 cm^{-1} using a 1 s acquisition time with a 2.30 mW irradiation power. Data were then processed using Horiba's LabSpec™ 4.2 software. The 532 and 785 nm experiments were conducted in a confocal Renishaw microspectrometer, model RM-2000. Spectra were collected with an incident power of 3.70 mW, and 3.89 mW respectively and 1s acquisition time. Previous studies using PDMS often show significant thermolytic and photolytic degradation of the analytes at laser powers higher than 4mW and irradiation times greater than 5s.^{78, 87, 119, 121} Therefore, power levels were kept below 4.0mW to ensure negligible effects at the irradiated surface, thus allowing a reliable reading and validation

of the SERS response. All measurements were normalized to enable a reliable comparison of the results obtained at each wavelength

Table 2: Bio-Inspired nanoarrays patterns and dimensions.

Asymmetric Group		
<p>Sunflower</p>  <p>L = 200 nm W= 100 nm H= 250 nm Gap= 300 nm</p> 	<p>Romanesco</p>  <p>L = 300 nm W= 100 nm H= 250 nm Gap= 300 nm</p> 	<p>Breadfruit</p>  <p>L = 330 nm W= 160 nm H= 250 nm Gap= 100 nm</p> 
Radially Symmetric		
<p>Lilium Ovary</p>  <p>L = 1150 nm W= 450 nm H= 250 nm Gap= 50 nm</p> 	<p>Asian Lilium</p>  <p>L = 1150 nm W= 450 nm H= 250 nm Gap= 50 nm</p> 	<p>Orchid</p>  <p>L = 1150 nm W= 450 nm H= 250 nm Gap= 50 nm</p> 
Bilaterally Symmetric		
<p>Acacia</p>  <p>L = 150 nm W= 450 nm H= 250 nm Gap= 50 nm</p> 	<p>Pinnate</p>  <p>L = 150 nm W= 450 nm H= 250 nm Gap= 50 nm</p> 	<p>Honeycomb</p>  <p>L = 150 nm W= 450 nm H= 250 nm Gap= 50 nm</p> 

3.2.2. Substrate Application

The use of the bio-inspired arrays as an alternative for the detection of pharmaceutical products were evaluated using the best four substrates in performance. For this, two pieces that contained the arrangements placed in two small petri dish. To each plate was added 3.00 mL volume of the solution of interest (Levo or 4-carboxy 1.00×10^{-4} M) then the plate was placed under the microscope. Each array was focused using a 50x objective and irradiated for 5 sec using the excitation line 638 nm at a power of about 2 mW. The solid sample of each drug was also analyzed for comparison purposes. This sample was irradiated for 30 seconds under the same conditions.

3.3. Results and discussion:

3.3.1. Initial Studies

Initial Studies

Proposed Bio-Inspired nano composite substrates were designed using Auto CAD® software with cell arrays of 40 by 40 of each design. Initial trials were performed using Polymethacrylimide (PMMA) as photoresist. The selection of this photoresist was made because of their use on several nanofabrication process reported on literature.¹²²⁻¹²⁴ Because of the diversity in morphology of the nanoinspired materials in addition to difference in packing density several electron beam doses were tested ranging from 1,000 $\mu\text{C}/\text{cm}^2$ to 1250 $\mu\text{C}/\text{cm}^2$. The results demonstrate poor particle definition especially for all patterns except the sunflower (less dense packing material). Increase in the dose results in overexposure patterns with poor definition as presented on Figure 13.

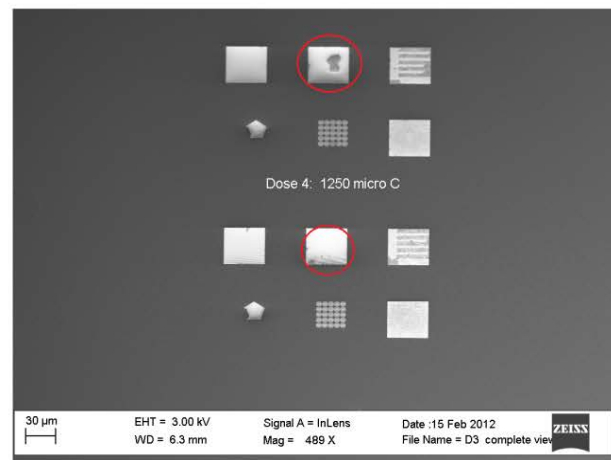
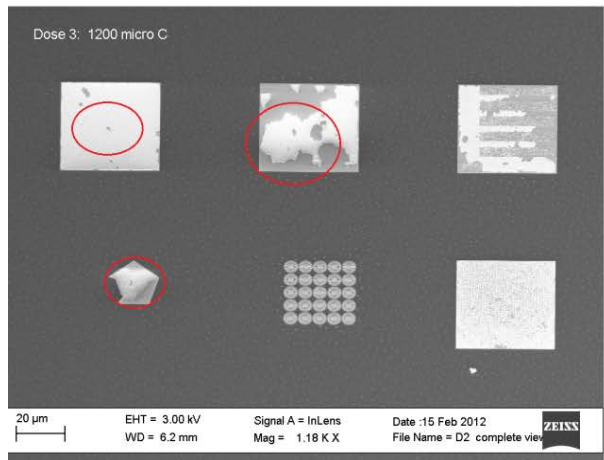
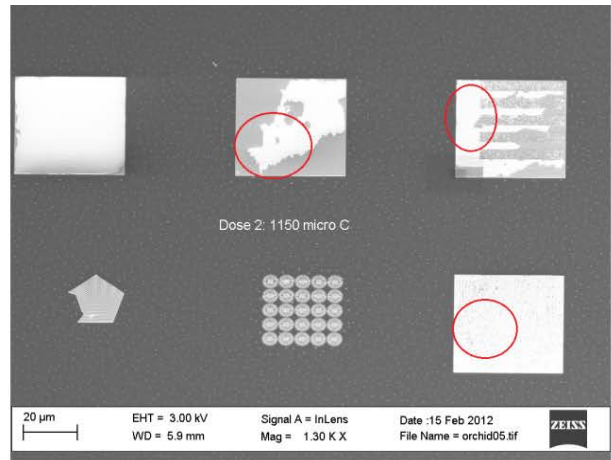
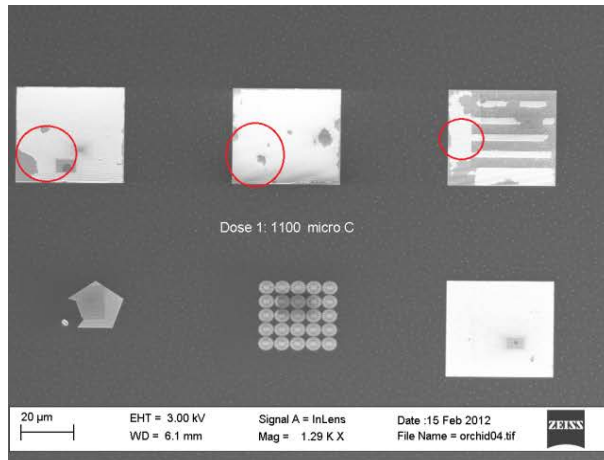


Figure 13: SEM micrograph for the four doses experiments performed. Circle shows over exposure of those areas led to incomplete development and poor liftoff efficiency for the most patterns.

To solve this situation a new study was performed using ZEP520A to decide which E-beam dose and photoresist would be suitable for the fabrication of the different Bio-Inspired patterns. ZEP-520A has several characteristics which made a suitable photoresist for these types of arrangements.¹²⁵ In addition a new design for the sunflower that resembles the natural Fibonacci spiral present in most of the nature patterns was included. Doses ranging from 275 $\mu\text{C}/\text{cm}^2$ to 1250 $\mu\text{C}/\text{cm}^2$ were employed to determine the optimum dose. The results of the dose study suggest that using the lower base dose and using proximity corrections methods to eliminate electron beam backscattering, offers the best combination to fabricate the proposed nine patterns.

3.3.2. Substrate Characterization

Biomaterials are the result of millions of years of evolutionary adaptation resulting in sophisticated designs with outstanding mechanical, self-cleaning, optical, adhesive, actuation, sensing, and responsive capabilities. As a result, nature offers a diverse number of functional surfaces, whose properties are unrivaled by most modern synthetic materials.¹²⁶ These properties arise from hierarchical self-organization and optimization for which asymmetric, bilateral or radially symmetric particle distributions from the nano to the micro and macro scales and determines the functionality and performance of the material. For instance, like many natural materials, the functionality of plasmonic substrates is accomplished through a tailored synergy between particle geometry, surface nanostructuring (roughness) and chemical properties. Previous work conducted by De Jesús, et al. using biomimetic honeycombs, acacia leaves and acacia pinnate metallized patterns have shown over 3 times improvement in the Raman signals of Rhodamine 6G

(R6-G) with respect to those from standard polydimethylsiloxane (PDMS) substrates.⁸⁸ The substrates have also shown potential for the detection of antimicrobial agents and carboxylic acids at the 1×10^{-6} to 1×10^{-8} M range. Recent collaborations with the center of nanophase materials (CNMS) at ORNL have allowed our team to extend the list of bio-inspired designs to include other naturally occurring patterns with potential application in plasmonics, such as from Fibonacci arrangements like sunflower seeds and romanesco broccoli (asymmetric); acacia leaves, and honeycombs (bilaterally symmetric), and Rhodonea flowers such as daisies and lilies (radially symmetric) as prospects for SERS applications. Thus, using the underlying principles developed by nature as a nanofabrication benchmark, to allow for a more efficient sampling of the substrate's morphological space, while expediting the identification of high performance plasmonic patterns. Original CAD generated patterns were rendered with a 50 nm inter-particle separation for eight out of the nine patterns. The sunflower pattern closest gap was defined to be 150 nm in order to preserve its Fibonacci ratio. Figure 14 shows micrographs with well-defined morphologies for seven of the nine bio-inspired patterns. Only the breadfruit and honeycomb patterns exhibited poor inter-particle definition per unit cell. The result can be related to low electron beam dose with respect to the pattern density resulting in underdeveloped structures. However, considering the various shapes and densities of the constructed nano-arrays, a use of low intensity dose proved to be the most reasonable tradeoff for the precise fabrication of at least seven of the nine patterns. According to the SEM analyses after the RIE step, inter-particle gap fluctuated in the range from 25 to 43 nm range for the highly dense arrays (Orchid, Asian Liliun, Acacia Leaf and Pinnate), while the mean gap of the sunflower array was at the 145 –195 nm range in reasonable agreement with expected gap. A 75 s RIE resulted in pillars with a height within the 212- 260 nm range for a

total of three measurements ($n = 3$), please refer to Table 3. Romanesco and breadfruit arrays which have the highest number of different elements, showed the lowest aspect ratios mainly affected by the poor development of the nano-structures.

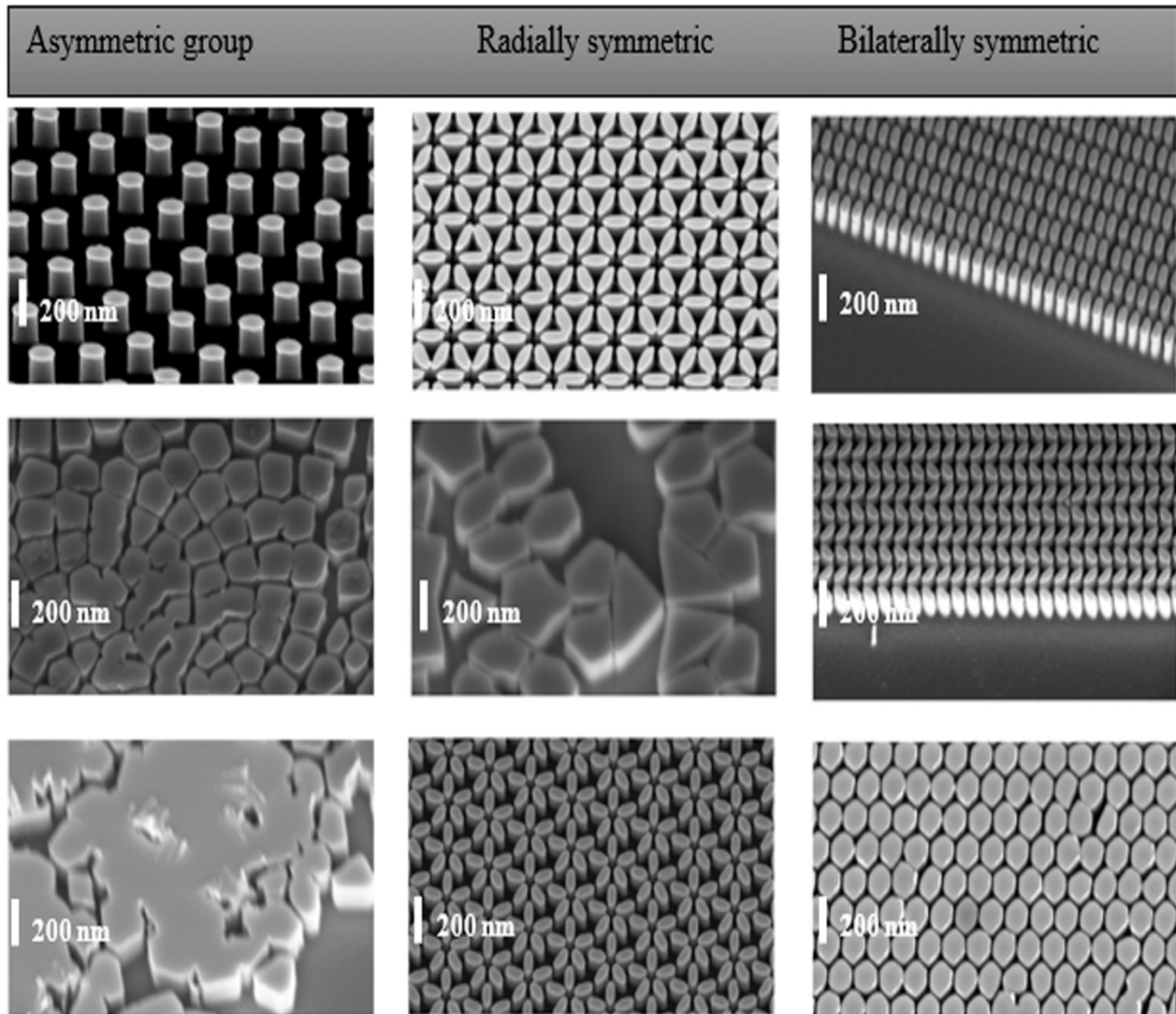


Figure 14: Bio Inspired arrays micrographs obtained with a Ziess Scanning electron microscope (SEM); Power = 3.0 kV; Magnification = 90.00 K X Tilted at 30 degrees; Detector Mode = InLens. Characterization of the nano composite substrates after the etching step was done to evaluate the efficiency of the nanofabrication process. Patterns are presented following the order defined on Figure 12.

Table 3: Dimensions for the fabricated Bio Inspired arrays:

Pattern	Long (nm)	Short (nm)	Height (nm)	Gap (nm)	Aspect Ratio
Sunflower	225(±19)	111(±8)	249(±29)	170(±25)	2(±0.3)
Romanesco	324(±18)	286(±28)	236(±35)	31(±8)	1.14(±0.05)
Bread Fruit	2926(±110)	2239(±409)	260(±2)	60(±10)	1.3(±0.3)
Asian	138(±13)	57(±9)	240(±3)	43(±10)	2.4(±0.5)
Ovary	728(±47)	421(±16)	249(±5)	24(±3)	1.7(±0.2)
Orchid	133(±17)	54(±1)	223(±16)	41(±10)	2.5(±0.4)
Acacia	147(±7)	67(±3)	226(±6)	33(±6)	2.2(±0.2)
Pinnate	122(±5)	53(±7)	212(±13)	26(±1)	2.3(±0.3)
Honeycomb	221(±34)	172(±38)	254(±6)	31(±11)	1.3(±0.1)

3.3.3. SERS Studies:

This work was focused on the design, fabrication and optimization of nine conceptual MNPs devised according to bio-inspired morphologies (Figure 12). The goal in this study was to use these patterns as point of reference to single out the morphological differences in relation to the array's ability to excite LSPs at 532, 632.8, and 785 nm. SERS performance of the developed nanostructures was assessed using 4-ABT and BT as standard reference materials to monitor the Raman responses at each wavelength and for MNs height optimization due to their self-assembly properties.¹²⁷ To accomplish this, each pattern was immersed for 15 min in a 0.1 mM solution of the respective standard to ensure proper monolayer coverage and rinsed in deionized water (DW). Characteristic Raman spectra and band for assignments for each standards are presented in Figure 15, 16 and Table 4. This includes the characteristics the 1050 cm^{-1} C-S stretching band, the 1500 cm^{-1} aromatic C-C stretching and the 1100 cm^{-1} C-H bending and stretching modes around are also observed. Enhancement of the Raman responses for each design pattern was assessed by calculating the 4-ABT and BT SERS Enhancement Factor (EF) at each excitation wavelength (Equation 10).

The number density of molecules present at the surface (N_{surf}) was determined calculating the total surface area, for instance an ellipsoid, for the elliptical patterns (acacia leaf, sunflower, acacia pinnate, orchid and asian liliun). The top area was empirically calculated using the average length and width of a particle based using the SEM images (Figure 14), Pattern heights were determined based on the thickness of the silver layer deposited on each substrate accounting for the amount of deposited silver. The calculated surface area was multiplied by the number of

particles at the diameter of the laser spot (5 μm for 532, 11 μm for 632.8 nm; and 12 μm for 785nm) respectively. For the arrays whose basic unit cells are irregular (honeycomb, romanesco, liliun ovary and breadfruit) measurement the individual dimensions of each particle is not practical. The average perimeter and the surface area of the most frequent pattern observed in the particles provide an estimate of the average surface area.

Table 4: Characteristic Raman spectra and band for assignments for 4-AminoBenzenethiol and Benzenethiol

4-AminoBenzenethiol			Benzenethiol		
Literature	Experiment	Assignment	Literature	Experiment	Assignment
536	521	C-C-C bending	417	403	
1011	1007	C-C bending/C-C-C bending		508	C-C-C bending
1077	1074	C-S stretching		678	
1142	1144	C-H bending	999	987	C-C-C bending
1178	1191	C-H stretching	1022	1010	C-H bending
	1310		1073	1063	C-S stretching
1387	1392	C-H bending +C-C bending		1100	
1430	1436	C-C stretching + C-H bending	1182	1172	C-H bending
1586	1576	C-C-C aromatic stretching;	1475	1465	C-C stretching
			1584	1566	C-C aromatic stretching; SH stretching

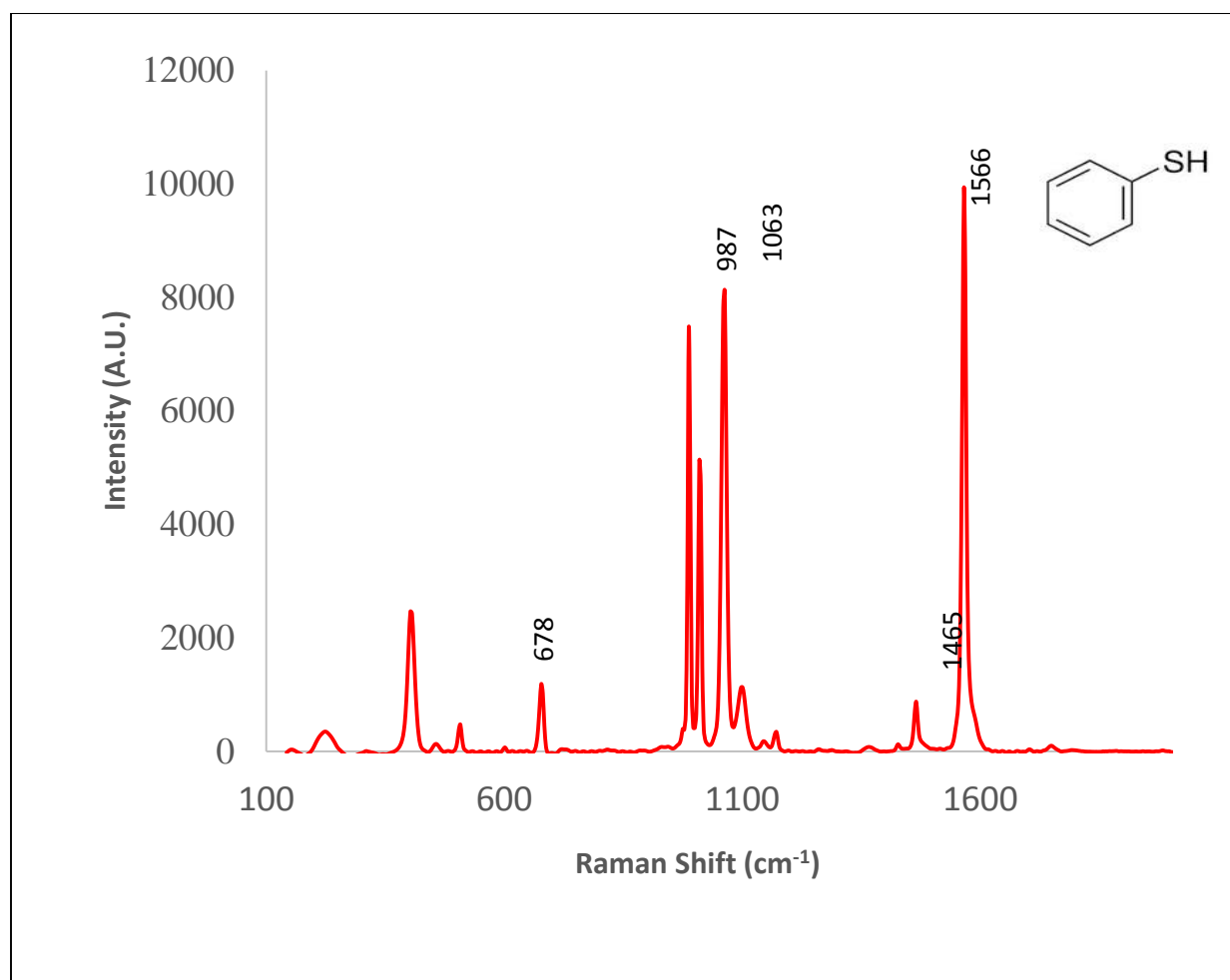


Figure 15: BT SERS spectra using the Sunflower array as substrate. This was collected using a 632.8 nm excitation source for 1 s with a 2.30 mW laser power.

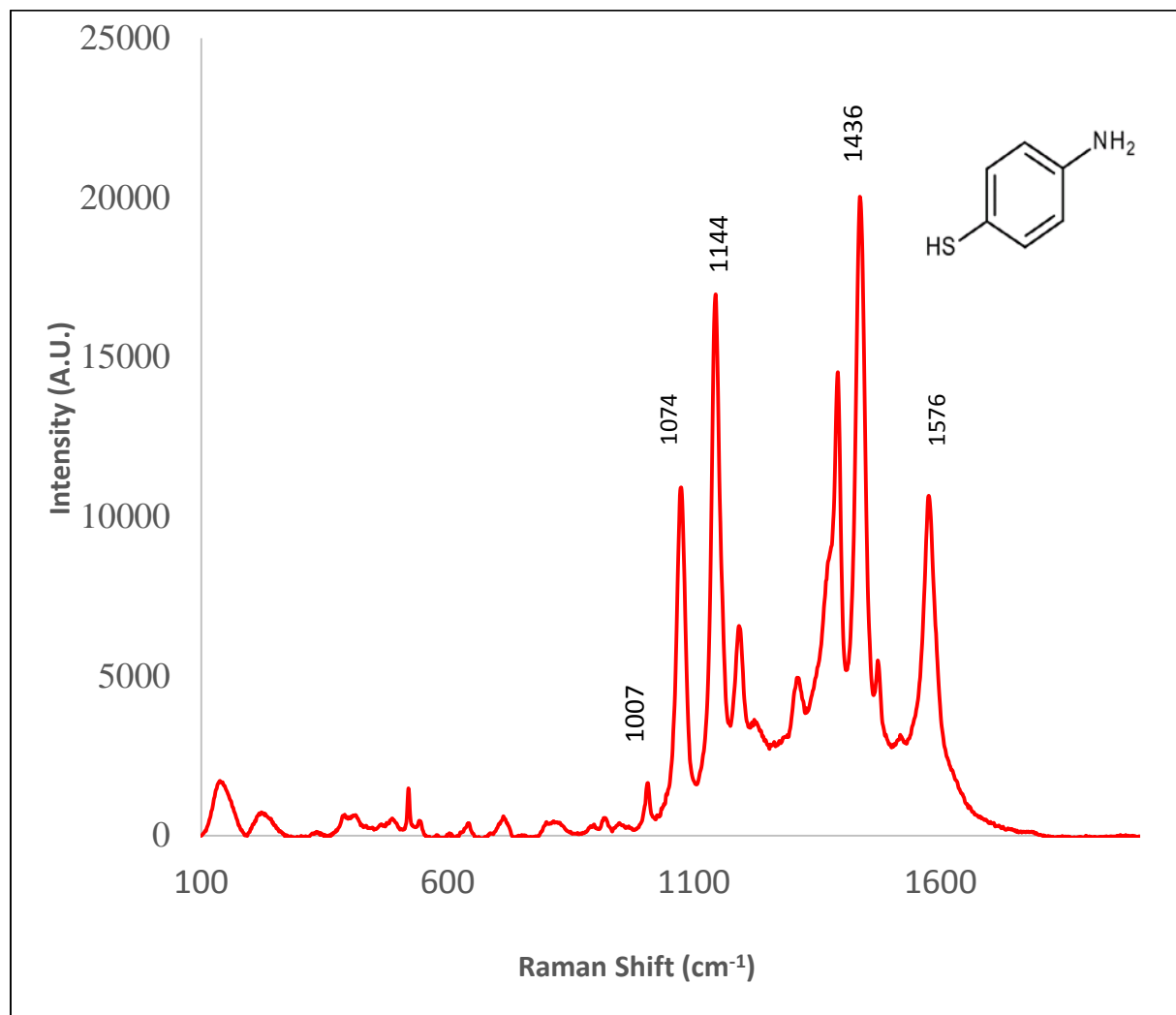


Figure 16: 4-ABT SERS spectra over the Sunflower Bio Inspired array. The acquisition was performed using a 632.8 nm excitation source for 1 s with a 2.30 mW laser power.

Natural LPR for silver is observed at a wavelength close to 420 nm. Efficient LPR excitation at the available wavelengths is function of size, shape, particle gap spacing and dielectric environment of the nanostructured arrays.¹²⁸⁻¹²⁹ These parameters can be modified promoting a red shift (displacement of the absorption wavelength close to the employed excitation line). Among these enhancement figures of merit particle morphology and spacing are key. For instance, studies conducted by our group and our team of collaborators at Oak Ridge have concluded that nanoparticles exhibiting an ideal length to width of 2.5 are suitable for 633 excitation (Table 3). In order to determine which figures of merit contributes more effectively on the EF the fabricated patterns were divided into groups of difference density and geometric complexity.

The bilaterally group, was chosen as the benchmark substrate based on a previous generation of nano composites that were fabricated without the RIE process.⁸⁸ The results at that time indicate the acacia was the more efficient pattern based on the design, and orientation of the particles.⁸⁸ The results of that study are confirmed by our findings. Close evaluation of the results shows that the separation between particles is not a significant difference between the gap of the acacia leaf and the pinnate group (33 vs. 26 nm respectively). However, for a SERS substrate shows an effective LPR it must be oriented in the same direction that the polarization vector of the laser. In this case this case from a two dimension perspective the vector is oriented aligned with the orientation of acacia leaf particles, which favors the generation of a strong LPS. This will result in a stronger enhancement effect for this pattern.

Radially Symmetric substrates followed a similar behavior with the orchid and the asian liliun showing the two highest signals intensities. The EF values however reflect a better enhancement for the orchid array. The gap between the particles in the orchid and the asian lilum is almost the same. Therefore, when particle orientation alter inter particle is less influential parameter. As consequence, the difference on the observed EF also is attributed to the orientation of the particles. This led to the generation of alternate light diffraction patterns which are in phase and out phase due to the complex level of those arrays. For that reason, the EF for those arrays are similar. The orchid array was the best of the evaluated substrate at 532 nm with a one order of magnitude greater than other patterns. The complex liliun ovary nano composite stayed as the less effective substrate.

The asymmetrical group, presents the sunflower which exhibit an apparent lesser density but a rather more complex spatial distribution. This presents an interesting situation because the effect of the Fibonacci distribution demonstrates that EF are not dependent exclusively on morphology as previously reported.¹³⁰ Evidently, inter-particle separation and distribution for this type of complex arrays also lays a significant impact on the EF. The other two asymmetric nano composite show modest EF values. This is attributed to the ratio between particle gap and its surface area. This also influence the efficiency of the fabrication affecting the dose and development performance on denser patterns, which also contributes to exacerbate the substrate EF.

As a conclusion, the figures of merits that have a more significant impact on the performance of these substrates are: morphology, gap and orientation. For systems that are geometrically simple, morphology and orientation are the key parameters. On more complicated systems like the asymmetric group the morphology, orientation and gap are the most important figures of merit.

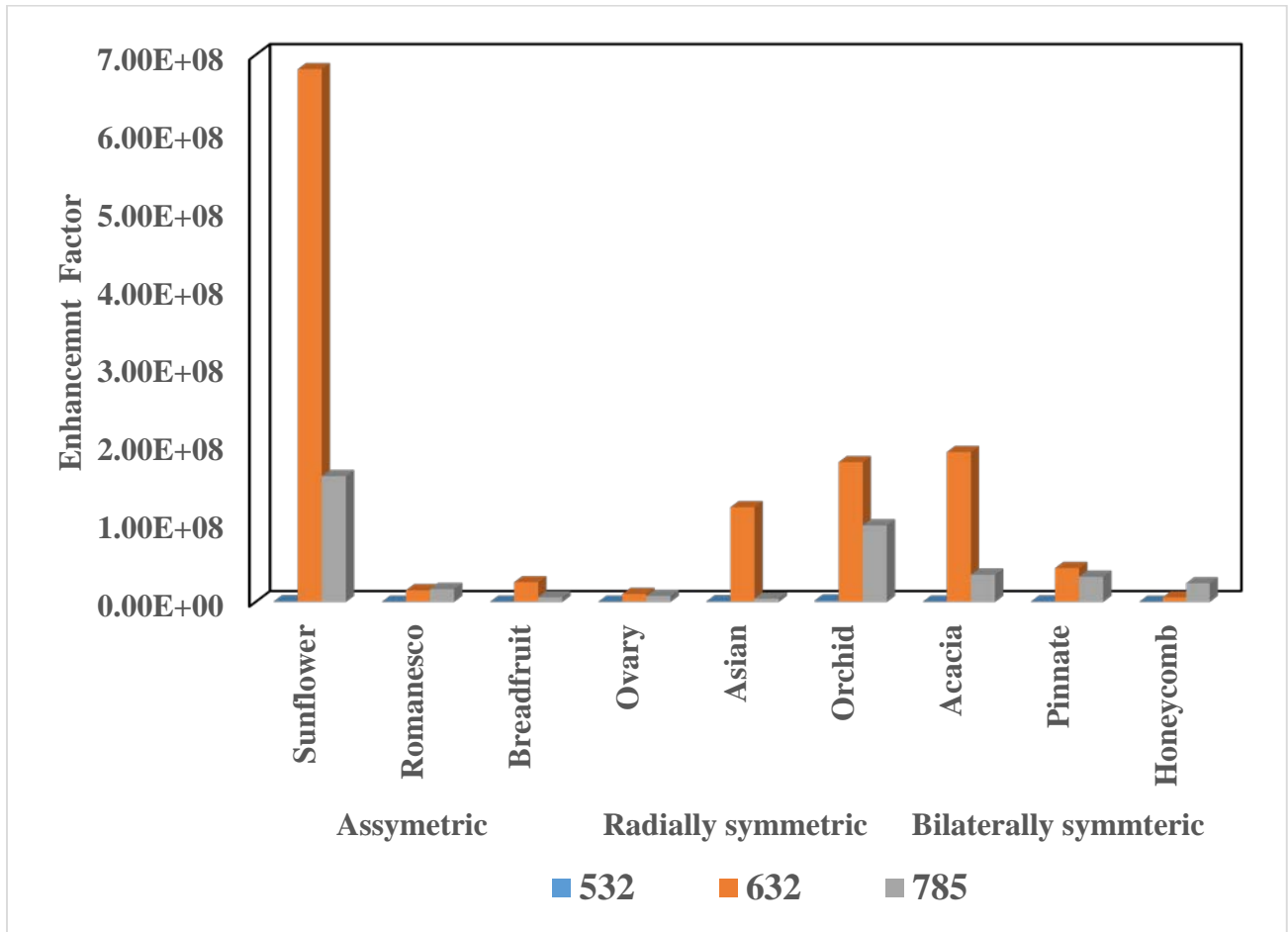


Figure 17: Enhancement Factor evaluation for the nine Bio Inspired arrays analyzed using excitation sources of 532, 632.8 and 785 nm.

Table 5: Enhancement Factors for the fabricated Bio Inspired arrays

Bio-Inspired Substrates EF for n=3 measurements				
Category	Pattern	532	632	785
Asymmetric	Sunflower	5.8(±0.8)E+05	6(±1)E+08	1.6(±0.3)E+08
	Romanesco	6(±2)E+04	1.4(±0.3)E+07	1.6(±0.1)E+07
	Breadfruit	7(±2)E+04	3(±1)E+07	6.0(±.3)E+06
Radially symmetric	Ovary	5.9(±0.4)E+04	1.0(±0.4)E+07	7.6(±0.3)E+06
	Asian	6.2(±0.8)E+05	1.2(±0.3)E+08	4(±2)E+06
	Orchid	1.7(±0.2)E+06	1.8(±0.3)E+08	9.8(±0.6)E+07
Bilaterally symmetric	Acacia	1.9(±0.5)E+05	1.9(±0.1)E+08	3(±3)E+07
	Pinnate	4(±4)E+05	4(±5)E+07	3(±3)E+07
	Honeycomb	5(±5)E+02	6(±1)E+06	2.4(±0.3)E+07

Evaluation of the substrate was done by the normalization of the different EF by the total area of each substrate, in order to get a deeper insight of the pattern activity. The surface area was determined using the experimental dimensions measure. The results presented on Table 6 demonstrate the substrates which smaller surface area on each category have the highest EF which correlates with the results presented on Figure 17. In addition the Sunflower and Orchid substrates show EF values with almost 3 times in intensity with one third of the surface area compared with the rest of the substrates for the highest power source (632 and 785 nm).

The results also present additional information about the efficiency of the substrate is related to the formation of Si pillars and to the increase in packing density. A previous work on orchid, pinnate, asian and acacia leaf arrays were fabricated without the use of the RIE process and using a less dense arrays in which the orchids are basically aligned on rows.⁸⁸ At that time, leaf and pinnate demonstrated to have better analytical responses over orchid patterns. This demonstrates that a denser array with increased pillar height improves substrate performance.

Table 6: Correlation of the normalized surface area vs. EF for the different Bio Inspired arrays at the different power source evaluated.

Category	Pattern	Surface Area(cm²)	NSA	532 nm	632 nm	785 nm
Asymmetric	Sunflower	3.54E-06	1.00	5.85E+05	7.20E+08	1.61E+08
	Romanesco	1.28E-05	3.62	5.95E+04	1.49E+07	1.64E+07
	Breadfruit	7.87E-06	2.22	6.99E+04	2.51E+07	5.98E+06
Radially Symmetric	Ovary	1.02E-05	2.88	5.87E+04	1.00E+07	7.56E+06
	Asian	1.05E-05	2.97	6.16E+05	1.21E+08	4.31E+06
	Orchid	4.46E-06	1.26	1.68E+06	1.79E+08	9.78E+07
Bilaterally Symmetric	Acacia	1.19E-05	3.36	1.89E+05	1.92E+08	3.47E+07
	Pinnate	8.46E-06	2.39	4.28E+05	4.33E+07	3.20E+07
	Honeycomb	1.40E-05	3.95	4.79E+02	5.80E+06	2.38E+07

* NSA = Normalized Surface

3.3.4. Pillar height Study

The influence of the nanocomposite structures height had been analyzed and studied since last decade due to their influence in the EF of the substrates.¹³¹ Latter research studies performed by Wen-Di et al¹³² on SiO₂ 3D cavity nano-antennas coated with gold, demonstrate the effect that pillar height has on the EF of the substrates showing that coupling the substrate backplane with the pillar result in an increase in SERS signal. This effect was determined to be dependent on both height and gap. Simulation studies showed that the LSPR can be further enhanced by systematically changing the height of the pillar nanostructure in relation that to those uniform substrates.¹³³ A recent study performed using silicon nanowires showed that such enhancement is limited up to the point of light trapping, where the signal quenching occurs.⁷⁵ Consequently a pillar height study was performed to assess its effect on the SERS performance of the bio-inspired substrates.

From the previous study, only the substrates with the highest EF and Raman intensities from their classes were selected to conduct peak height analyses. Based on the above findings the selected arrays were the sunflower, asian liliun, acacia leaf and the orchid (also used as pattern marker). Asian liliun was chosen because it has the fourth highest EF and considering the possible improvement in their analytical signal with the variation of the pillar height make this array an interesting alternative. SEM results for the corresponding patterns are summarized in Figure 18 and Table 6. According to this, changes on etching time resulted in pillars ranging from 53 nm to 596 nm. A SERS analysis of the six different pillars heights (Figure 19 A-D) demonstrate that the sunflower array exhibited the highest response for 5 of the 6 pillars heights. The EF value for the

pillars with the lowest height for this array showed an acceptable response but not at the same level as the results observed for the other heights for the sunflower. Orchid pillars also show good response intensity for pillars in the 120-275 nm range. Like the sunflower, lowest pillars did not show the same response. Quenching of the SERS signal could be caused by the result of a decreased morphology after the silver deposition. This could lead to a continuous surface in which the polarization of the substrate is not favored in the same ways as the pillar height increase. Asian liliium array did not show a remarkable improvement on the EF values with respect to the first study. Optimum pillar height for this array is close to the 195 nm. Acacia leaf substrate showed the best EF results for the lowest pillar height (≈ 56 nm) which is not expected based on the behavior of the other three nanostructures. The aligned orientation of the ellipses in this type of substrate may induce the formation of several hot spots and its effect is enhanced by the surface of the Si-Ag wafer.

All the EF reported were the average for almost 422 scans acquired over each 40×40 (μm^2) array. Evaluation of the points in which each substrate presents the highest response signal at the 1560

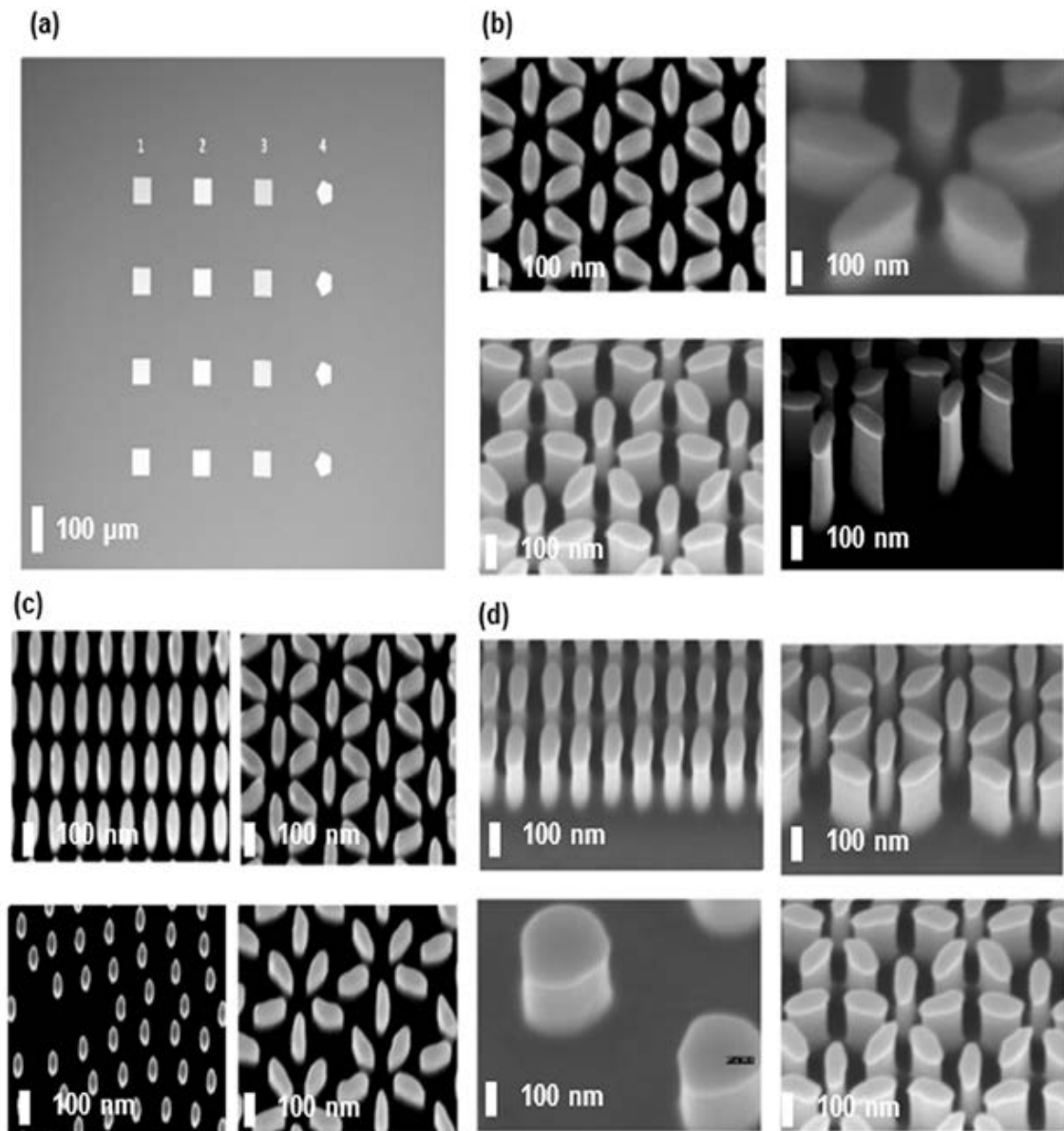


Figure 18: Long range view SEM micrograph using a Ziess Scanning electron microscope (SEM); Power = 3.0 kV; Magnification = 19 X Tilted at 30 degrees; Detector Mode = InLens, of the Acacia(1),Asian Lilium(2) Sunflower (3) and Orchid (4) arrays for one of the Bio-inspired chips etched at 45 seconds. (B) Micrographs were acquire with a magnification of 315Kx, Orchid arrays (clockwise direction) images after 30, 60, 120 and 150 seconds of etching. Pillar heights differences are clearly observed. Images for the four arrays selected using a 30 seconds (C) and 120 seconds (D) etching time. (E) Pillar Heights measurements results for the 4 selected Bio-Inspired arrays.

Table 7: Experimental Heights for the Pillar Height study of Bio Inspired arrays

Pillar Height in nm for n=3 measurements				
Etching time (sec)	Sunflower	Orchid	Acacia leaf	Asian liliium
30	72(±7)	53(±3)	56(±6)	79(±6)
45	159(±6)	121(±16)	136(±9)	105(±8)
60	181(±6)	189(±3)	171(±8)	195(±17)
75	249(±29)	223(±16)	226(±6)	240(±3)
90	274(±6)	251(±11)	268(±12)	264(±14)
120	285(±15)	275(±4)	293(±14)	275(±12)
150	442(±12)	422(±15)	596(±17)	539(±5)

cm⁻¹ region was considered. The average band area for this signal (n = 3) was reported and the corresponding EF calculated and compared with the average EF calculated at each height (figure 19). EF values at highest intensity points are in the order of 10⁹ for the sunflower and the orchid patterns. Meanwhile, the Asian and the acacias patterns showed EF's one order of magnitude lower than the former two arrays. Reproducibility of the measured highest intensity spots were measured for all the arrays at this point. Percent RSD values (%RSD) demonstrate acceptable results with values that range between the 8 – 10% for the sunflower, orchid and acacia arrays. Asian Liliium variability is close to the 24% at the optimum height (195 nm) and by 7% at heights close to 275 nm. It is important to clarify that small variation on substrates morphology gaps and height could lead to dramatic changes on analytical signal. The four bio-inspired patterns seem a promising alternative for Raman applications for pharmaceutical and environmental applications.

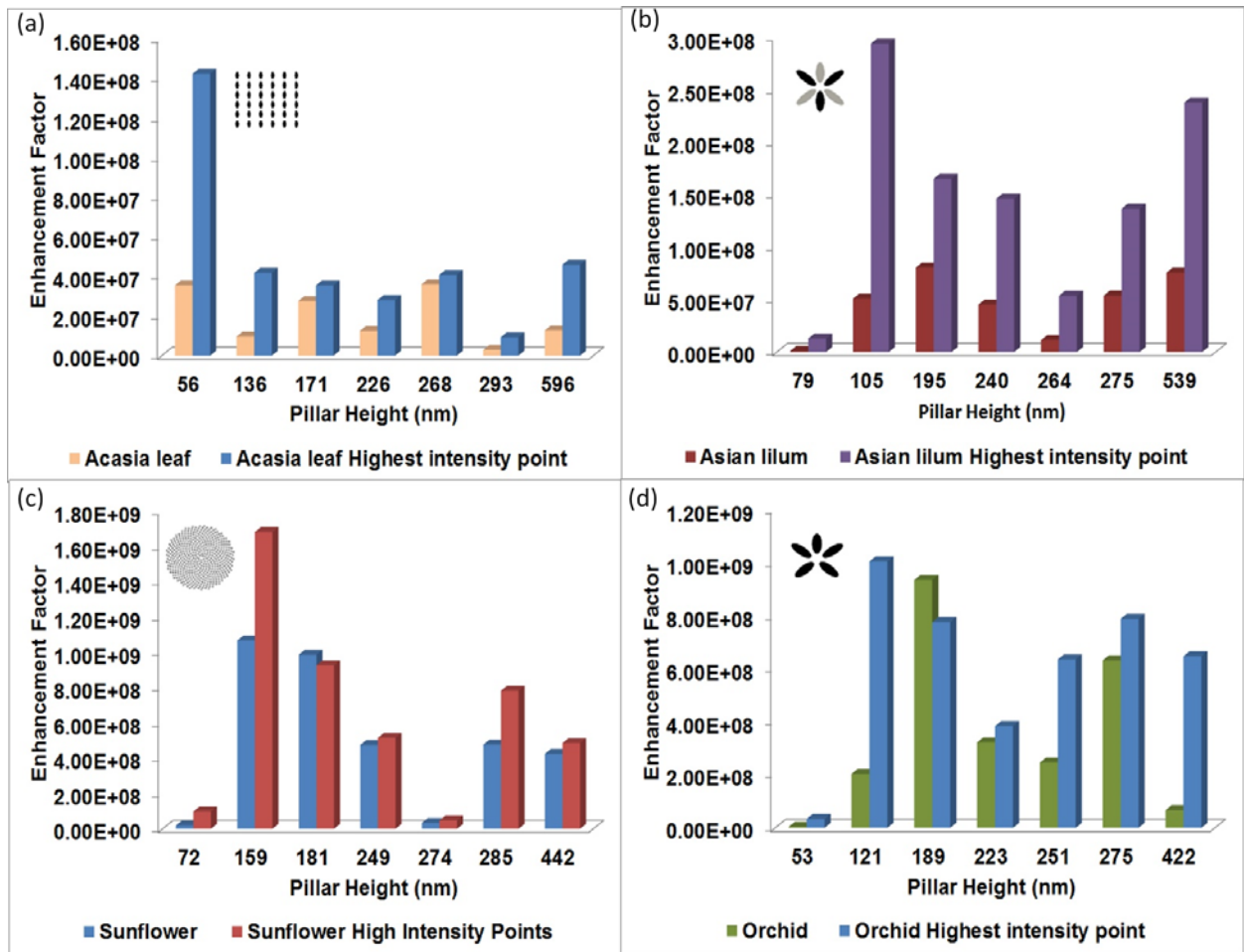


Figure 19: Benzenethiol EF plots of the average and the high intensity point for the (a) Acacia leaf, (b) Asian lily, (c) Sunflower and (d) Orchid Bio Inspired arrays. Optimum pillar heights are between 105-189 nm for all of the patterns except the Acacia.

3.3.5. Detection of Fluoroquinolones and Sulfonamide:

The arrays selected by availability at the time of the experiment were the ones which etching time of 75 s. The evaluation of the four more prominent substrates determined before, with a fluoroquinolone (Levo) and the sulfonamide (4-carboxy) samples demonstrate that acacia and the orchid arrays offers the highest signal intensity followed by the asian lilum and finally the sunflower (figure 20 and 21). The SERS spectra corresponding to Levo showed an increase in all the bands presents on in the range between 1340 and 1625 cm^{-1} . This indicates that the bonding between the molecules and the nano structure composite occurs by the piperaziyl and the aromatic group of the compound (please refer to chapter #4, table 8 for a detail band identification). This behavior is expected based because the size and complex structure of the molecule does not offer so many alternatives to the adsorption on the surface of the nanoparticles.

The 4-carboxy bands SERS spectra showed the increase in the intensity of some of the bands but varies depending on the substrate morphology. The bands corresponding to the 1621 and 1401 cm^{-1} frequencies on the orchid arrays presents a more dramatic increase. This caused by the adsorption on the surface threw the aromatic ring and the sulfoxide group (1401 cm^{-1}). This situation changes on the acacia array in which are the band around 1080 of the carbonyl group which present the highest increment in intensity. The band of the sulfoxide group meanwhile is not enhanced in the same way.

The sunflower which was the array with the highest EF does not produce and enhancement similar to the acacia or the orchid. This array has the less amount of particles under the laser spot compared with the other arrays. Under this circumstances the surface area available is less, also

the system under study is a dynamic one in which the analytes are continuously been adsorbed and desorbed otherwise than the benzenethiol and 4-ABT. This molecules are fixed to the nanoparticles by the time they for the SAM. The apparent increase in signal expected by the EF is because this parameter is higher on a substrate that has the less surface area and has the less amount of molecules adsorbed.

3.3.6. Substrate working life and cleaning procedure.

In routine analyses, it has been observed that the substrate retain its SERS activity for as long as 10 consecutive uses as long as adequate cleaning procedure is used. Extremely care should be taken to avoid the destruction of the characteristic elements of each substrate. Cleaning procedure must be done using Aqua Regia (1 part concentrated Hydrochloric Acid and 3 parts of concentrated Nitric Acid). The chip is immersed in a define volume of the Aqua Regia for 10-15 minutes. Then rinsed with DW and dried using Nitrogen. An alternate method employs a plasma microwave system. This instrument provide several stripping methods in order to clean silicon wafers preserving the original arrays in a 7-10 minutes period. Prior to use this method is necessary to remove the metal coating using Aqua Regia.

3.3.7. Hyphenated Bio Inspired arrays with a sample translational device

The concept of lithographically constructed substrates with a sample rotational device had been reported with success.⁷⁰ The main requirement to this is that the substrate has an extended area of clone units in order that when the substrate is been rotated the individual elements shows a similar orientation and distribution in order to get reproducible responses. The array that has this

intrinsic characteristic of the four most prominent substrates is the sunflower. The infinite orientation symmetry of this array make it a viable prospect for translation since it allows its use without altering the effective orientation of the substrate with respect to its polarization vector. This substrate represent an opportunity to merge nanofabricated patterns to our new sample translational device for SERS analysis. The development, fabrication, validation of the new translation device as a complementary tool for SERS will be discussed on the following chapter.

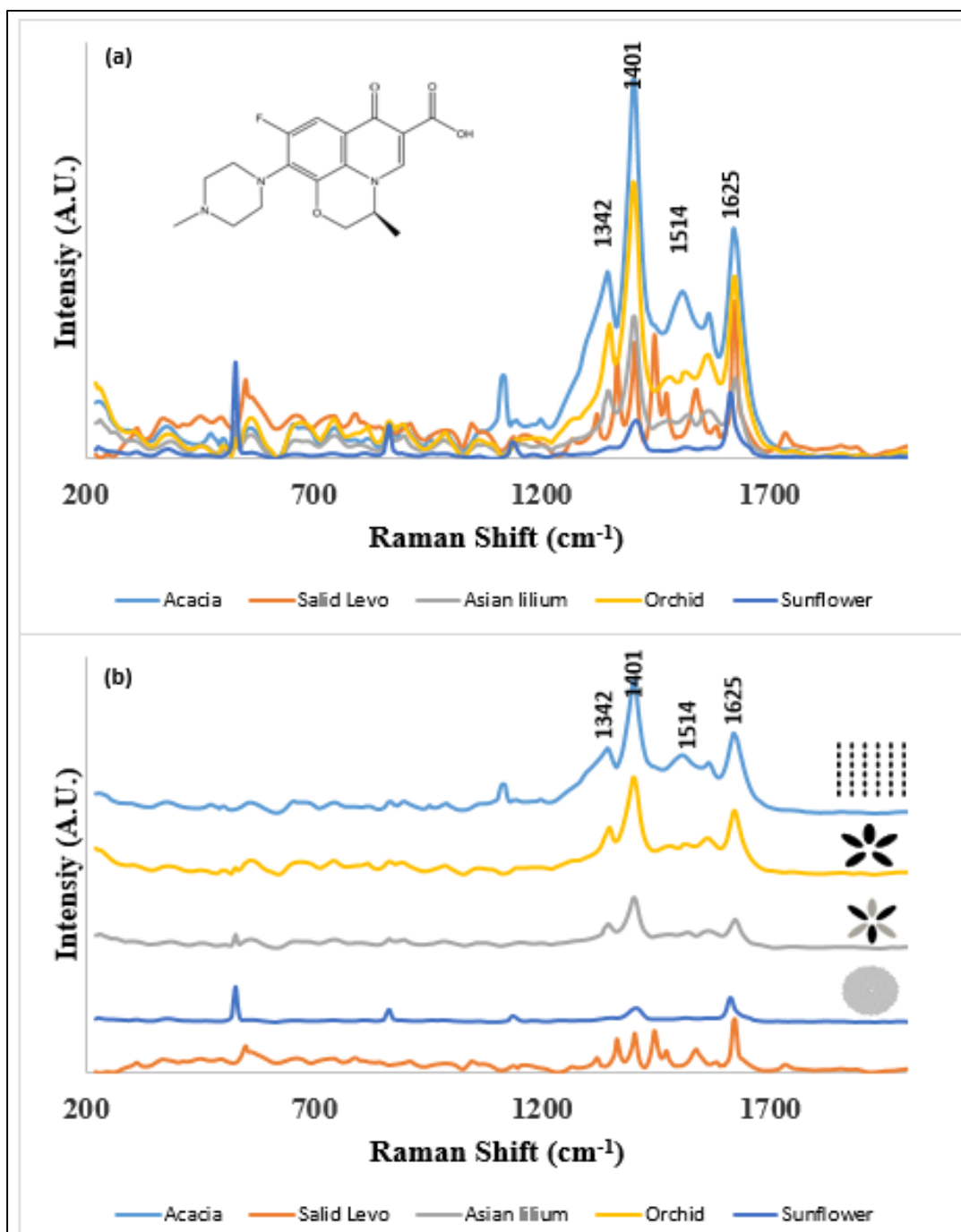


Figure 20: Levofloxacin analysis with the Bio-inspired arrays. (a.) overlay (b) stacked

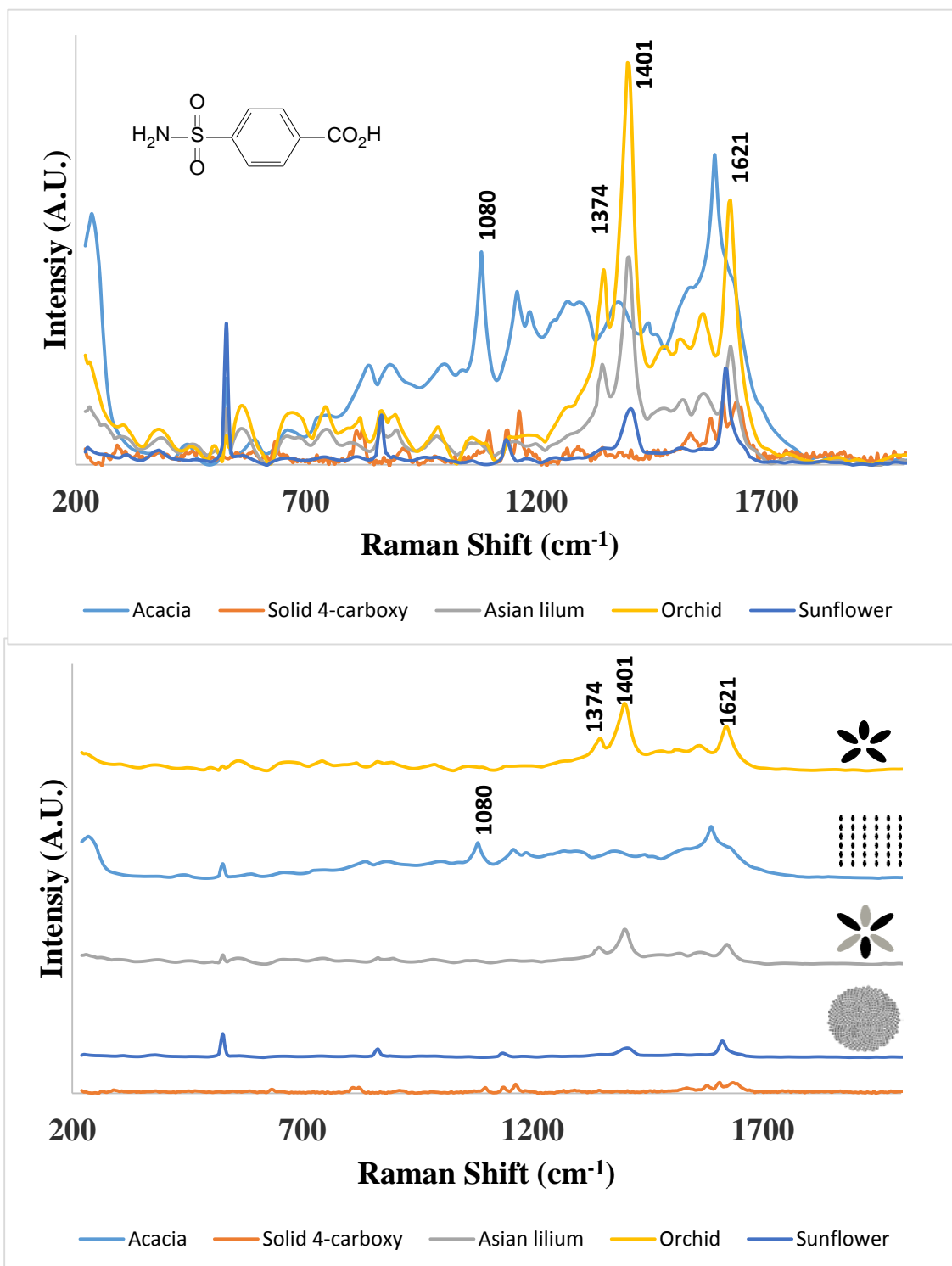


Figure 21: 4-Carboxybenzene sulfonamide analysis with the Bio-inspired arrays. (a.) overlay (b) stacked

Chapter #4: USB sample translation probe to enable the reproducible detection of photo-labile drugs by Surface Enhanced Raman Scattering (SERS)

4.1. Introduction

The presence of pharmaceutical products in aquatic environment was first discovered during the mid-80's by Aherne, English, & Marks.¹³⁴ The discovery received little attention until Thomas Ternes, discovered several human pharmaceutical products, present in sewage treatment works (STWs) effluents.¹³⁵ A study by Joblin et al. (1998), later found out that one particular pharmaceutical product ethinyl estradiol (EE2), was responsible for feminization of male fish in rivers, where the effluent from STWs were dominant.¹³⁶ So far, approximately 100 different pharmaceutical products have been found in STWs effluents and aquatic systems.¹³⁷ The pharmaceutical products range from selective serotonin reuptake inhibitors (SSRIs), steroids, beta-blockers, anti-epileptics, analgesics, and fibrates.¹³⁸ These findings suggest that these products are not removed by the waste water treatment plants. Studies have shown that the pharmaceutical products, have a significant impact on the ecological environments, as well as aquatic systems.¹³⁹

A study by Oaks et al (2004), demonstrated that presence of diclofenac in South east Asia waters, caused dramatic decrease in population of old world vultures of the genus *Gyps*. The wild species were found to have been accidentally poisoned by diclofenac present in water, as the vultures are very sensitive to diclofenac. There is therefore need to promote the development of some detection and quantitation techniques, which would help in the identification of such pollutants.¹⁴⁰

One of the pharmaceutical products pollutants that is of great concern is the fluoroquinolones. This is because the products are toxic to pregnant women and their presence in drinking water

poses great risk to the pregnant women.¹⁴¹ Fluoroquinolones are broad spectrum antibiotics, which possess *in-vitro* activity against both gram negative and grand positive bacteria. The fluorine atom is usually located at the sixth atom and it enhances potency against organisms.¹⁴² The general structure of fluoroquinolones consists of '1-substituted-1, 4-dihydro-4-oxopyridine-3-carboxylic moiety' that is attached to an aromatic ring.¹⁴¹ This study will focus on the analysis of two fluoroquinolones namely: Ciprofloxacin and Levofloxacin. The study will also explore sulfonamides, specifically 4-carboxybenzene sulfonamide. As mentioned on chapter #2, Ciprofloxacin and levofloxacin are commonly used in treatment of ailments such as typhoid, upper and lower respiratory tract infections, among others. Sulfonamides on the other hand, are derived from sulfonamide and it prevents the growth of bacteria. They usually contain a 4-aminobenzene ring and act by stopping the growth of bacteria.¹⁴¹

One of the techniques that is currently in use, as a quantification technique of the pharmaceutical agents present, is the SERS. The SERS technique, can only be used to analyze a small number of the significant organic chemicals. The technique has also not been widely used, for traditional trace analysis because it lacks analytical figures of merit.⁸⁷ De Jesus et al. (2004), proposed the use of silver-polydimethylsiloxane nanocomposites (Ag-PDMS) for quantitative and qualitative analysis. The study involved model environmental pollutants, which were analysed using sample translation technique (STT). The study examined the response characteristics of 4-hydroxybenzoic acid (*p*-OHBA), 4-chlorobenzoic acid (*p*-CIBA), 4-aminothiophenol (*p*-ATP), PABA and phenolphthalein. The effects of laser irradiation time, translation rate and laser power on the SERS signals of the compounds above was also studied. The new approach was found to improve the reproducibility and sensitivity of SERS and also minimises the photolytic and thermal

effects of SERS.⁸⁷ The SERS technique has also been found to have problems of gross decomposition of sample analyte, as a result of continuous irradiation of laser beam. This greatly decreases the intensity of the observed spectral bands and can also cause photolytic or thermal fragmentation of analytes. This results in alteration of observable bands that can cause inaccurate conclusions. The technique can be enhanced through sample translation technique (STT). This is done by rapidly spinning the sample, which dramatically decreases the analytes residence time and substrates present in the irradiated zone. This reduction does not affect the analyte density in the zone or spectral acquisition time. The method was used to study riboflavin, Naproxen USP, 4-aminothiophenol, Rhodamine 6G and folic acid. The study used Ag-PDMS) composite substrates and silver islands on glass in varied spinning and stationary conditions.¹¹⁹ Recently, had been demonstrated the used Raman spectroscopy to analyse drugs surface-enhanced Raman spectroscopy (SERS), together with a fabricated optical fiber nano-probe coated with gold nanoparticles, to determine the levels of levofloxacin lactate in mouse blood. The optical fiber nano-probe revealed the characteristic band frequency of the drug. The study demonstrated that Raman spectral techniques, can be used with optical fiber nano-probes to analyse drugs.¹⁴³ A variety of quinolones like Ciprofloxacin, Norfloxacin, Ofloxacin, Nalidixic acid, Enoxacin, Oxolinic acid, Lomefloxacin, Cinoxacin, Sarafloxacin, Moxifloxacin and Flumequine were analysed by Raman. The investigation was done using micro-Raman spectroscopy at 275, 257 and 244nm and DFT calculations were done to assign vibrational mode and identify the hydrogen bonding motif. The Raman spectroscopy was found to be effective in determining low concentrations of fluoroquinolones.¹⁴⁴ A study by Sahoo et al. (2011), analysed three pure fluoroquinolones namely: Ofloxacin, Norfloxacin and Ciprofloxacin using Raman Spectroscopy.

The study was carried out using a portable Raman Spectrometer of low resolution, having fibre optic sampling probe and using a 785 nm solid state diode laser. The Raman spectral analysis showed that fluoroquinolones had prominent characteristic peaks for piperazinyl ring and fluorine substituent, carboxylic acid and pyridine. The results also showed characteristic peaks at 797.5 cm, 771.47 and 872.7 for Ofloxacin, Ciprofloxacin and Norfloxacin respectively. The spectral patterns of the drugs were also assigned to vibrational normal mode of C-F bond containing molecule, which were fully symmetrical. In addition, the analysis was done using a portable device to rotate the sample in order to improve the SERS reproducibility of the analytical measurements. The study demonstrates that Raman spectroscopy is a promising method for fluoroquinolones identification.¹⁴⁵

The SERS technique characterizes the spectrum of a particular molecule, using vibrational spectroscopy. The Raman spectrum, is used to directly identify the biological agents or molecules present.¹⁴⁶ The technique has however been found to have poor signal reproducibility and is not appropriate for low level detections. This is because the polymer was found to interfere with the detection of low level signals of analytes.¹⁴⁶ The SERS technique can therefore be enhanced using the practical array method. This can be done through the fabrication of higher enhancement, uniform and bigger SERS substrates. The fabrication of a microwell-arrayed SERS chip, on a microscope slide with standard glass (2.54 cm×7.62cm). This technique was used to produce SERS-active surface and a well –array patterning mold that has addition of liquid PDMS. The curing is done at low temperatures by heating, which provides a cost effective and time efficient use of SERS substrates for many individual sample analysis. The avian influenza was analyzed

using this technique. The spectra of patterned substrates showed high reproducibility and less variation compared to the non-patterned ones.¹⁴⁶

4.2. Initial Studies and Justification

This research initially was focused on the fabrication of new bimetallic substrates that could be used as analytical tool for the detection of PPCPs. The new design was focused on combining layers of different metals that exhibits the capacity of produce strong LSP's. In this case the combination of metal selected was Silver and Copper. In order to determine the efficiency of the new substrates they were compared with the Ag-PDMS substrates. The experimental set up is described on Figure 22. The thickness of copper layer on top of the substrates were increased from zero to four nm.

The substrates were tested using a 1.00×10^{-4} M solution of PABA, with a 532 nm excitation line for 10 s and a 2.00 mW laser intensity. The results of this experiment are presented in Figure 23. The results show an inverse relationship between the intensity of the Raman signal of PABA and the thickness of the copper layer. By using just four nm copper the PABA bands disappears completely. This behavior is due to the possible oxidation of copper on the substrate surface in a way that inhibits the generation of the LSP.

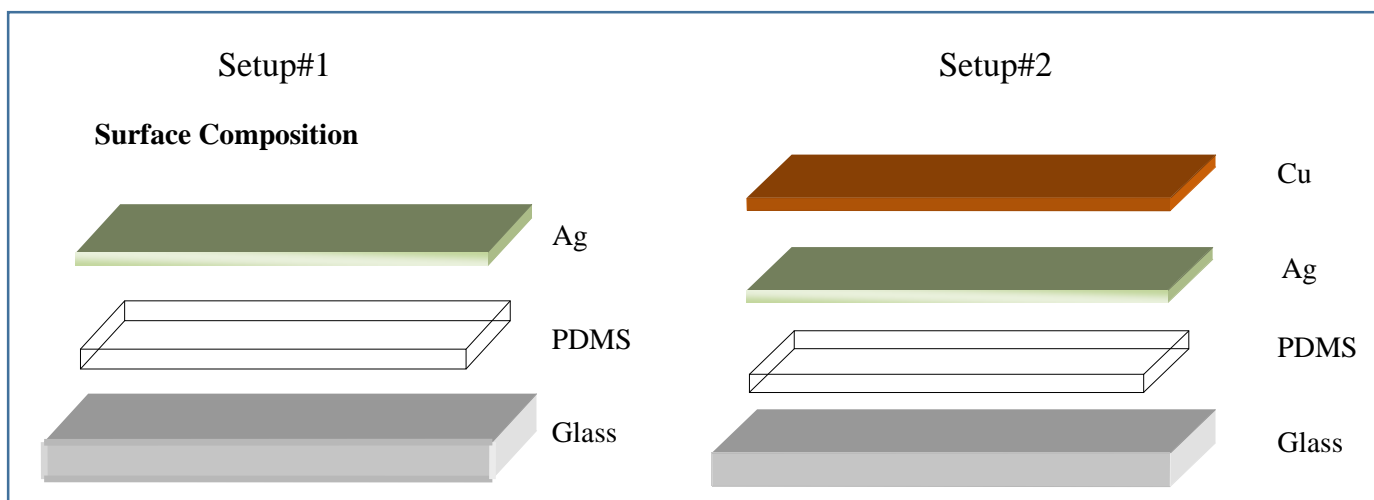


Figure 22: Setup designs for the evaluation of bimetallic substrates.

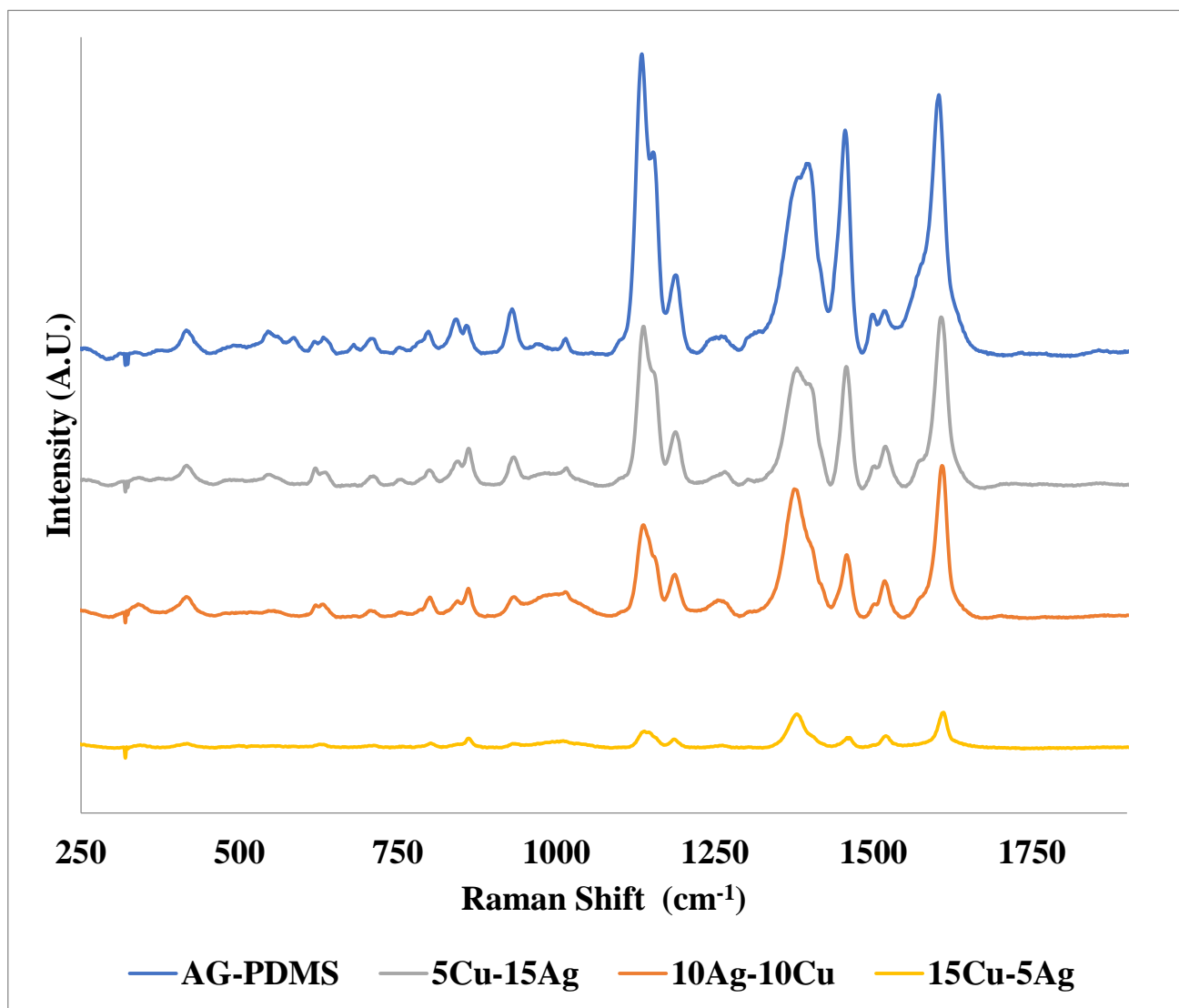


Figure 23: PABA SERS spectra for the bimetallic substrates evaluation

The results of this testing lead to the conclusion that a bi metallic substrate does not offer the results to support a further development of this substrates as an alternative. Several options were tried in which the copper was deposited first follow by the silver layer in order to have 20 nm of metallic substrate, but the results do not encourage that you continue to use copper with silver as an alternative for the preparation of a bi metallic substrate.

Another factor that is important when an analyst is performing SERS experiments with an immobilized substrate like Ag-PDMS is the fact that the surface morphology still have some variation (as explained on chapter #1). This source of variation lead to irreproducible measurements that decrease the potential of SERS as an analytical tool for different uses besides the qualitative analysis. Example of this is presented on two measurements of PABA on Ag-PDMS using the same experimental conditions taken with just 50 μm of separation (Figure 24). The two measurements differ in intensity by more than 10,000 counts. This situation can explain the non-linear behavior (figure 25) observed in a simple experiment in which a series of standard solutions of Cipro analyzed to study the possible quantification of this compound using Ag-PDMS as substrates over a range from 0.00 to 6.25×10^{-4} M standard solutions.

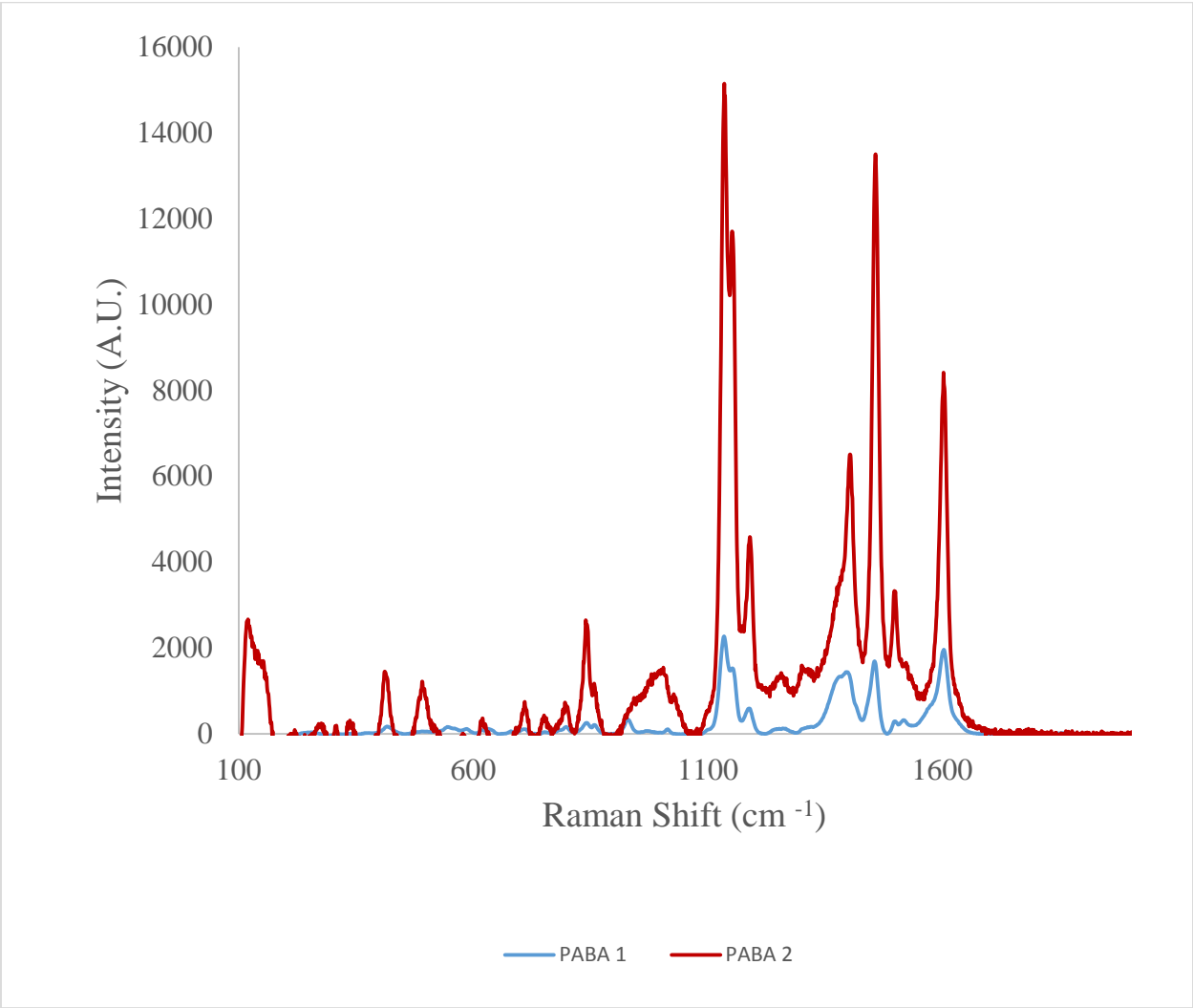


Figure 24: PABA SERS spectra showing the reproducibility issues with the use of an immobilized substrate

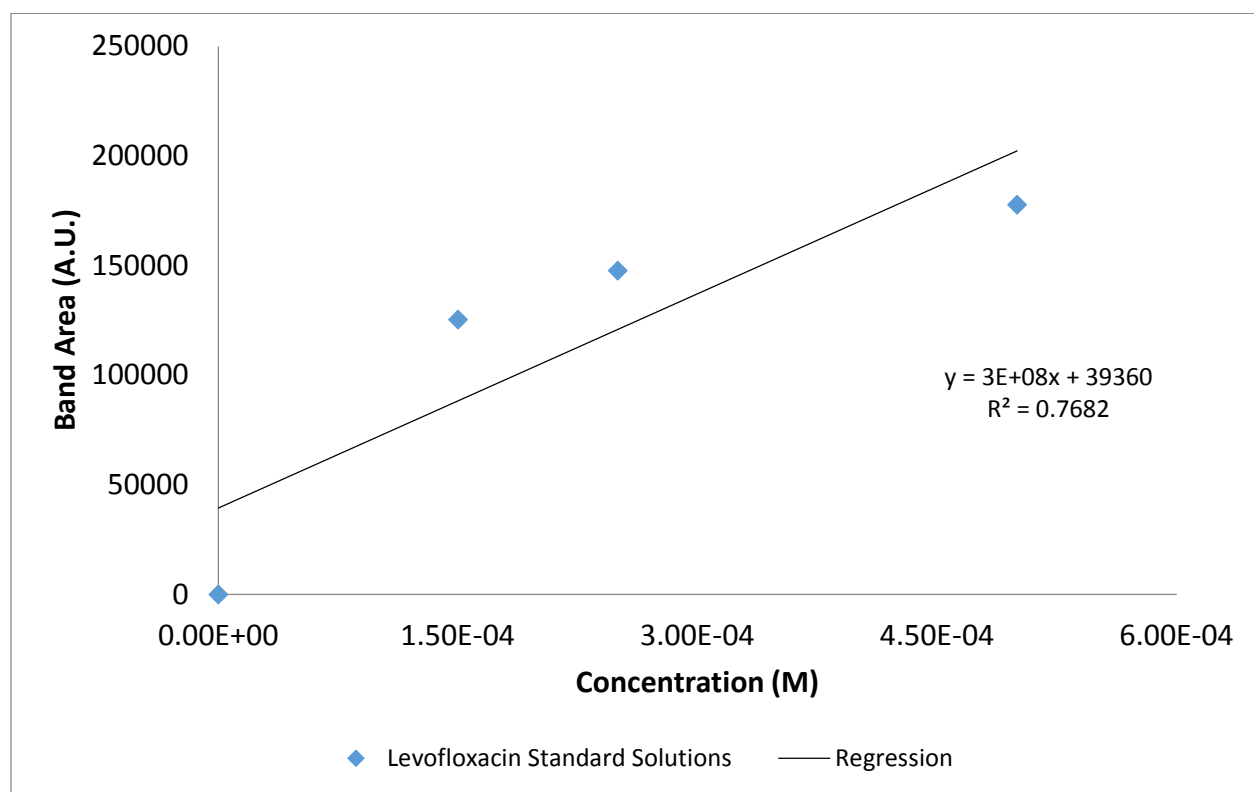


Figure 25: Calibration Curve for the analysis of levo using a PDMS slide.

This situation and the results in several preliminary studies in which the inconsistency of the measurements is the basis for the fabrication of a new translation sample system like the one previously designed.¹¹⁹ This system, has the disadvantage of the high cost of manufacture and it is fixed to the Raman Spectrophotometer. Our research laboratory has developed a prototype system of rotation that offers the advantages of being more economical than its predecessor as well as one laptop that can be used for analysis in the field (environmental area) and could be adapted to phases of manufacturing processes for analysis (process analytical technology) for generating data on manufacturing lines. The fabrication, evaluation of this device and their use as tool for the analysis of a group of fluoroquinolones and a sulfonamide drug will be presented on the following sections.

4.3.Experimental

4.3.1.Portable Sample Translational Technique Device

The PSTTD was made using a 3 volt DC motor from a portable cd player. Electrical power was provided in a direct current mode using four 1.5 V AAA batteries or by a USB power cord to regulate spin rates in a 700 – 2500 rpm range (Figure 26). The rotation disk was coated with a thin layer of PDMS elastomer and curing agent in a 10:1 proportion to ensure an adhesive surface for the substrates. Computerized control was performed using a motor bee® control board acquired from PC-Control Ltd at https://www.pc-control.co.uk/motorbee_info.htm. Operational Conditions were done using the Motor Way® version 2.5 software also from PC-Control Ltd.

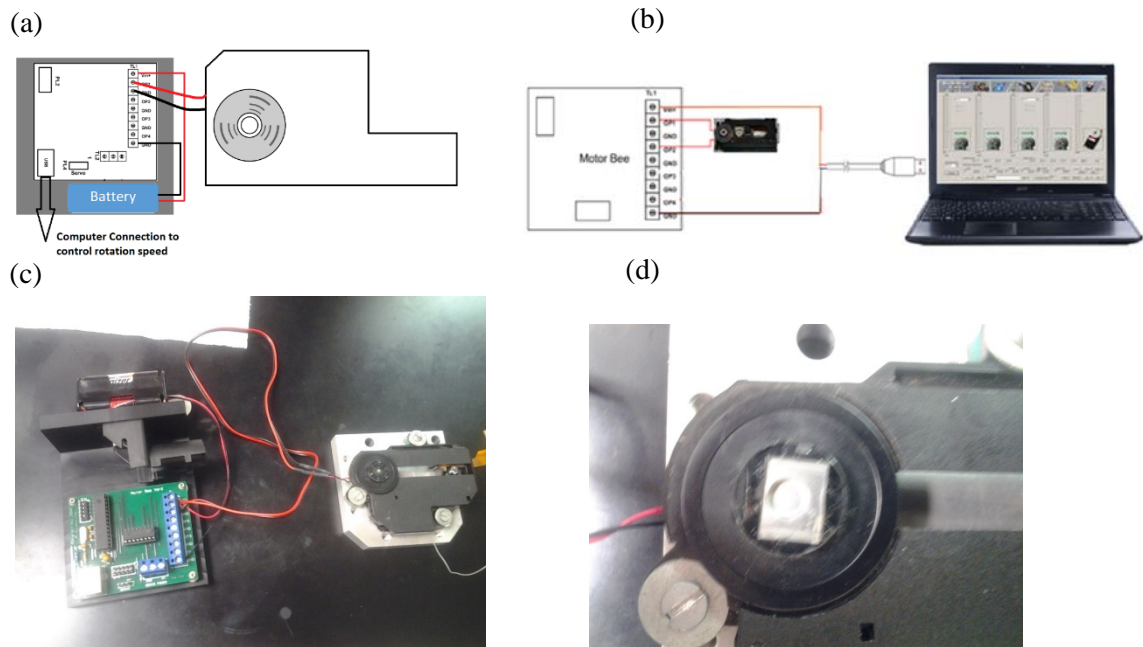


Figure 26: (A, B) Schematic of the PSSTD using both power options. (C) Photo of the designed device (D) Image of the Ag-PDMS substrate to be analyzed

4.3.2. Instrumentation:

All SERS spectra were acquired using a Horiba® Xplora Raman Spectrometer using a 638 nm excitation wavelength. In general the instrument used an Olympus 10X objective with a numerical aperture NA = 0.25. A computer controlled X-Y-Z stage was used to perform the raster and radial analysis of the substrates. The working spectral window was set from 200 cm⁻¹ – 3000 cm⁻¹ with acquisition times varies from 1s to 5 for the Rhodamine 6G, 1- 10s for 4-carboxybenzenesulfonamide analysis and 10 to 20s for the different Fluoroquinolones. Laser power was adjusted to 3.00 mW using an optical density filter.

The Ag-PDMS, SERS multi-wells active substrates preparation were prepared using a clean Lego® plate which had been polish to remove the logo. The PDMS polymer was prepared in a 10:1 elastomer: curing agent ratio. The mixture was deposited over the plate and heated at 75°C in an oven until solid surface was observed. Depending on the amount of polymer used, the number of wells produced with this procedure are close to 45. The polymer is cut in individual wells and coated with silver as presented on Figure 26 d.

The deposition process uses silver 99.9999%, with an Edwards® physical vapor deposition instrument at 0.5Å/s rate and pressure of 3x10⁻⁶ torr until a 20 nm layer is produced. Mean thickness is measure with a quartz crystal microbalance sensor included on the instrument. The resulting substrates were stored under vacuum conditions until the moment of the analysis.

4.3.3. Sample Preparation : pH Study and Adsorption Time study

A series of 1.00×10^{-4} M solutions of each fluoroquinolones, Levo, (Fluka HPLC grade 99% +), Cipro (Fluka 98% +), sulfonamide (Sigma Aldrich 99%+) and 1.00×10^{-5} M of R6G (Sigma Aldrich 99.9%) were prepared to evaluate the characterization, adsorption time and the spinning rate experiments. The sample volume used for all the measurements were 25 μ L and all samples were covered with a cover slip to avoid sample lost during each experiment.

4.3.3.1. pH effect study:

Evaluation of the acidity and alkalinity effect were performed using this solutions under static conditions. Samples aliquots were adjusted to the desire pH using 0.01M Nitric Acid or Sodium Hydroxide to cover a 3 -8 range. The SERS experiment were conducted using the conditions described on section 4.3.2. Each solution was analyzed in triplicate and the acquisition time was 10 seconds with one acquisition for each of the drugs. The R6G was analyzed with an acquisition time of 5 seconds with one acquisition as well. The most intense signal of each compound at each pH were plotted for comparison purposes.

4.3.3.2. Revolutions Study:

This study was carried out analyzing a solution of each drug and R6G in triplicate under different rotatory conditions. The range of revolutions used were between 0 and 1595 RPM. The acquisition time were 10 seconds for each drug and 2 seconds for R6G.

4.3.3.3. Adsorption Study:

The Adsorption time study was performed under static and the spinning conditions. The revolutions determined on the previous section were used as the rotation speed for this experiment.

4.3.4. Precision Study:

A 1.00×10^{-5} M standard solution of R6G solution was used for the precision analysis. This study evaluates the precision of the PSTTD on repeatability, reproducibility over a complete well and Intermedia Precision over three different wells. The number of measurements are listed as follows:

Repeatability:

To evaluate the repeatability of the experimental data a series 5 measurements over the same spot were analyzed with 5 seconds irradiation time and 1 acquisition using a 638 nm excitation line.

Well Precision (reproducibility)

One PDMS well were prepared using the deposition conditions and experimental conditions were described before on section 4.3.4. Linear Raster over a distance from -600 – 600 μm with a 50 μm using the same conditions of the repeatability study.

Intra well precision (intermedia precision):

Three PDMS wells were prepared using the deposition conditions and experimental conditions were described before on section 3.6.4. The wells were analyzed using a

raster technique from -600 – 600 μm with a 50 μm using the same conditions of the repeatability study.

4.3.5. Linearity study:

A series of standard solutions covering a range from 1.00×10^{-3} M to 2.5×10^{-4} M for Levo, (representing one of the fluoroquinolones), 4-carboxy and R6G standard solutions covered a range within 1.00×10^{-6} M - 1.00×10^{-5} M were prepared using DW (18 M Ω pure). Each solution was analyzed in triplicate. Data analysis was performed using PLS toolbox®

4.4. Results:

4.4.1. Evaluation of the spinning Limits of the PSTTD

Determination of the real spinning capabilities of the hyphenated DC motor under the two possible power sources was done using a digital tachometer. The averaged (N= 4) experimental revolutions against the software scale to determine the real spinning speeds. Figure 27 presents the revolutions per minute (rpm) correlation chart that demonstrate that independently the power source a linear relation is observed. The lowest spinning rate that can be achieved was 840 rpm. Below this level the cd player motor does not response independently the power source used. Higher resolutions values were obtained for the DC power source (1000 - 2700 rpm) than the USB power (800 -2150 rpm). This behavior was expected because the combined amount of energy provided by the four AAA batteries is slightly higher (6V) than the voltage output of the USB cable (5V).

Deviations between the experimental measurements for each level are minimum for each power source. Relative Standard deviation (%RSD) for the USB connection showed a 3.5% as the maximum deviation for the slowest spinning rate, which are acceptable. DC power variation are smaller with a 0.5%. Both power alternatives demonstrate the real capability of the PSTTD to employ different sources which could be useful for a direct field analysis and monitoring.

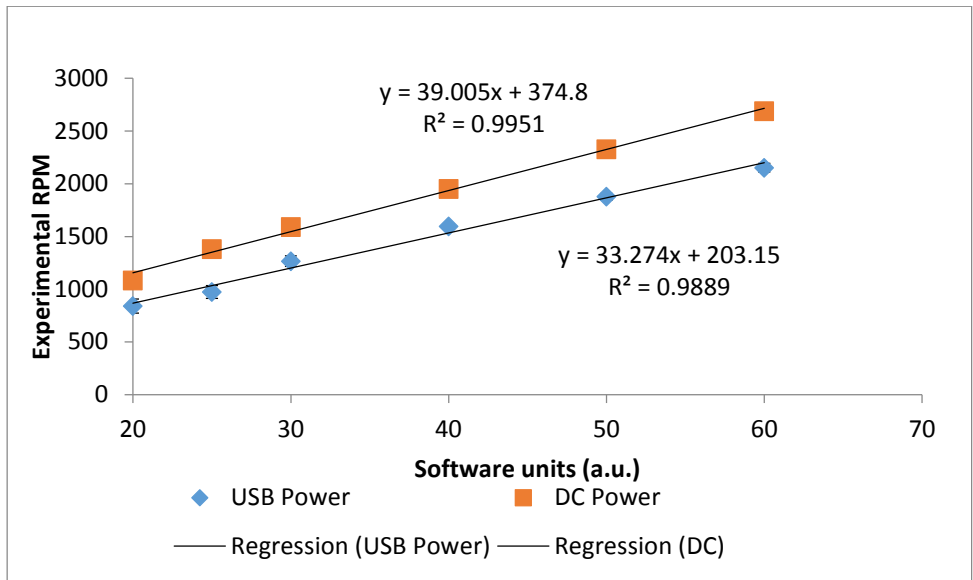


Figure 27: Revolutions per minute correlation chart revolutions per minute correlation chart for the evaluation of the PSTTD using a DC and USB power

4.4.2. Fluoroquinolones and Sulfonamides SERS characterization

Figures 28-30 presents the SERS spectra for the 4-carboxy, Levo and Cipro respectively. Each compound presents a group of well define signals on the 1250 -2000 cm^{-1} range. Characteristic bands for each compound are detailed presented on Table 8. 4-carboxybenzene sulfonamide presents a group of well define bands. The most prominent is the 1600 cm^{-1} which is the result of the double bonds C=C of the aromatic ring. The sulfonamide group, C-SO₂N, shows two characteristic bands at 1386 cm^{-1} and 1108 cm^{-1} corresponding to the asymmetric and symmetric vibrations respectively. A small shoulder around the 1064 cm^{-1} is related with a weak carbonyl vibration. Finally, a moderate intensity band around the 840 cm^{-1} is related with the out of plane vibrations associated with the C-H group in a 1,4-disubstituted aromatic ring.

The analysis of fluoroquinolones by SERS is rarely reported on literature.¹⁴⁷ In addition, there is no reference associated with the characterization using PDMS as substrate. The identification of the most important Raman signals can be done using the conventional Raman analysis reported on the literature.

Both fluoroquinolones, shows prominent signals around the 1600 cm^{-1} associated with a mixed vibration of the C=C of the aromatic rings¹⁴⁷, and the COO⁻ group. The most intense band near the 1380 cm^{-1} is associated with the stretching of the carboxyl group. At 1352 cm^{-1} Cipro presents a shoulder related with a mixed vibration of the piperaziyl group. This signal appears in a well-defined shape close to the 1136 cm^{-1} on Levo. Between the first two bands a group of medium intensity signals are presented. Cipro present a 1477 cm^{-1} band attributed to the O-C-O vibration. Meanwhile, Levo has a the doublet peak around 1516 and 1562 cm^{-1} is assigned to the

Piperaziyl and to the Quinolone group respectively which is in agreement to the findings on the literature. Cipro only shows a weak peak close to the 1570 cm^{-1} . Finally Cipro present a peak around 750 which had been associated with the bending deformation of the CH_2 groups. Although the similar structures of Ciprofloxacin and Levofloxacin, identification of each one is possible based on specific characteristics bands.

Structures presented on Figures 7, 8 and 10 denoted the acidic character of the three compounds. Based on this fact and the evidence which relates the aromatic character of several compounds with their attraction to metallic surfaces; a pH study to evaluate the spectroscopic behavior of the compounds was done.

Table 8: SERS characterization of pharmaceutical drugs under Static and rotational mode

4-carboxybenzene sulfonamide Raman bands assignments			
Stationary	Rotational	Literature	Assignment
1600	1611	1610-1550	Aromatic Stretching C-C + COOH band
1386	1390	1387	CH bending + C-C bending; SO ₂ asymmetric
1189		1170-1145	SO ₂ symmetric stretch
1112	1111	1200-1140	S=O sulfonamide band
1069	1068	1073	C-O stretching
849	847	880-780	p-disubsti aromatic
Ciprofloxacin Raman bands assignments			
Stationary	Rotational	Literature	Assignment
1623	1620	1628	C=C aromatic ring; C=N; COO ⁻
1564	1567	1554	Quinolone ring
1484	1483	1481	O-C-O symmetric
1389	1381	1386	O-C-O asymmetric
1334	1359	1354	Mixed vibration pyrazine ring
753	747	720-800	C-F
Levofloxacin Raman bands assignments			
Stationary	Rotational	Literature	Assignment
1623	1626	1621	stretch C=C ; stretch C=N
1561	1561	1547	V C=C of the Quinolone ring
1515	1512	1530-1490	RNH ₂ R ⁺ piperaziyl group
1466		1447	O-C-O symmetric
1398	1398	1401	OH (bent)
1331	1343	1322	Mixed vibration pyrazine ring

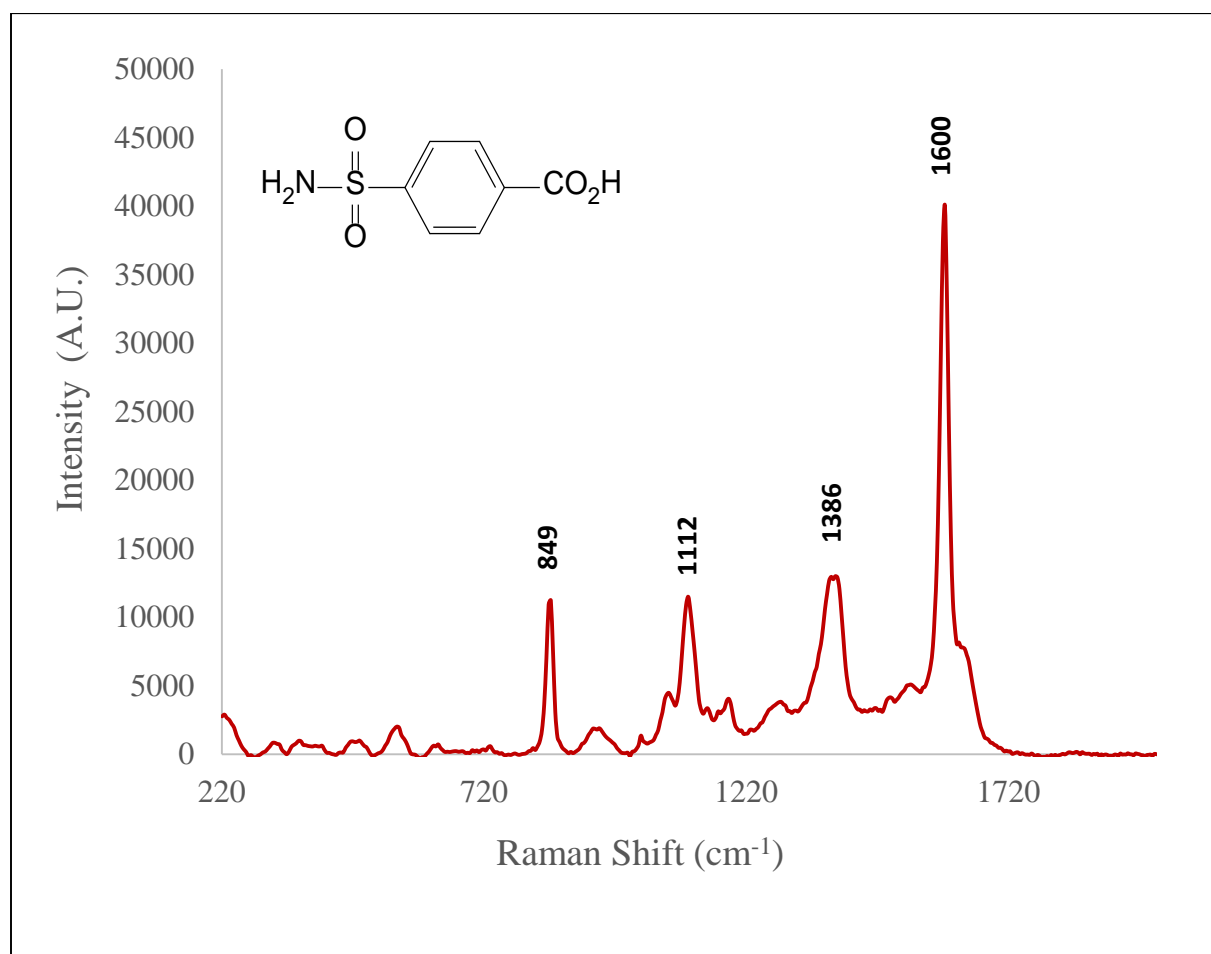


Figure 28: SERS spectra for 4-carboxy. Acquisitions was made using a 638 nm emission line for 10s acquisition using 3.00 mW laser power.

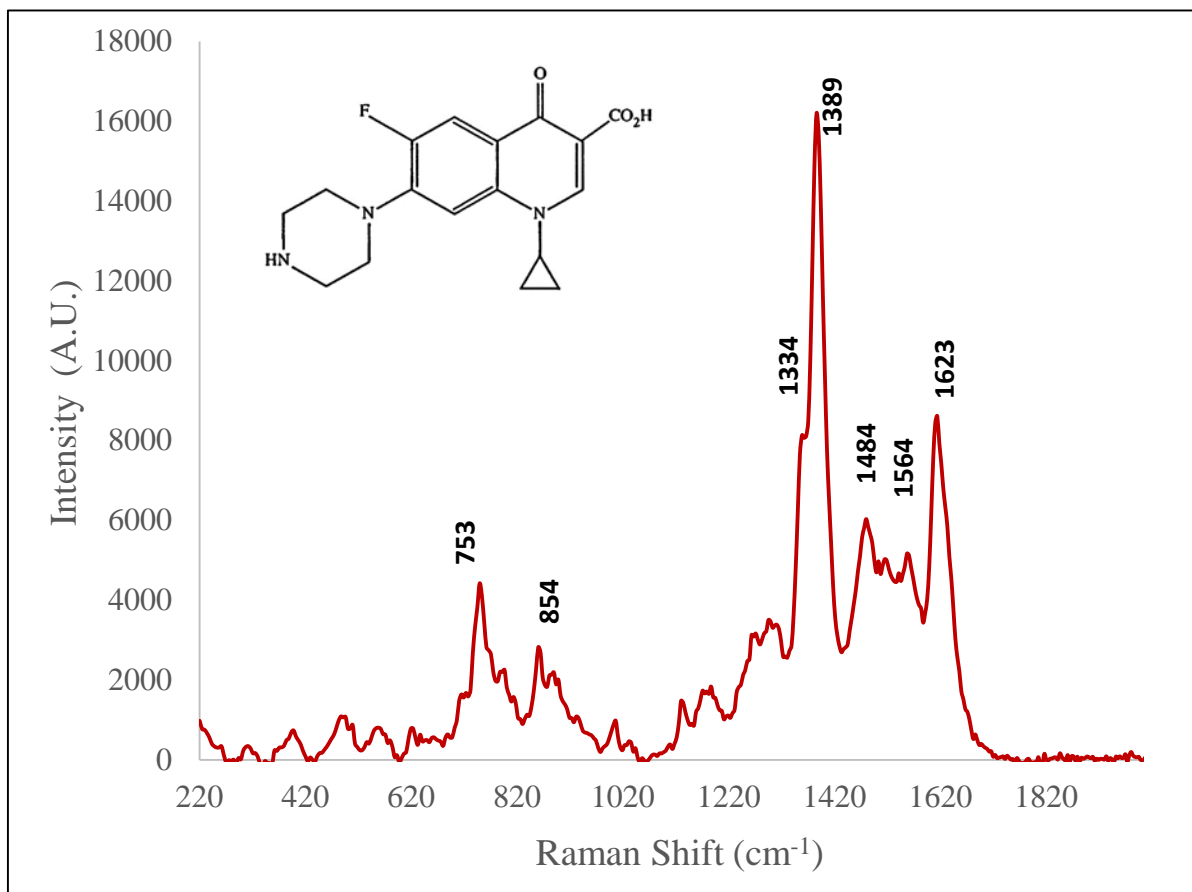


Figure 29: SERS spectra for Cipro. Acquisitions was made using a 638 nm emission line for 10s acquisition using 3.00 mW laser power.

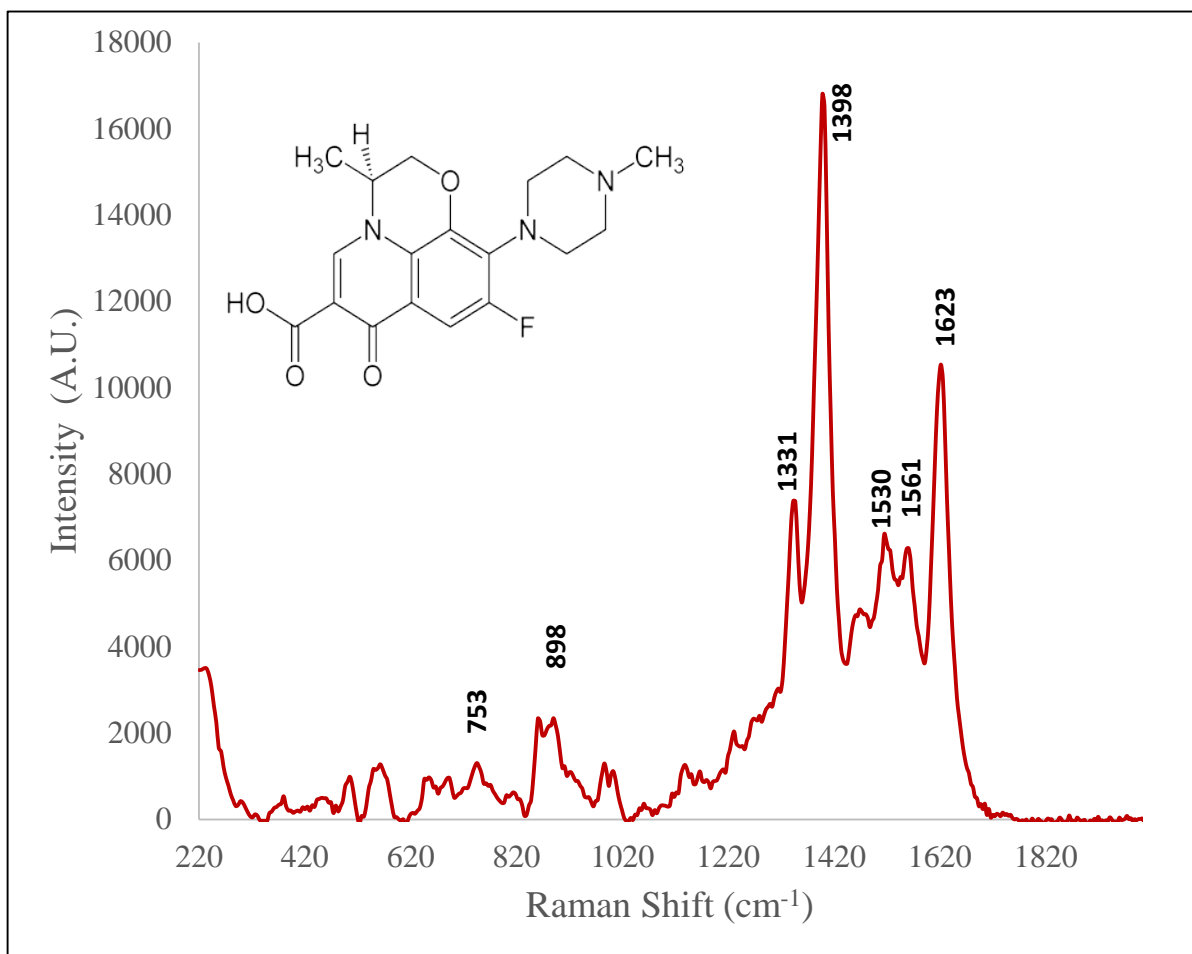


Figure 30: SERS spectra for levo. Acquisitions was made using a 638 nm emission line for 10s acquisition using 3.00 mW laser power.

4.4.3. pH studies

As described before, the three compounds under study has characteristic acidic groups. This suggest that changing the pH of the solution of the analyte would have an impact on the selectivity of the drug toward the PDMS polymer and at the same time affecting the adsorption on the metal. A pH study was made evaluating the samples at pH above and below their pKa values in order to determine the effect on the SERS spectra. The pKa values for Cipro are 6.42 and 8.49, Levo has pKa values of 5.70 and 6.05 and finally 4-carboxy has a pKa value of 3.60. This study was made under static condition with the idea of determine the effect on the compounds by means only of the pH change (Figure 31).

The results demonstrates that for 4-carboxy at pH below its pKa (3.6) the SERS spectra presents a higher intensity than the other pH values. This suggest that the attraction between the protonated silanol groups and the fully protonated carboxylic acid group is favored by hydrogen bonding intermolecular attraction. This help the molecule to move through the polymer network and reach the silver particles.

The fluoroquinolones behavior is similar to the one exhibit by the sulfonamide. Levo had the most intense signal at pH lowers that the first pka, (pH =5) and below that value. Like the sulfonamide it is expected that the dominant species at pH below 5.70 are the protonated form (Chapter 5 figure 46) which favors the hydrogen bonding between the PDMS. As the pH changes it can be concluded that the adsorption occurs by means of the OH terminal of the carboxylic group. This is supported by the inspection of the Figure 31 b, in which the signal close to 1400 cm^{-1} still present while the rest of the signals disappears.

Cipro presents a similar behavior to Levo, as it should be due to their similarity in chemical structures. The best SERS spectra are observed at values close and below the pKa. The intense of the signals however are superior to the Levo signals. Analyzing the chemical structures of each fluoroquinolone, Cipro has a cyclopropane substituent bonded to nitrogen against levo that has a bigger group attached to the same nitrogen. This by steric effects could be the reason for the difference in band intensities.

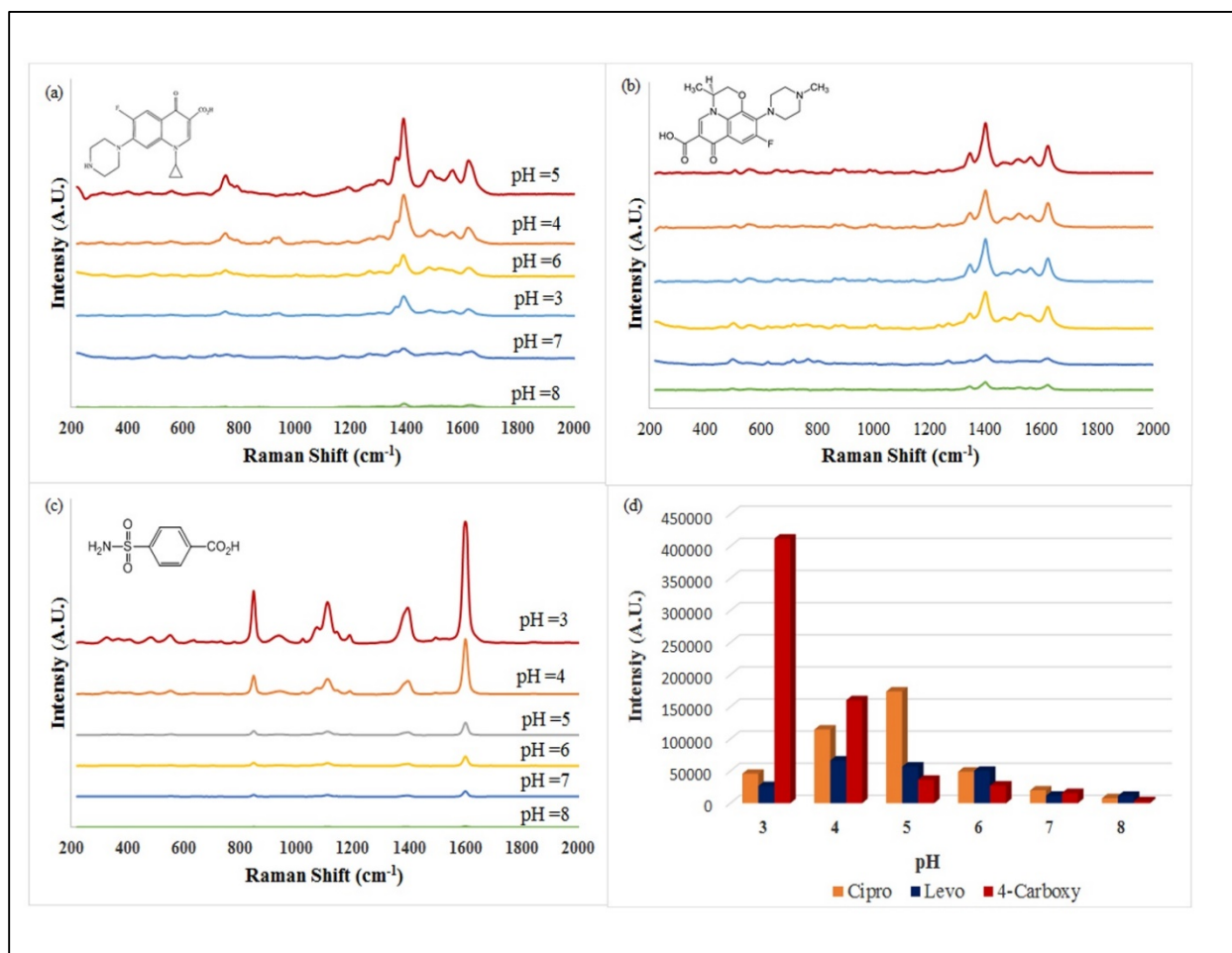


Figure 31: Effect of pH on the intensity of each pharmaceutical drug

4.4.4. Translation Study

The spinning effect on each analyte was tested to determine the effect on the analytical signal. This study, provides information about what are the best rotation conditions that presents the highest analytical signal with the best reproducible results. Evaluation was done using the most intense band of the SERS spectra for each analyte a. In general, the results demonstrate that at the lowest spinning conditions each analyte maintains an acceptable response compared to their response under static conditions (0 rpm) (Figure 32). This behavior is expected because under rotatory conditions the scatter radiation from the excited analyte is moving away from the detector on a contrary of the static mode in which the analyte is in a fixed position. This results in a less amount of radiation reaching the detector and produces less define spectra. The R6G intensities maintain a 75 % of the original peak area for their 1510 cm^{-1} band at 840 rpm. After that, the signal begins to decrease and by the 1595 rpm the signal is about 20% of the original intensity. The 4-carboxy shows a similar behavior, in which at the lowest spinning rate the 1600 cm^{-1} band still preserves 82% of the original response. In the case of Cipro and Levo, these spectral areas have decreases in their areas of more than 50 % for the revolution of 875. It has been reported that the fluoroquinolones require high concentrations to produce significant signal in SERS. However with the PSTTD it offers the advantage of increasing the irradiation time with minimal damage to the substrate.

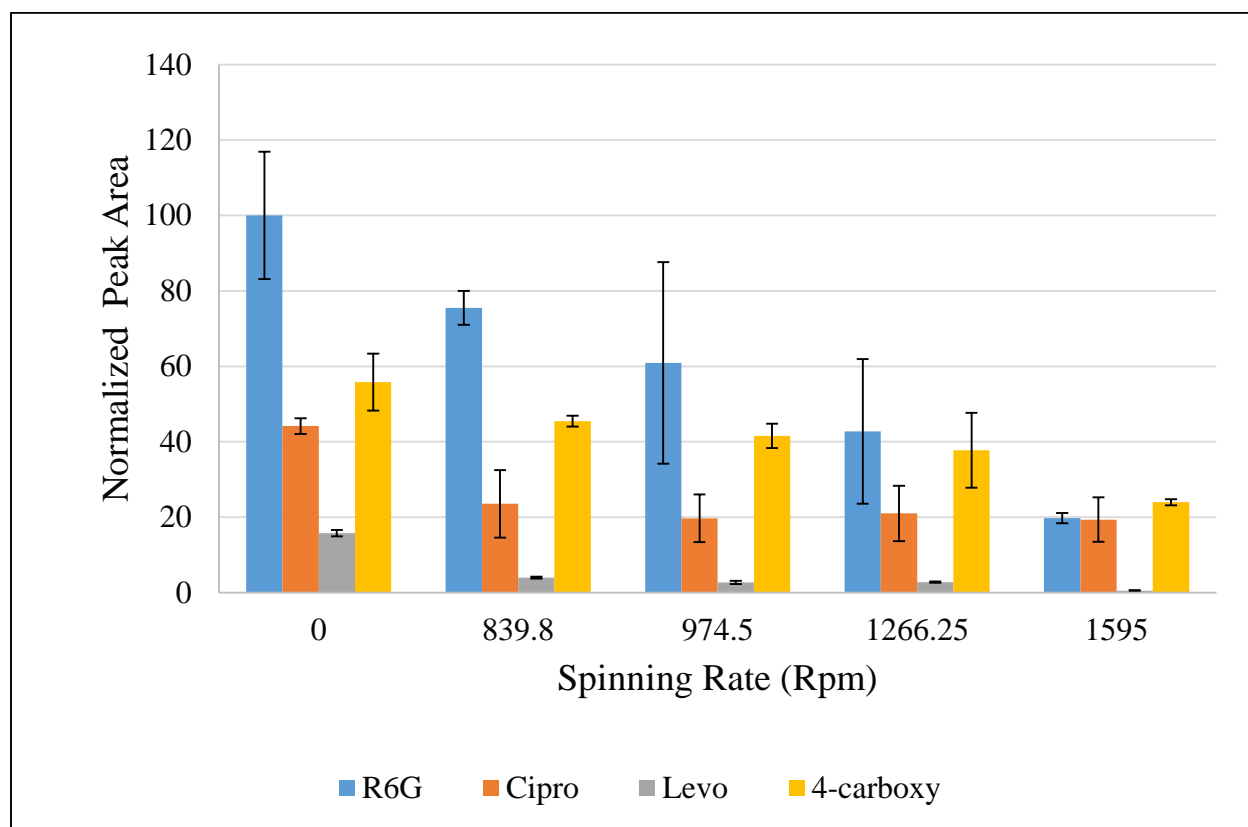


Figure 32: Spinning rate effect on the analyte signal for PSTTD

4.4.5. Adsorption Time

The use of PVD technique for metallization of the substrate has the peculiarity that forms small aggregates or silver islands. These penetrate to some depth influenced the metal deposition rate. The ability of the analyte to percolate or migrate through the PDMS is influenced by several factors such as, the size of the molecules, the kind of intermolecular attraction the analyte has to the silanol groups of the polymer and the dominant specie of the analyte (cationic or anionic). These factors influence the time it may take the analyte to be adsorbed on the metal surface to exhibit plasmonic response. For this reason a study of the adsorption time for each analyte was done. Measurements were made considering the time the compound exhibit the high response. The analysis was performed until constant responses were observed in the areas of the more prominent band of each compound in both static and rotational mode. The spinning speed tested was 850 rpm using a USB power. The results for the 4-carboxy demonstrate that the maximum response is observed during the first five minutes of analysis in the static mode. This can be explained based on the relative small size of the 4-carboxy molecules compared with the other studied compounds. Studies reported for a similar molecule shows similar adsorption times.

After this time, significant decrease is observed, mainly produced by possible photolytic degradation of the analyte. The RSD for the complete analysis in this mode is about 85%. Significant improvement is observed on the translational mode in which a constant response is observed over the whole period of analysis with a 4.5% RSD. The decrease in the measured response is one of the inherent disadvantages of the translational technique as previously reported. But this can be overcome with a small increase in the irradiation time that will result on an increase in the signal to noise ratio. In addition, the constant response that for this type of compound offers

the advantage of getting consistent results over a relative large period of time which is demonstrate the capability of the PSTTD for field analysis. Similar results are observed for the different compounds (Figure 33-36) tested.

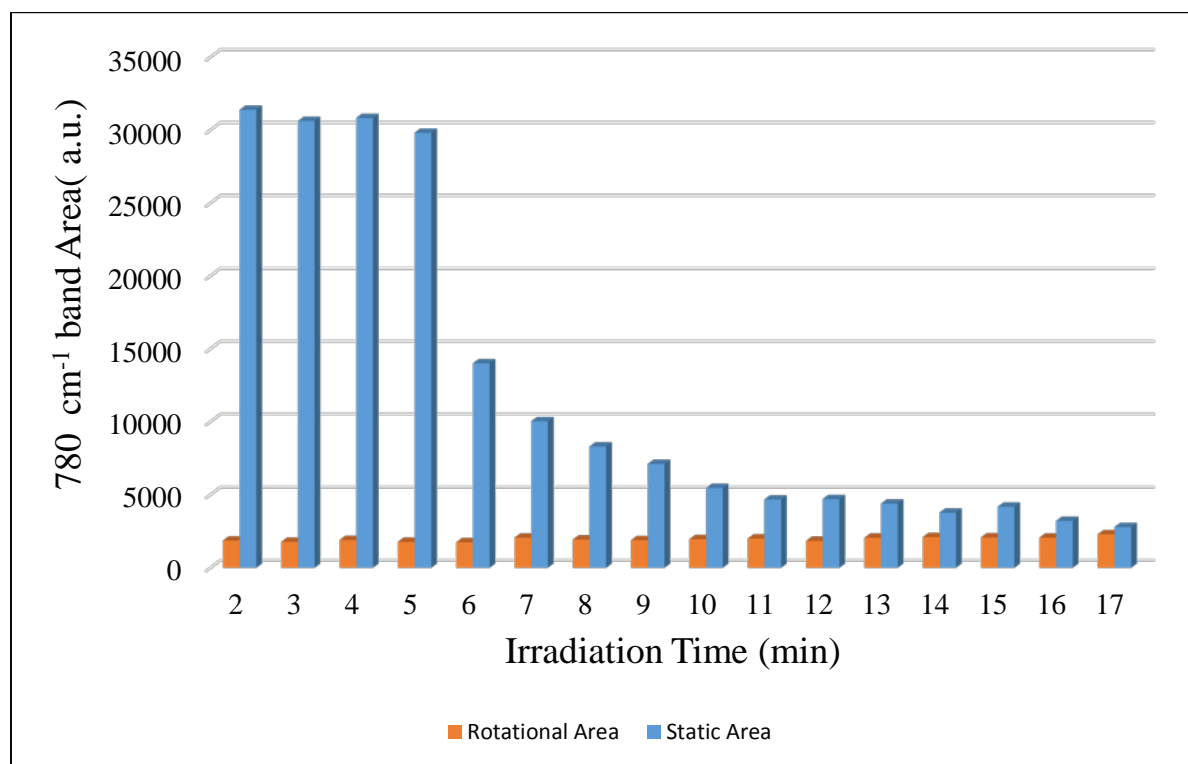


Figure 33: Time adsorption study for the 4-carboxy analysis. Reproducible measurements can be observed over the seventeen minutes analysis over the rotational mode

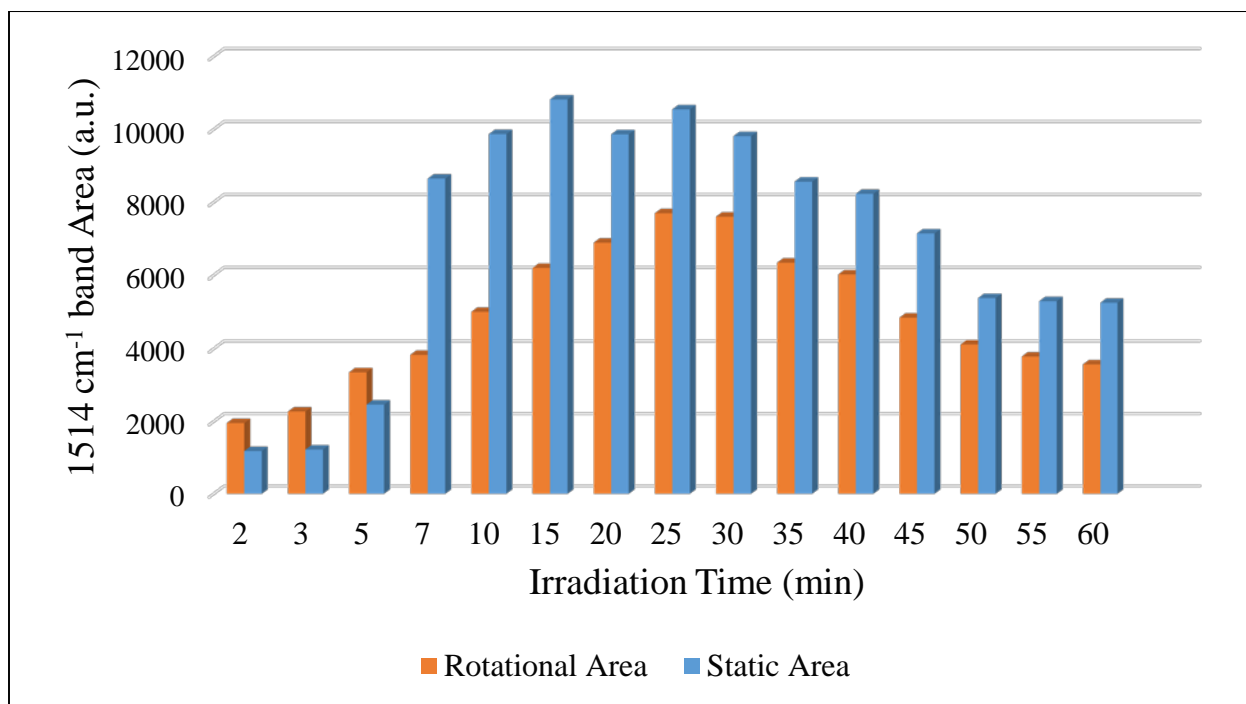


Figure 34: R6G adsorption study. The maximum intensity was achieved in a short time analysis over the static mode

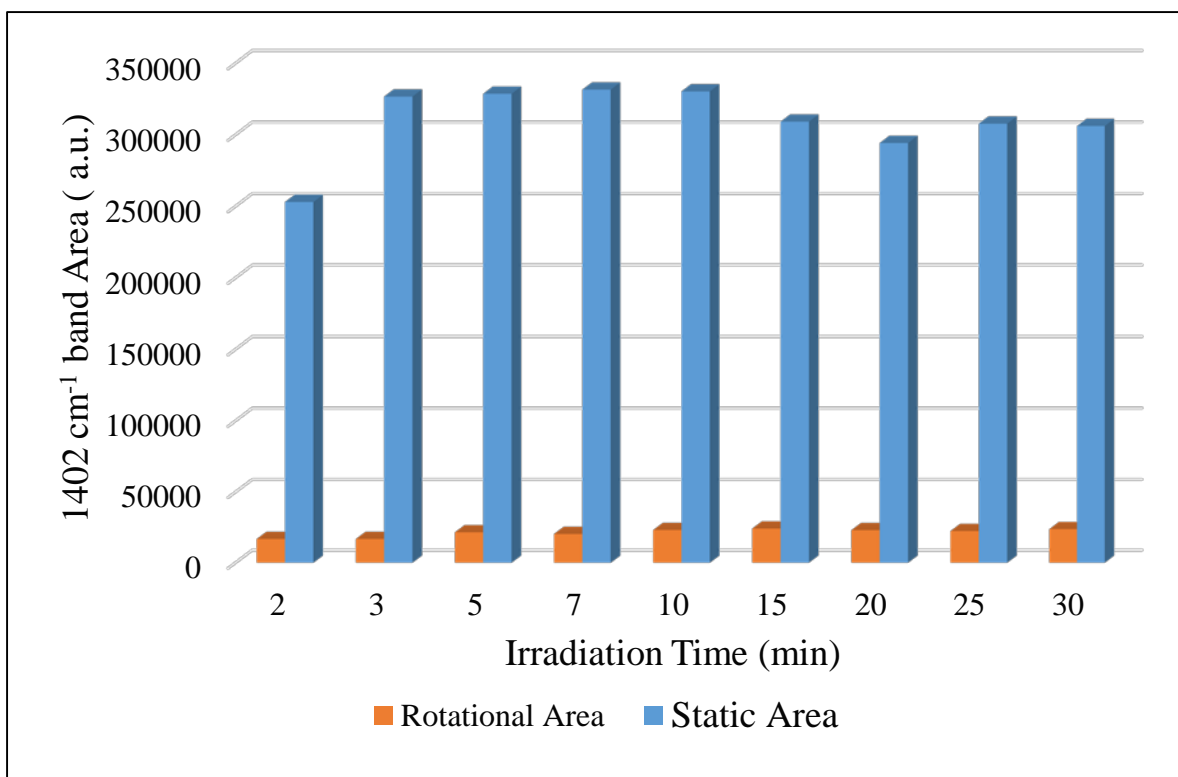


Figure 35: Levo adsorption study for a 30 minutes analysis. The rotational analysis show a constant response over the entire analysis

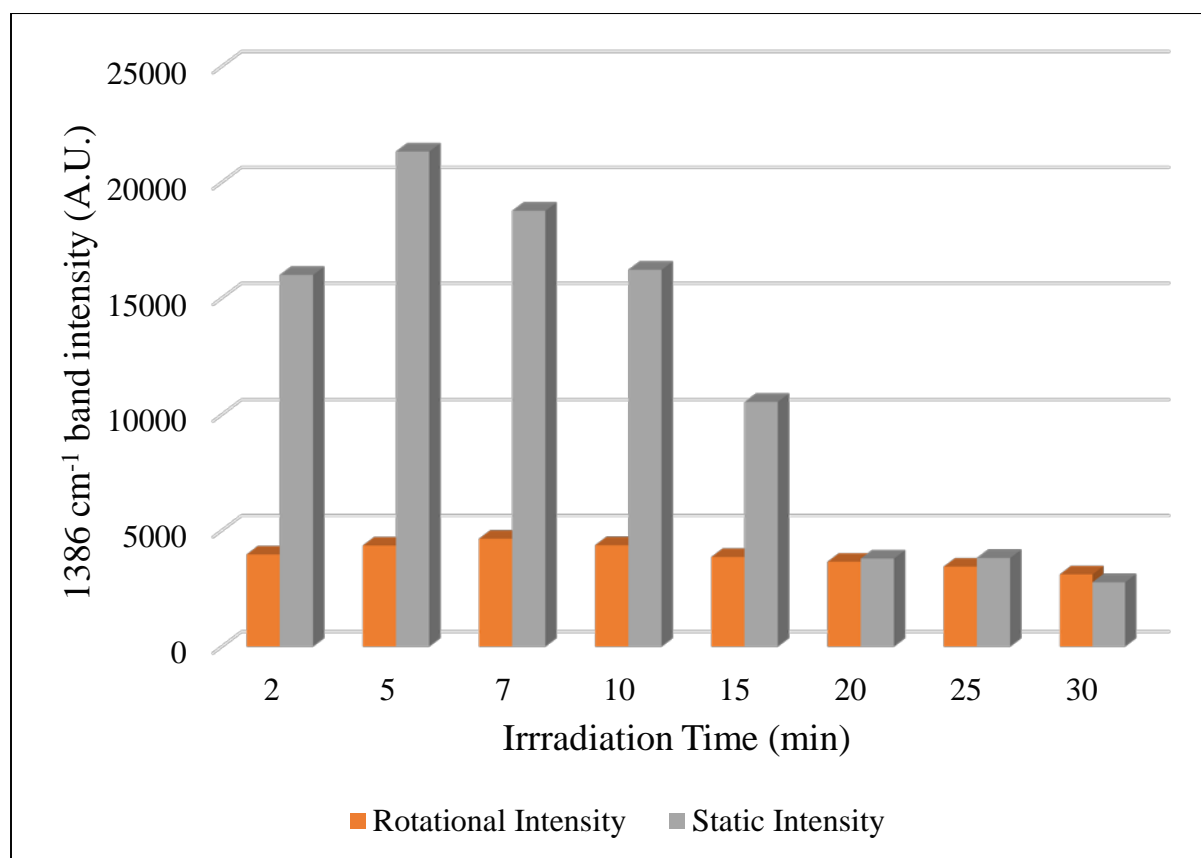


Figure 36: Levo adsorption study for a 30 minutes analysis.

4.4.6. Precision Evaluation for the PSTTD

The capabilities of the PSTTD were tested to evaluate the precision on several measurements. Figure 37 and Table 9 summarizes the findings for the different measurements. The results clearly present the effect on the rotation mode against the static mode. The %RSD for the repeatability measurements demonstrate a significant improvement on the precision of the results compared with the static results. As expected when the reproducibility parameter was evaluated an increase on the %RSD (8.83% vs. 17.0%) is observed.

Table 9: Precision study results for the PSTTD

Parameter	Result Rotational	Results Static
Repeatability n=5	2.74 %	13.6%
Intermedia Precision n= 20	8. 83 %	17.0%
Intra-well Precision n=3	27.6%	150.%

The intra well results presents the most dramatic difference between both modes. The main reason for this behavior is due to the combination of several factors like the variation on silver (Ag) deposition and possible substrate oxidation. Others factors like thermal degradation of the substrate and photolytic degradation of the analyte arise on the static mode as well. Figure 37 presents the raster analysis performed for the reproducibility study using R6G. The plot presents a consistent spectra acquisitions for the whole well which results on an 8.83% RSD. This results are less than one normally reports for SERS.²⁶

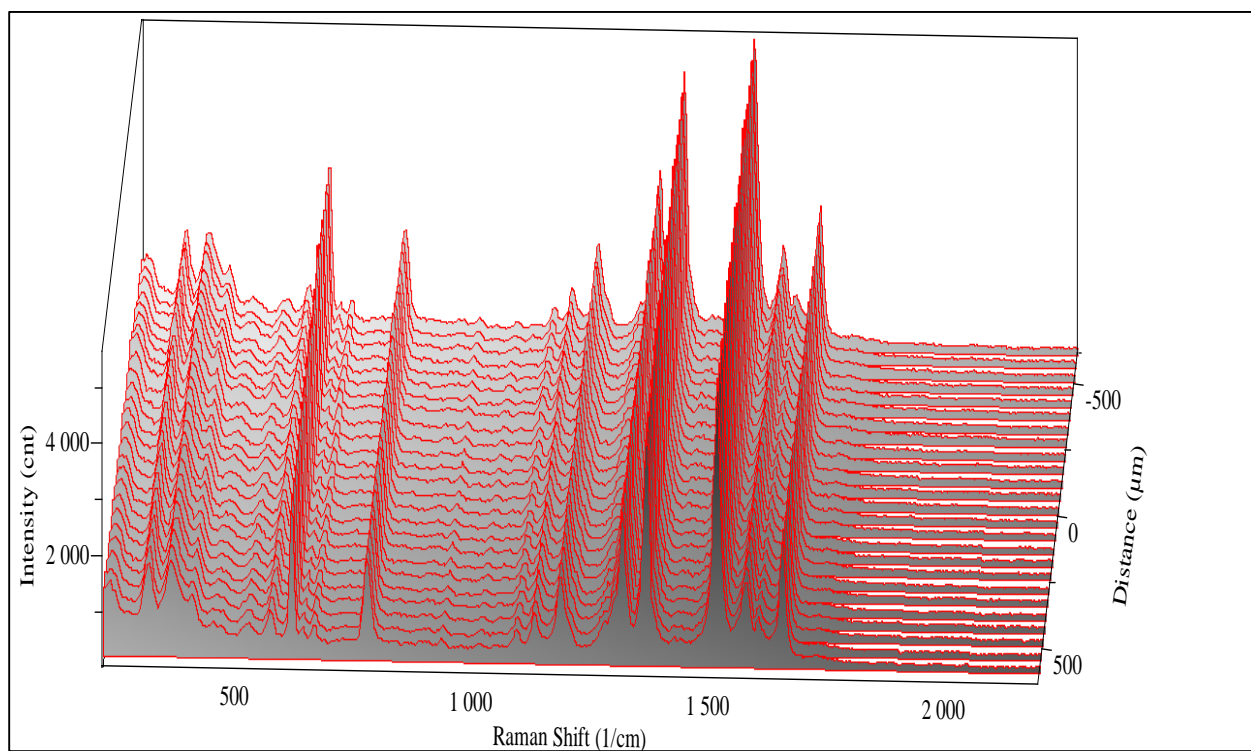


Figure 37: R6G SERS spectra for the 1.00×10^{-5} M solution for the raster acquisition of 1s and 3 acquisition from -600 μm to 600 μm .

4.4.7. Linearity Evaluation for the PSTTD

Initial linearity studies pursuits the use of the traditional working curves models with the PSTTD. Results for the different compounds (4-carboxy, levo and R6G) did not show the characteristic behavior of an univariable model (Figures 38-39). Spectral interference and other degradation process could be contribute to these lost in linearity.

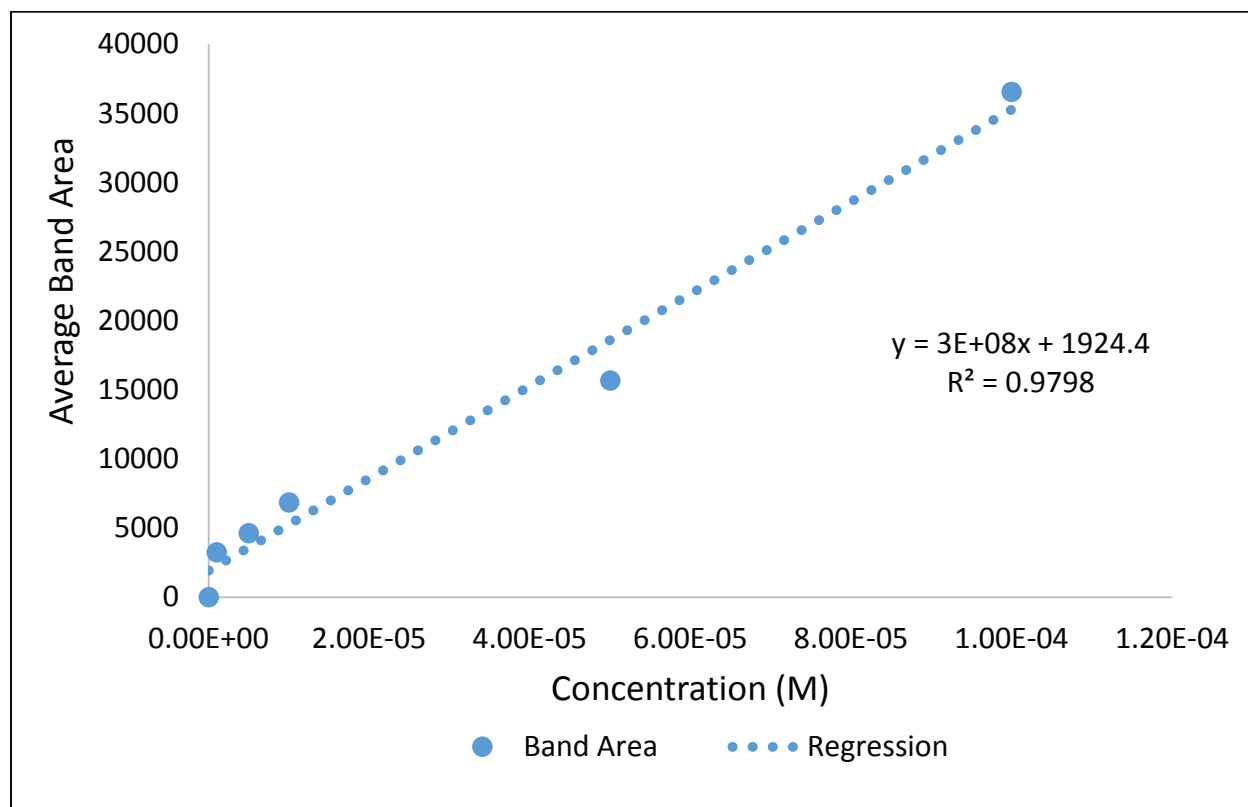


Figure 38: 4-carboxybenzenesulfonamide Calibration Curve using PDMS wells analyzing the 830 cm^{-1} band using 10 s acq at 638 nm

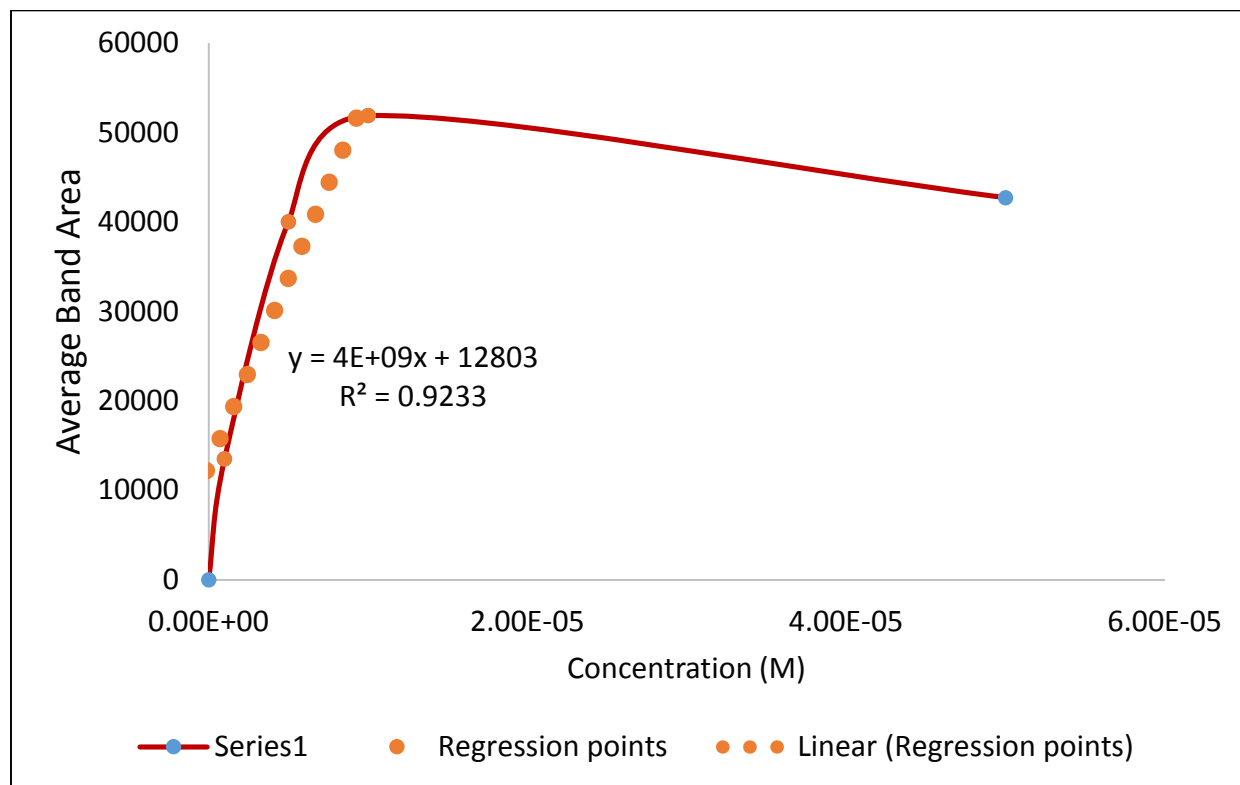


Figure 39: Rhodamine 6G Calibration Curve using the 770 cm^{-1} Band using 2 sec acquisition at 638.

The results observed guide the study to a new focus using partial least square analysis (PLS). Using PLS tool box a Mathlab® extension add ins it was possible to identify the best region of analysis for the different spectra of each pharmaceutical compound and R6G. Figure 40 shows the selected area for the R6G spectrum. The same procedure was done for the Levo and the 4-carboxy data.

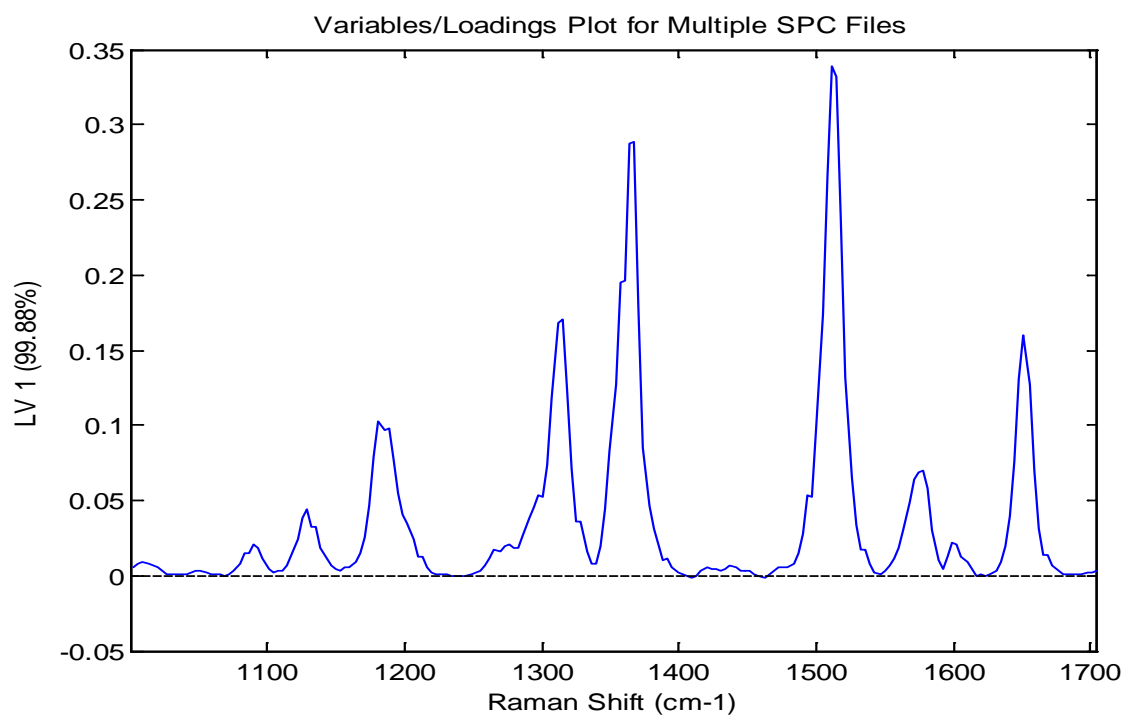


Figure 40: SERS Spectra Region for R6G for Partial Least Squares for R6G

The PLS analysis performed shows an improvement on the linearity results as table 5 summarizes. The correlation coefficient (R^2) showed an improvement in their value from the working curves to the new method. The Root Mean Square Error of Calibration which value should be as low as possible to ensure that for the proposed model there is a relation between the variables also supports the PLS method as an efficient one. The results suggest that the use of PLS in combination with the PSTRD to perform quantification of the tested compounds using SERS. This part was a proof of concept, full validation is required to implement this approach as an established procedure in the detection of pharmaceutical contaminants.

Table 10: PLS regression results for the PSTTD

Analyte	R² working curve	R² Calibration	RMSEC
Rhodamine 6G	0.9233	0.9996	3.58228e-008
4-Carboxy	0.9798	0.9988	1.85151e-010
Levofloxacin	0.8975	0.9894	2.93695e-005

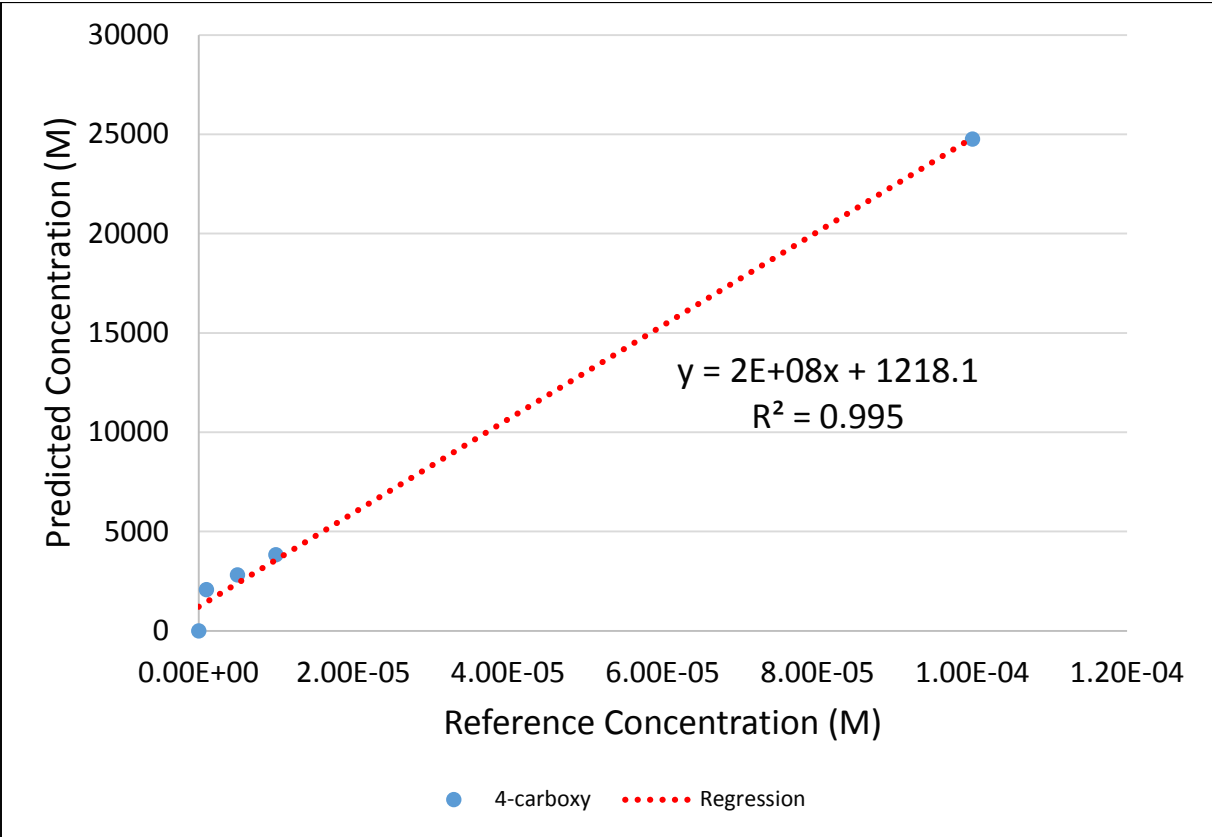


Figure 41: Partial Least Squares results for the analysis of 4-carboxy

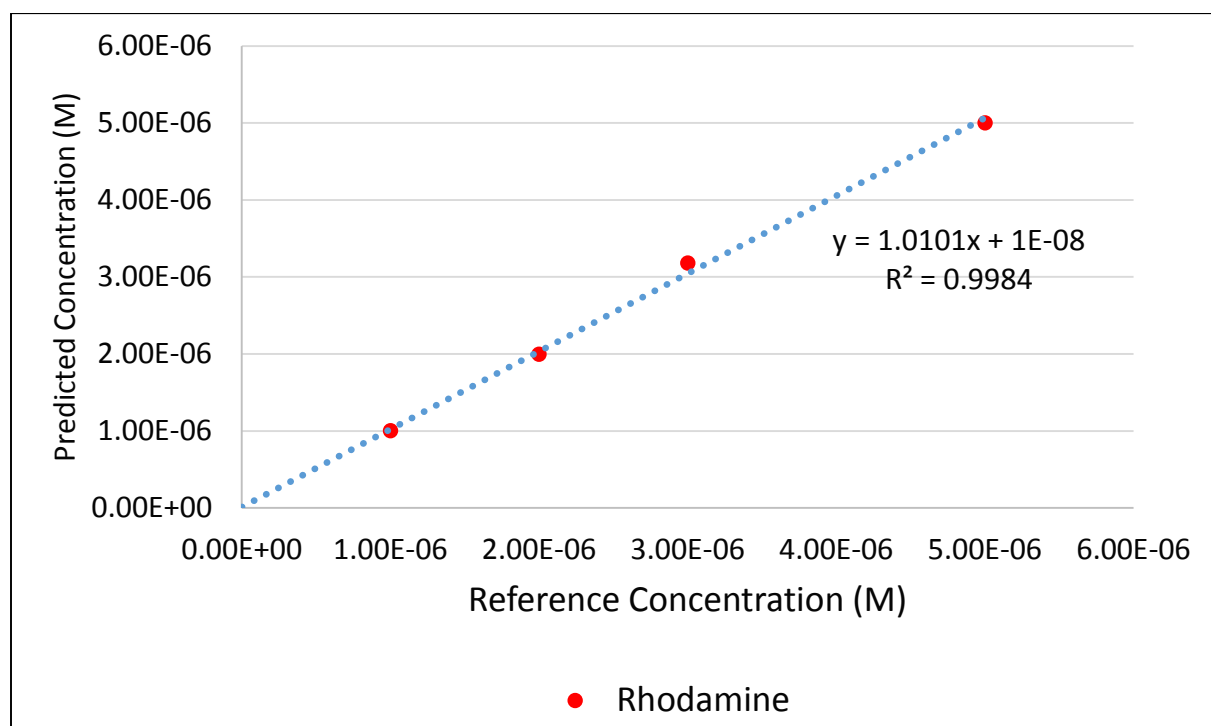


Figure 42: Partial Least Squares results for the analysis of Rhodamine 6G

Chapter 5: Remediation alternatives for the fluoroquinolones and Sulfonamides Removal

This chapter contain a modified version of an article published in Advances in Optical Technologies by Beer Pal Singh, Ravish Kumar Upadhyay, Rakesh Kumar, Kamna Yadav, and Héctor I. Areizaga-Martínez

Beer Pal Singh, Ravish Kumar Upadhyay, Rakesh Kumar, Kamna Yadav, and Hector I. Areizaga-Martinez; “Infrared Radiation Assisted Stokes’ Law Based Synthesis and Optical Characterization of ZnS Nanoparticles”. Advances in Optical Technologies, vol. 2016, Article ID 8230291, 6 pages, 2016. doi:10.1155/2016/8230291

My primary contributions to this article included: (A) part of the fabrication of the nanopaticles (B) collection and interpretation of a part of the analytical data.

Copyright © 2016 Beer Pal Singh et al. This is an open access article distributed under the Creative Commons Attribution License, which permits unrestricted use, distribution, and reproduction in any medium, provided the original work is properly cited.

5.1.Introduction:

During the previous chapters the successful development of novel bio inspired nano composites and the use of polymeric substrates for the detection and quantification of a selected

number of fluoroquinolones and sulfonamides had been demonstrated. But, as part of an environmental research group it is also necessary to develop strategies that can be used as an alternative for the removal of pollutants from surface waters and or wastewaters. Those strategies have some specific requirements that need to be considered for the development of effective products that could solve the problem. The most important requirements are cost, toxicological effects and efficiency. These aspects are normally considered at the time waste treatment plants were built. But the removal process of the pollutants and contaminants does not consider the presence of pharmaceutical products in waste water streams. For that reason most drugs that are discharged over the sanitary or landfills systems are not removed during the treatment process. Leaving the final fate of those compounds as unknown as sometimes most of the treatment water is returned to the surface waters or rivers.

Most of the studies done of the presence of PPCPs are in agreement that the concentration of such compounds are not significant enough to have an impact on the water systems. But, the long term exposure (chronic) to such agents in the ecological systems had not been considered as significant. There are some proposed alternatives over the past years to help solving this situation like the phyto remediation, which recall the use of plants to remove pollutants from different sources. These alternative present a problem of disposition of the contaminated bio mass once the removal efficiency of the plant is achieved. The use of activated carbon is another alternative explored for the removal of pollutants but lack of information about their efficiency with complex molecules is available.

The use of metallic and metallic oxide nano particles had been explored as a remediation tool for the removal of several contaminants. Several studies using iron oxide nanoparticles had been demonstrate acceptable efficiency on the removal of simple contaminants like solvents such as methanol. The use of cerium oxide nano particles for the removal of PPCPs represents an interesting alternative based on the medical uses of those particles in recent years. This chapter will focus on the development of a chromatographic method for the detection of the proposed fluoroquinolones and for the 4-carboxy compound. In addition a new sulfonamide (sulfadiazine) was included to demonstrate the capability and roughness of the method. Also, the efficiency of the nanoparticles in the removal of the studied drugs we discussed.

The use of chromatographic techniques for the isolation, detection and quantification of pharmaceutical compounds had been the standard procedure for decades. Several methods had been develop for the analysis of different types of fluoroquinolones using High Performance Liquid Chromatography (HPLC)UV and Fluorescence detection and reverse phase C18 columns. Those methods usually requires the combination of buffered salt solutions and acetonitrile solvent. This combination provides problems in terms of the possible deposition of salts that can block up the instrument lines and decrease the column life. The waste material is also an environmental concern that also represent a disadvantage of this current methods which most of the waste are organic solvents.

The Sulfonamide chromatographic determination follow more aqueous conditions for the same reverse phase determination.¹⁴⁸ Nevertheless, there is no record that a chromatographic determination had been performed for 4-carboxy and for a simultaneous determination of

sulfonamide and fluoroquinolones. This situation provides the need for the development of an analytical method that uses more green solvents and provide an efficient separation of the selected drugs in a short period of time using a common HPLC system with UV detection. The method development was achieved at first considered the separation of the two fluoroquinolones and sulfadiazine (sulfa). The rationale for this was based on the fact that the literature presents evidence that HPLC separation can be achieved for the three selected compounds. Once the optimal conditions were determined, the 4-carboxy drug was added and experimental conditions readjusted.

5.2. Method Chromatographic Method evaluation

The development of any chromatographic method in which the analytes have a chromophore as part of their chemical should be started with the determination of the optimum wavelength at which each compound showed the highest absorption of light.

Experimental:

For this a wavelength scan was performed in a 200- 400 nm range, using a 1.00×10^{-3} M of each drug except the Sulfa which concentration was 1.00×10^{-4} M. Using a Thermo Evolution 210 UV-Vis Spectrophotometer

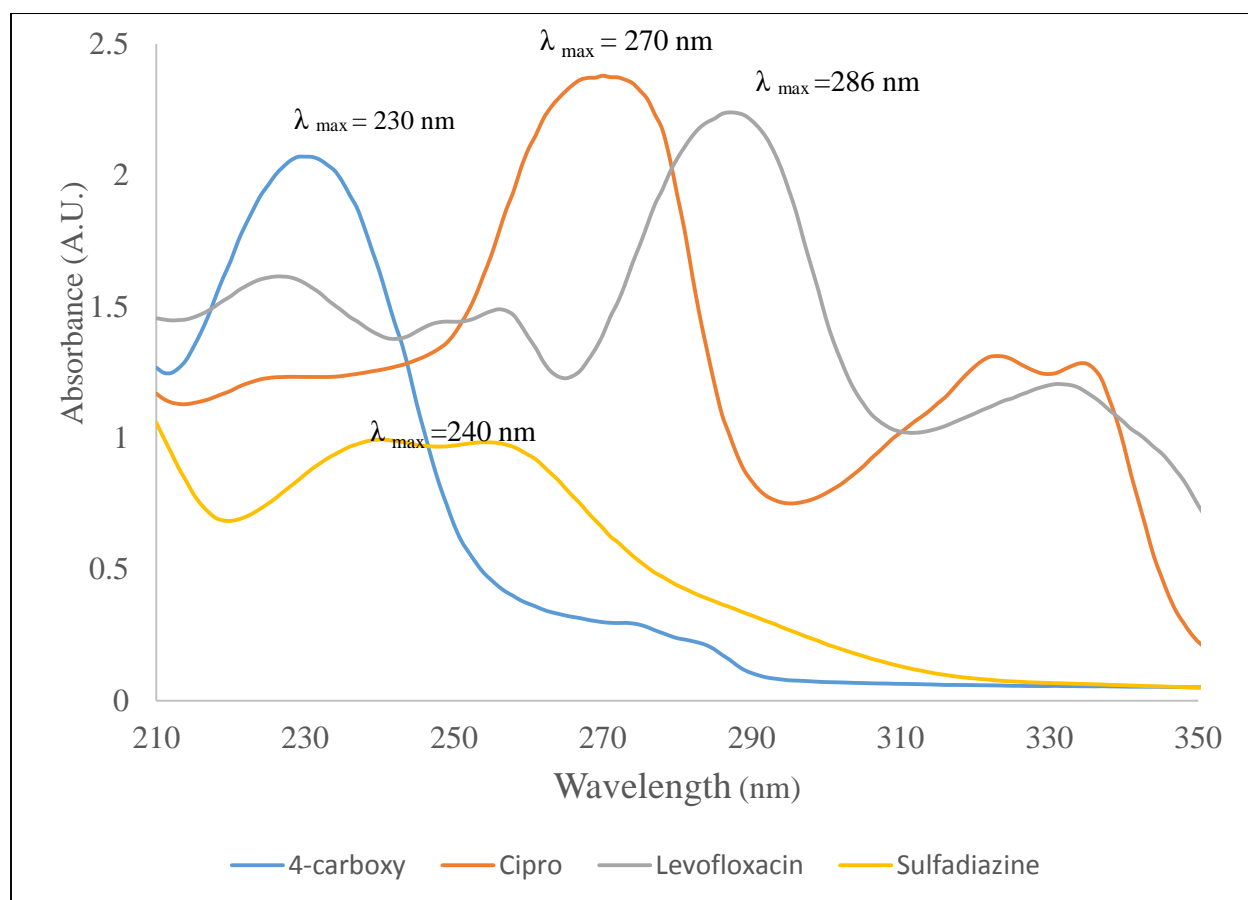


Figure 43: Ultraviolet spectra for the four pharmaceutical drugs to determine their maximum absorption wavelength

Figure 43 presents the spectrum of the scan analysis for each pharmaceutical drug. The scan results demonstrate that the Cipro maximum absorption occurs at 270 nm, for Levo it occurs at 286 nm. This results are expected because the conjugation level they has on their chemical structures. The sulfonamides which also has aromatic functional groups but also has the sulphone and amine group which typically are responsible of the displacement of the absorption band to shorter wavelengths.

Evaluation of the spectra suggest that a selection of a wavelength close to the 286 nm as the analytical wavelength of analysis. At this wavelength Levo and Cipro has relative high absorption and Sulfa which almost has a constant response over the 200-300 nm range.

Once the maximum absorption wavelength was determined a mobile phase evaluation was performed having acid water as the principal component. Methanol was selected as organic solvent, because of its cost which is lower than other solvents like acetonitrile and their toxicity is lower compared to acetonitrile. Several proportions of aqueous/organic solvent were tested, resulting the 80% acid water and 20% methanol the combination which had the best separation. The flow rate used was 2.0 mL/min, a Zorbax Rx-C18 was used with a 40°C temperature. Triethylamine at 1% was added to the aqueous mobile phase to improve peak shape.

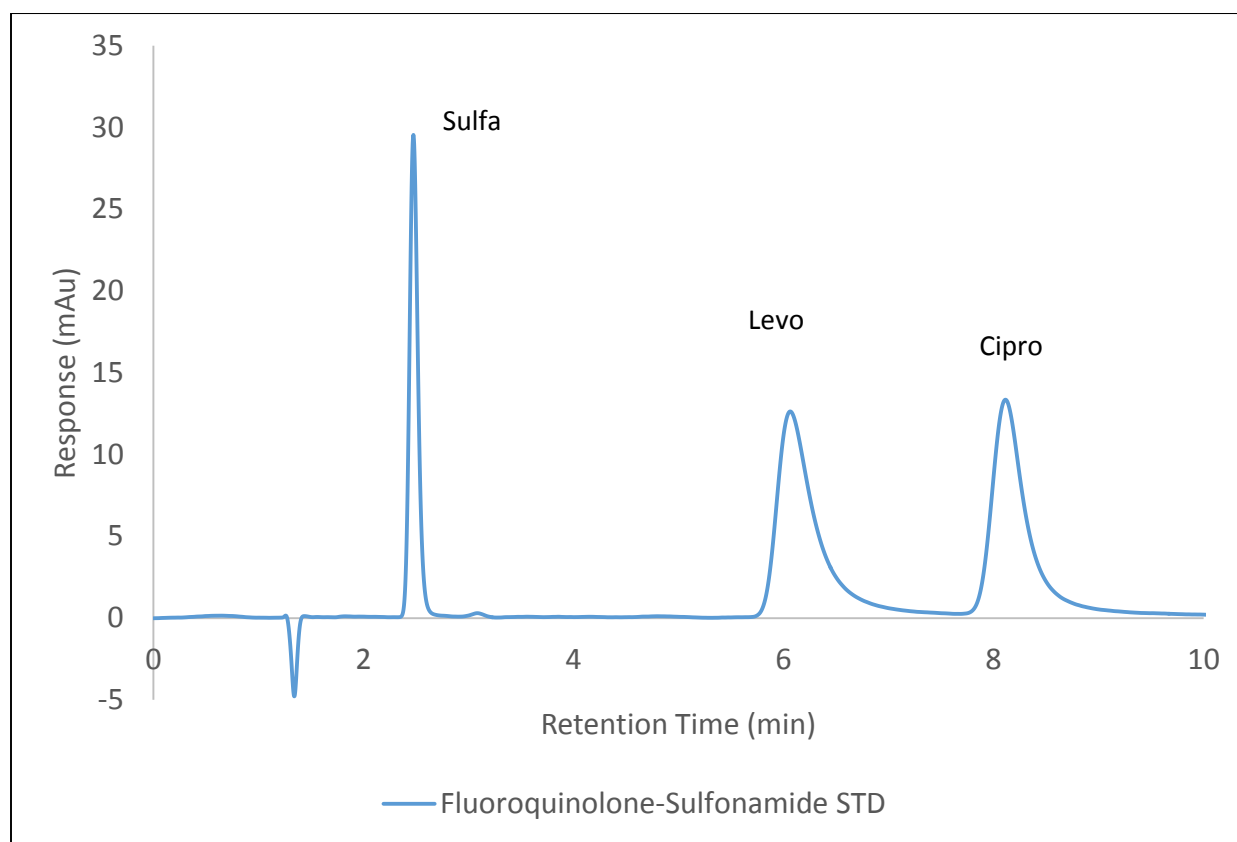


Figure 44: Chromatogram for the separation of the antimicrobial drugs

The chromatogram presented on Figure 44 shows a complete separation for the 3 drugs analyzed. Separation is achieved in a relative short period of time. Once the detection wavelength had been determined and the mobile phase composition evaluated, the next step was to perform the method validation for the separation of the three selected drugs. The conditions and results of this validation will be discussed on the following section.

5.3. Method Validation for the Pharmaceutical Products Separation

5.3.1. Experimental

The method validation was performed preparing a series of standards solutions of each drug to evaluate performance of the detector (linearity, accuracy and precision) and separation capacity of the column. The separation was achieved using an Agilent 1100 with a Quaternary pump system and Variable Wavelength Detector (VWD). The column used was a Zorbax Rx-C18 (Serial Model: USCU013660) and the detector was set to 286 nm with a run time of 10 minutes. As mentioned on section 5.2 the column was heated to 40°C and the flow rate was 2.0 mL/min. The injection volume was 10 µL.

The mobile phase was prepared using the following reagents: Methanol HPLC Grade (Fisher Scientific Lot#126273), distilled water, Phosphoric Acid H₃PO₄ (EMD Lot#48350925) and triethylamine - N(CH₂CH₃)₃ (JT Baker Lot#420146). The mobile phase composition as mentioned before was a mixture of 80% aqueous and 20% methanol with 1% Triethylamine. The pH of the aqueous phase was fixed to 3 with phosphoric acid. The mixture was filtered using a 0.45 µm filter. Five mixed standards solutions covering a range of 9.00 x 10⁻⁵ M - 1.00 x 10⁻⁵ M were prepared. The method used was the successive dilution method starting with a 9.00 x 10⁻⁵ M stock solution of each compound. Quality Control (QC) Solutions were prepared with a 5.00 x 10⁻⁵ M label concentration. The solutions were analyzed in triplicate and the average results were calculated for the response and times of each drug.

Suspended Solid Experiment:

The presence of suspended material in the surface waters especially after rainfall precipitation brings an interesting hypothesis; can the presence of this suspended solids will act as a degradation source of PPCPs? That possibility lead our research team to do a simple experiment in order to determine the effect of suspended solids in the possible degradation of pharmaceutical products. For this, a sample water from “Quebrada Oro” was splitted on equal volumes. The first half was filtered using a 0.45 μm filter and then spiked with a volume of the stock solution to led a final concentration of 5.00×10^{-5} M This sample was label as water without suspended solid particles (SSP). The other half sample was also spiked leading to the same drug’s concentration and label as water with suspended solid particles (SSP). This sample as not filtered until the moment of the analysis to avoid the chance the column was clogged with the particles.

5.3.2. Results and Discussion

The method validation process demonstrates if the proposed method is suitable for its intended use. The parameters commonly evaluated are linearity, precision, accuracy, limit of detection (LOD) and limit of quantitation (LOQ). In addition System suitability was evaluated in terms of capacity factor, theoretical plates and resolution. The acceptance criteria limits selected for the different parameters were chosen from the United States Pharmacopeia and International Conference of Harmonization. The criteria for those organizations are higher than the parameters recommended by the Environmental Protection Agency (EPA). The Table’s 11-12 summarizes the results for the different parameters evaluated for each compound.

Table 11: Suitability results for the method validation of the sulfonamide and fluoroquinolones

Linearity Parameters	Sulfa	Levo	Cipro	Acceptance Criteria
Theoretical Plates (N)	4695	1671		>2000
%RSD	0.88%	1.9%	2.2%	≤2.0%
Capacity Factor (k')	23.8	59.6		≥2.0
Resolution	---	9.7	3.6	≥2.0

Capacity factor parameter for the three drugs reflects acceptable results with values that exceed the acceptance criteria with Cipro with the highest value as expected based on the compound retention time. The separation capacity measure by the resolution, also exceeds the acceptance criteria. In the particular case of the two fluoroquinolones, the separation which chemical formulas are quite similar, the method is capable to discriminate them completely with a value of 3.6.

The theoretical plates is the system suitability parameter which the method does not meet the acceptance criteria for the Cipro and Levo. This result is affected mostly by the tailing observed for both compounds (Figure 42), which increase the peak width and as consequence decrease the number of theoretical plates. Considering that the method was designed to measure pollutants at trace levels the number of theoretical plates presented are not far from the criteria set for an active ingredient. This can be overcome increasing slightly the amount of Triethylamine on the mobile phase help in the decrease of the tailing factor. The precision values for five consecutive measurements also presents acceptable values with Cipro a slightly outside the acceptance parameters by only 0.2%.

Table 12: Linearity and Accuracy results for each compound

Linearity Parameters	Sulfa	Levo	Cipro	Acceptance Criteria
Correlation Coefficient (R²)	0.9999	0.9993	0.9997	≥ 0.995
Slope	4.27E+06	7.77E+06	7.29E+06	N/A
Intercept p value	0.258	0.632	0.203	> 0.05
LOD	9.49E-07	2.44E-06	1.52E-06	N/A
LOQ	3.16E-06	8.15E-06	5.06E-06	N/A
Accuracy Evaluation				
Percent Recovery	98.4	97.6	101.7	80-120

Linearity parameters and Accuracy (Table 12) were also evaluated on this validation. Correlation coefficient (R^2), which describes the relation between the dependent and independent variables, are in acceptance criteria for all the drugs. The calibration plots (Figures 45-47) for each compound clearly present the linear relation for the selected concentration range. The remaining linearity parameters also are in compliance with the acceptance values. The intercept p-value is a parameter used in method validation to describe the change the intercept has a zero value. If the value is higher than the limit the probability that the intercept is zero is statically probable. This means that the possibility of matrix interferences is not significant. This is also supported by the intercepts values of the 3 plots which are close to zero. The limit of detection and quantification values confirm that the selected concentration range is suitable for the analysis, because they are below the concentration of the standard #1 (1.00×10^{-5} M) In addition, the limit of quantification results, suggest that a lower concentration can be experimentally tested to expand the useful range of the method. The percent recovery confirm the accuracy of the method. The percent range from 97(sulfa) to 101%, values that at this level of concentration is considered more than appropriate. The results also support that nevertheless some of the acceptance criteria in the suitability evaluation are not completely meet the method is robust enough to accurate measure the sulfonamide and fluoroquinolones.

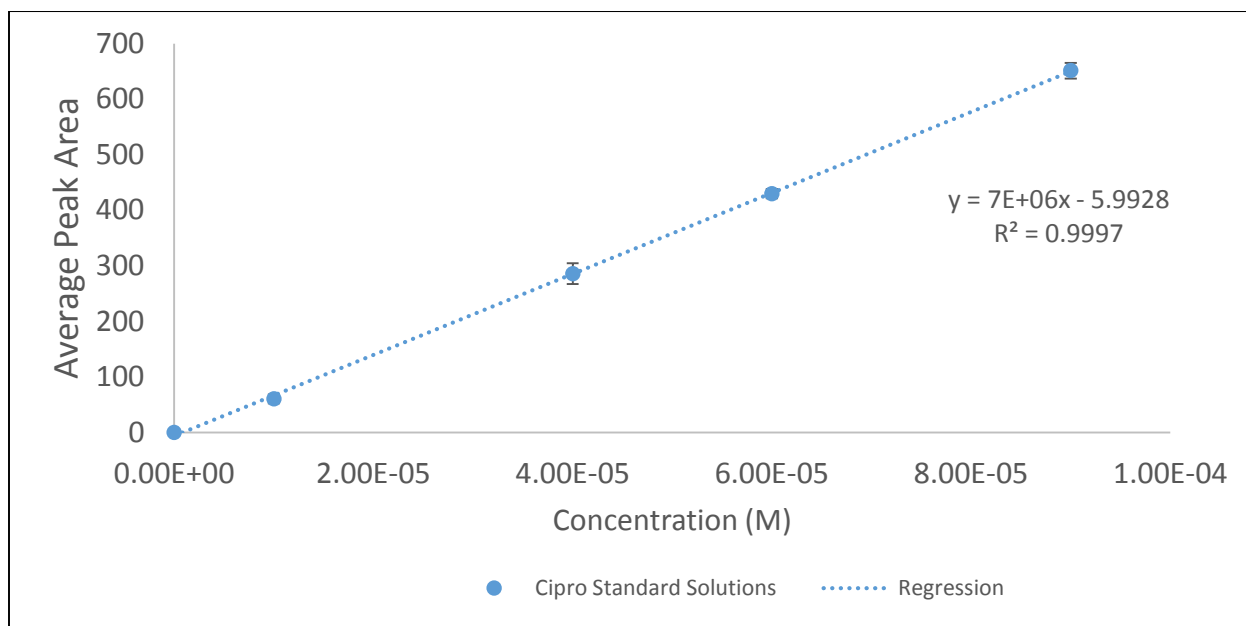


Figure 45: Calibration curve for the linearity evaluation of Ciprofloxacin.

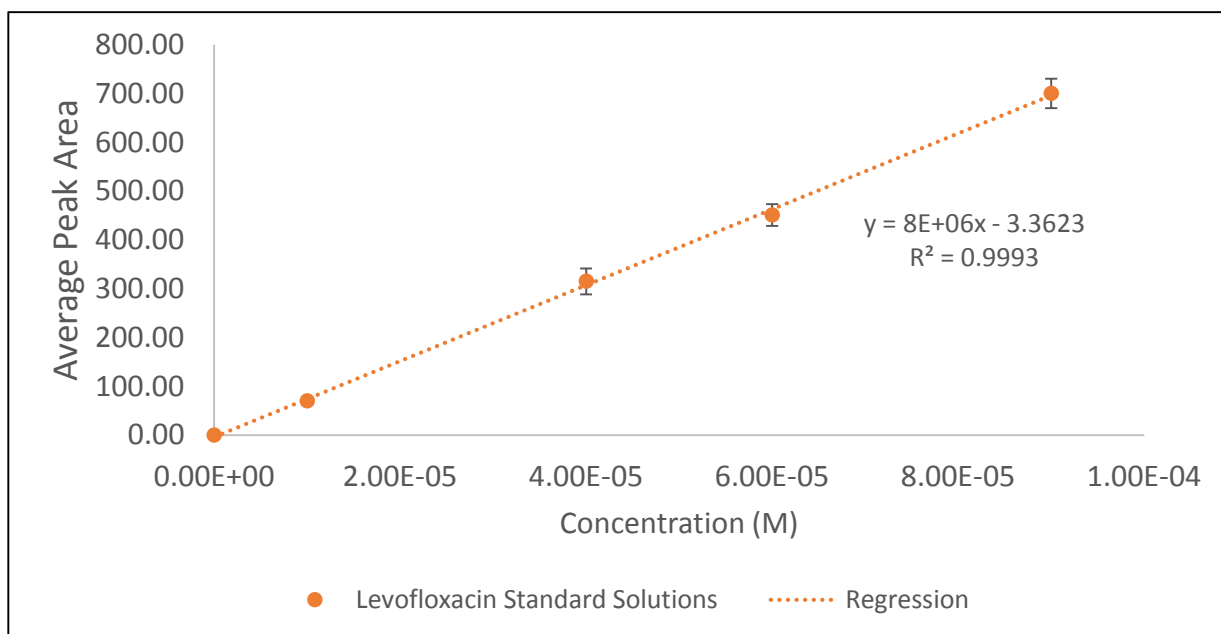


Figure 46: Calibration curve for the linearity evaluation of Levofloxacin.

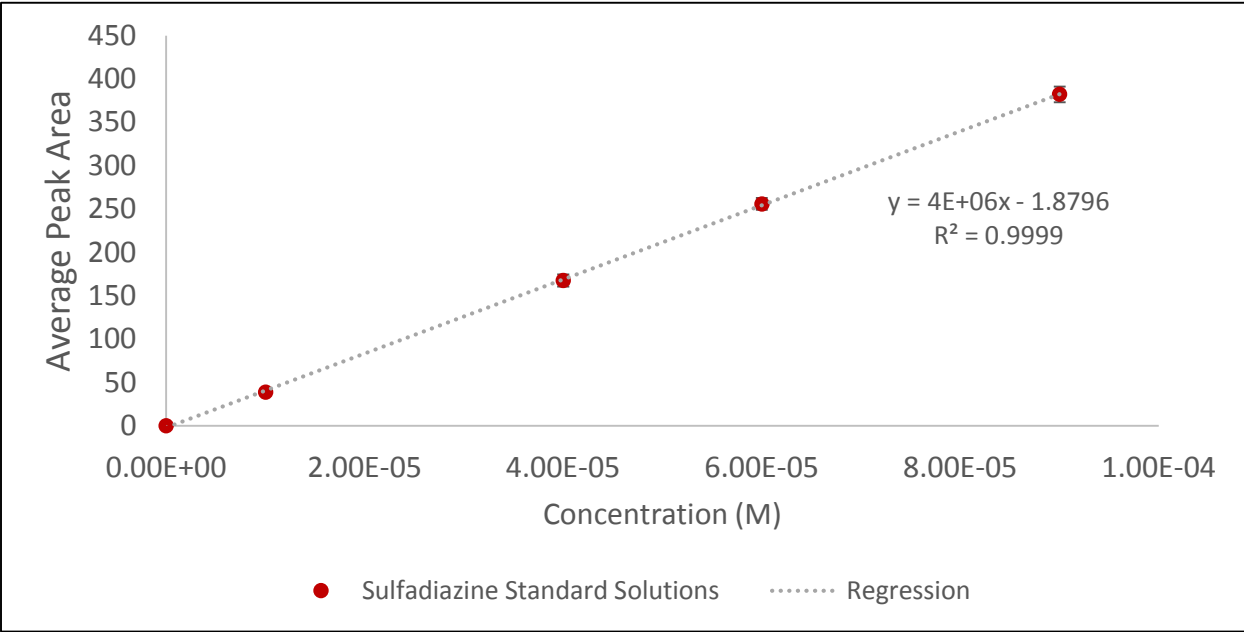


Figure 47: Calibration curve for the linearity evaluation of Sulfadiazine

Suspended Solid Analysis:

The analysis on the effect of suspended solids in the removal of surface water pollutants was evaluated by means of determining first the experimental concentration of the QC sample. Then, the percent recovery was calculated for the sample to determine the presence of any error associated with the sample preparation. The results demonstrate no difference between the calculated and the theoretical (label) concentrations (Table 13). The Cipro experimental concentration, which present the highest concentration (5.09×10^{-5} M) had a percent of error of 1.80%. The recoveries for the QC solution are within acceptance criteria with values between 98.6-101.8 %. The results for the solution without SSP showed that percent recovery for all drugs are between the 101-110%, although the experimental concentrations are higher compared to the label concentration. It should not dismiss the fact that this sample contains a more complex than the QC solution matrix. Therefore, the presence of other possible interference like organic material or dissolved materials may contribute to increased average signals. The solution with SSP present diverse results, for the sulfa there is no evidence of removal by the suspended material as the percent recovery value was 103%. The fluoroquinolones recoveries on the other hand, were decreased to a concentration 4.55×10^{-5} M and 4.38×10^{-5} M, for Levo and Cipro respectively. This represent a decreased between 8-14% compared to the experimental concentration of 5.00×10^{-5} M. This behavior can be explained in terms of the ionizable functional groups that dictates which species are present in solution due to the pH of the water sample (Figure 48). Levo has pKa values of 5.45 and 6.20¹⁴⁹, meanwhile the pka for Cipro are 6.42 and 8.49.¹⁵⁰ The pH of surface waters typically this 6-8 units. In these circumstances Cipro it's in is neutral and therefore can experience hydrophobic attractions to the surface of the particulates suspended. This also explains

the reduction observed with Levo. In case of the Sulfa compound, the reagent used was the sodium salt. This in water exists as a negatively charged ion which experiences no attraction to the surface of suspended materials.

Table 13: Suspended Solids results for the analysis of “Quebrada Oro” sample

	Sulfa	Levo	Cipro
Experimental QC concentration (M)	4.99E-05	4.93E-05	5.09E-05
Theoretical QC concentration (M)	5.00E-05	5.00E-05	5.00E-05
Percent Recovery (%)	99.9	98.6	101.8
Experimental Results for the surface water sample			
Water without SSP concentration (M)	5.20 E-05	5.20E-05	5.59E-05
Percent Recovery (%)*	104	101	110
Water with SSP concentration (M)	5.16E-05	4.55E-05	4.38E-05
Percent Recovery (%)*	103	92	86
Experimental QC concentration (M)	4.99E-05	4.99E-05	5.09E-05
Percent removal**	N/A		

* Experimental Percent recovery was calculated using the Experimental QC concentration determined on row #3

** the percent calculated using the experimental QC concentration.

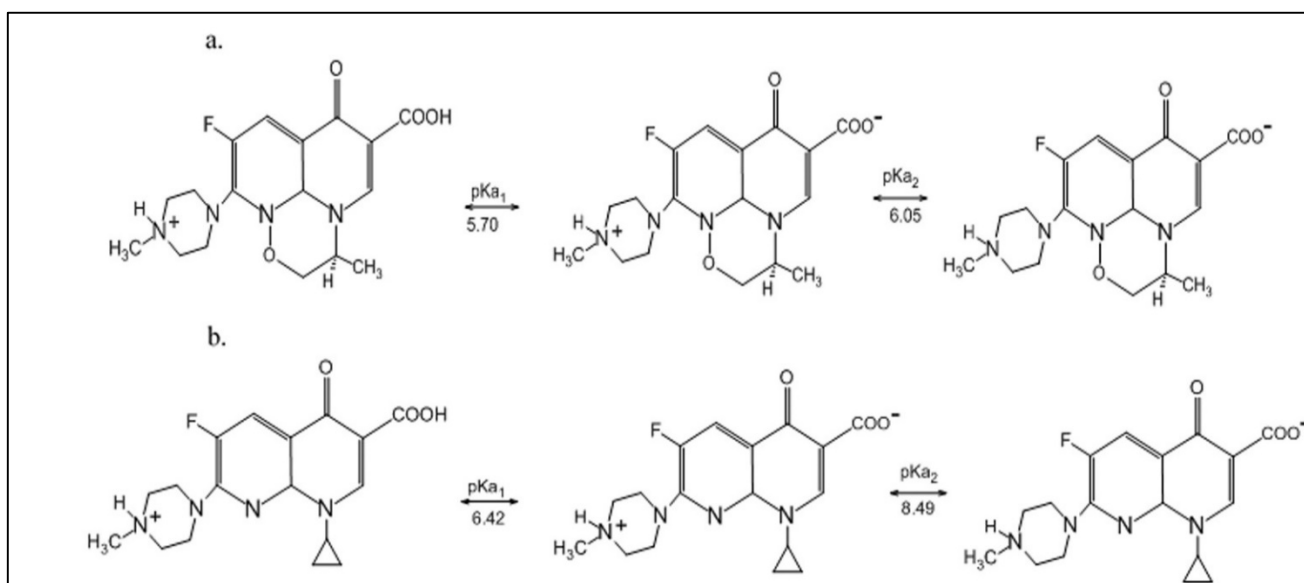


Figure 48: Acid Base Equilibria for: a. Levofloxacin and b. Ciprofloxacin

5.4.4-carboxybenzene sulfonamide HPLC determination

The inclusion of 4-carboxy in the methodology designed for the detection and quantification of antimicrobials drugs motivates a re-validation of the designed protocol. The major changes that need to be addressed was the selection of a new detection wavelength. According to the UV spectra (Figure 43) 4-carboxy has its maximum absorption at a wavelength close to 230 nm, but the Cipro and levo compounds does not absorb energy with the same intensity and the same behavior is observed for 4 carboxy at the actual analysis wavelength. In addition, due to the fact that we did not have an equipment that has a diode array detector available at that moment. The designed approach was to perform an analysis in which during the sample run the wavelength changes from the 230 nm to 286 nm. The rationale for this is the gap in time between the elution of sulfa and levo compounds. The 4 minutes window offers enough time to the UV detector to balance and get a stable baseline in order to detect effectively the rest of the compounds. This is not the common approach for chromatographic separations but the reliability of the method was tested with acceptable results. The chromatogram presented on Figure 48 demonstrates the effectiveness of the change in wavelength method. Because the 4-carboxy was not evaluated for the remediation experiments that will be discussed in the following sections, validation data of this new method is available on Appendix 2.

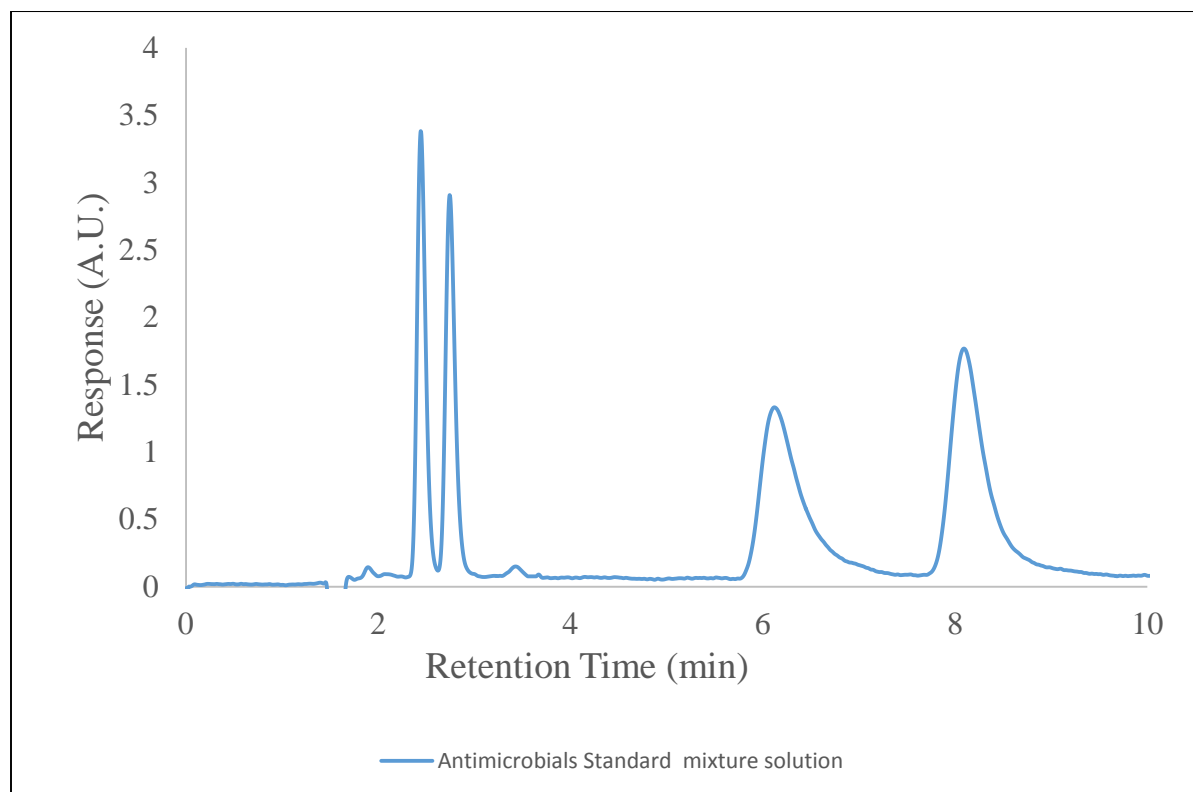


Figure 49: Antimicrobial standard mixture containing: 4-Carboxy, Sulfa, Levo and Cipro at 10^{-6} M range

5.5. Cerium Oxide nanoparticles for PPCPs remediation

The use of Cerium Oxide (CeO_2) nanoparticles over the years had been focused mostly on their use as therapeutic¹⁵¹, chemotherapy¹⁵², neurological¹⁵³ and pharmacological¹⁵⁴ agents. Nevertheless, new approaches had been used to bring a new dimension to the use of this nanoparticles for remediation purposes. He, L et.al proposed the synthesis of Cerium Oxide nanoparticles and report their use on certain dyes.¹⁵⁵ This group proposed that the mechanism of action is based on the catalytic degradation of the organic compounds by action of the CeO_2 material. Other groups reported the use of CeO_2 as excellent arsenic III and V adsorption capacity.¹⁵⁶ Meanwhile, recently it had been reported the use of this material in combination with active carbon for the removal of a selected group of chlorinated solvents.¹⁵⁷

The information presented suggest that this type of material could be used as a mitigation tool in the removal of antimicrobial drugs. The proposed design was to prepare a filter with certain amount of nanoparticles to evaluate the efficiency and loading capacity against each of the fluoroquinolones and the sulfa drug. This approach had the advantage the nanoparticles are confined on a certain area against the technique of releasing the material on the environment in which already had been reported the effects on certain aquatic ecosystems.¹⁵⁸ The experimental conditions, results for each of the drugs will be presented on the following section.

5.5.1. Experimental

CeO₂ nanoparticles were donated by Dr. Martha López, from the US Research Nanomaterial with the following specifications: purity CeO₂, 99.97%; particle size 10-30nm. Solvents, reagents and chromatographic conditions had been described on section 5.3.1. An amount of 0.01g was weighted by difference inside a 5 mL syringe that contains a PTFE disk at the bottom to avoid material loss. Figure 50 presents the filter setup.

25-30 mL of a 1.00×10^{-4} M solution of each Antimicrobial drug were discharged in volumes additions of 1.00 mL. Filtration process was done by gravity and the residual liquid was collected on a HPLC vial for further analysis.

Determination of the initial percent removal

For this experiment the rationale is to measure how much amount of drug can be removed by using a laboratory sample containing the drugs, a surface water sample spiked with a mixture of the drugs. Table 14 present the information in detail.

Table 14: Experimental conditions for the initial percent removal determination

SolutionID	Filter CeO ₂ amount (g)	Antimicrobial Concentration (M)
1	0.01	1.00 x 10 ⁻⁵ M
Surface Water “Quebrada Oro”	0.01	1.00 x 10 ⁻⁵ M

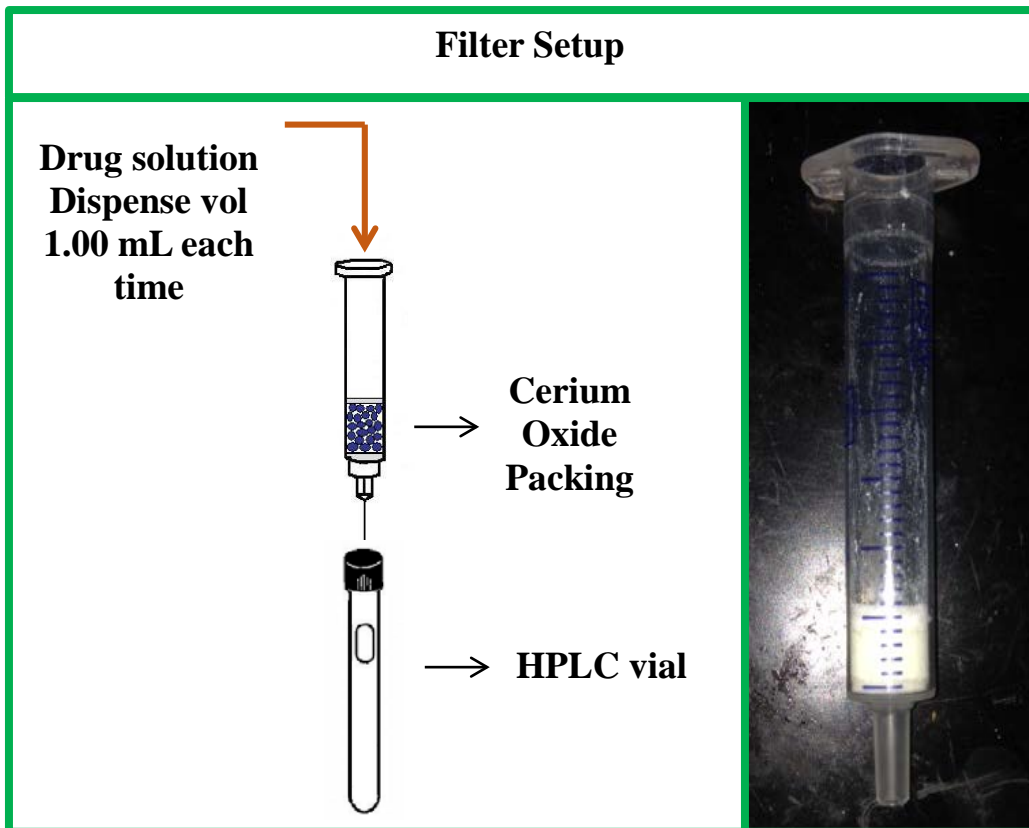


Figure 50: CeO₂ filter setup containing 0.01 g for antimicrobial removal evaluation

5.5.2. Results

This study was done to investigate the capacity of removal of the CeO₂ nanoparticles for the different antimicrobial compounds. This was a proof of concept study, the plots that this section refers are with the idea to measure of how effective could be the nanoparticle in the process of remediation. The results obtained are not final and conclusive because there are some other experimentation activities required to be done by the established protocols in order to get a complete understanding of the process involve.

The removal of the sulfa was tested and a loading capacity plot was prepared in order to determinate if the nanoparticles had an effect on that compound and how much concentration can be removed before saturation is observable. Saturation concentration was found to be 7.00×10^{-4} M (Figure51). The Chromatogram for that analysis present with illustration purposes (Figure 52) the difference between the first volume added and the subsequent additions for this drug. The other fluoroquinolones present higher removals as it can be appreciated on Levo (figure 53 and 54) in which the chromatogram show the removal of the drug from the first addition and across the several continuous addition until the last one. Levo saturation concentration was determined to be 2.10×10^{-3} M. Cipro (not showed) has a saturation concentration of 9.00×10^{-4} M.

The results presented supports the concept that the CeO₂. For each drug the initial percent removal was determined. This is the amount of drug removed based on the peak area of the analyte in the first volume (1.00×10^{-4} M) and the peak area of the same solution without been filtered. For this experiment the amount of cerium oxide was changed according to the amounts indicated on section 3.

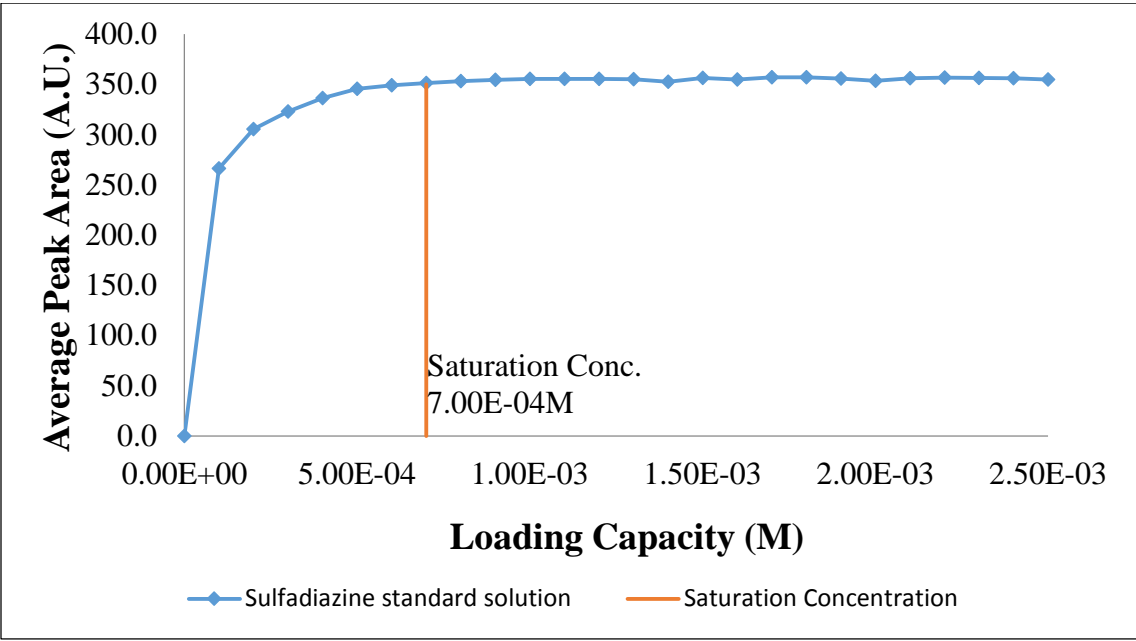


Figure 51: Loading plot for the 1.00 x10⁻⁴ M sulfa standard solution

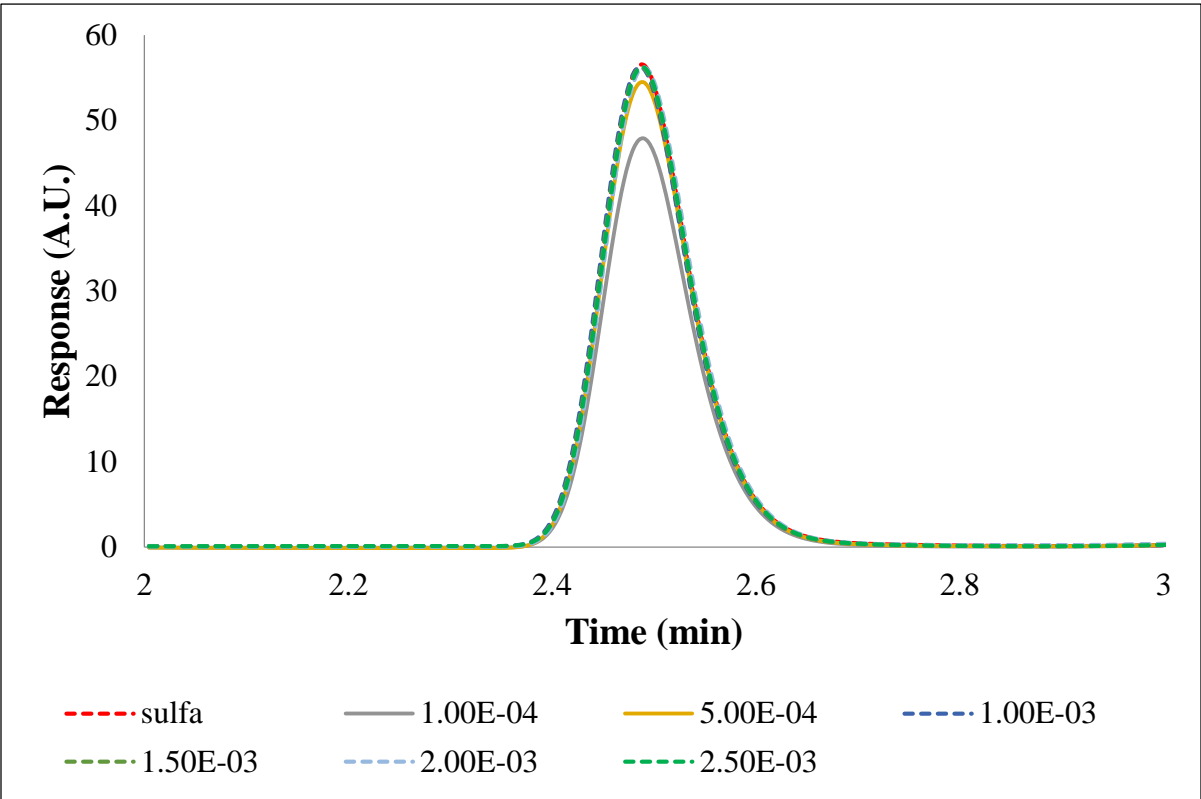


Figure 52: Sulfa chromatogram for the loading experiment.

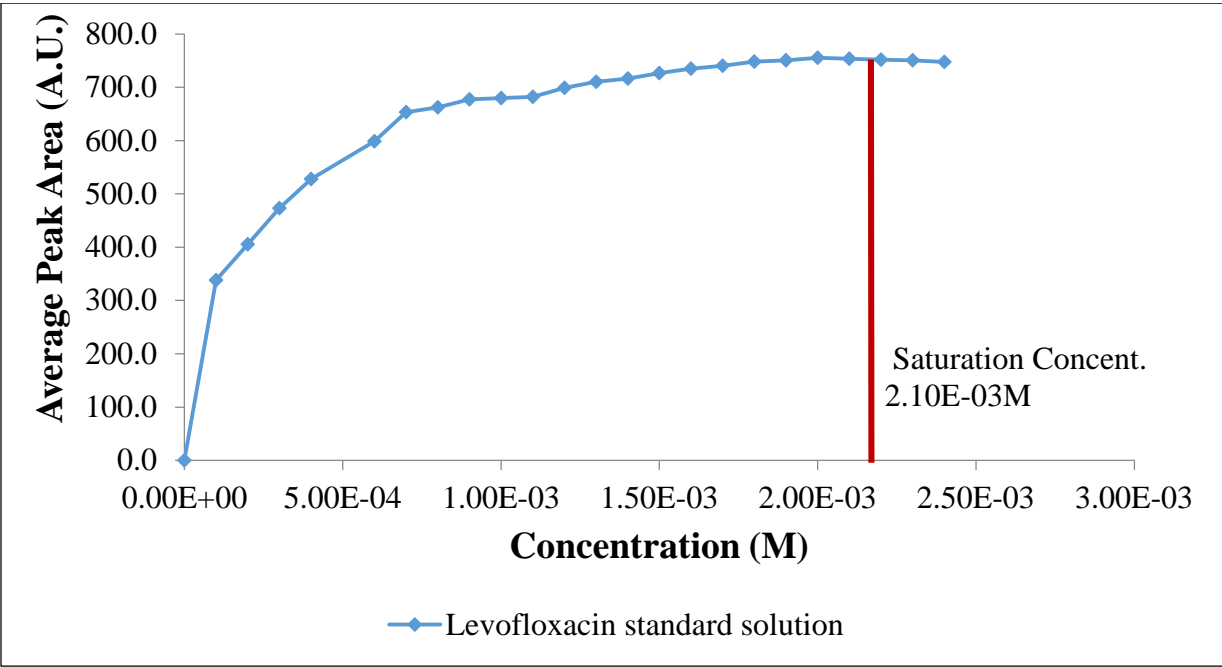


Figure 53: Loading plot for the 1.00 x10⁻⁴M sulfa standard solution

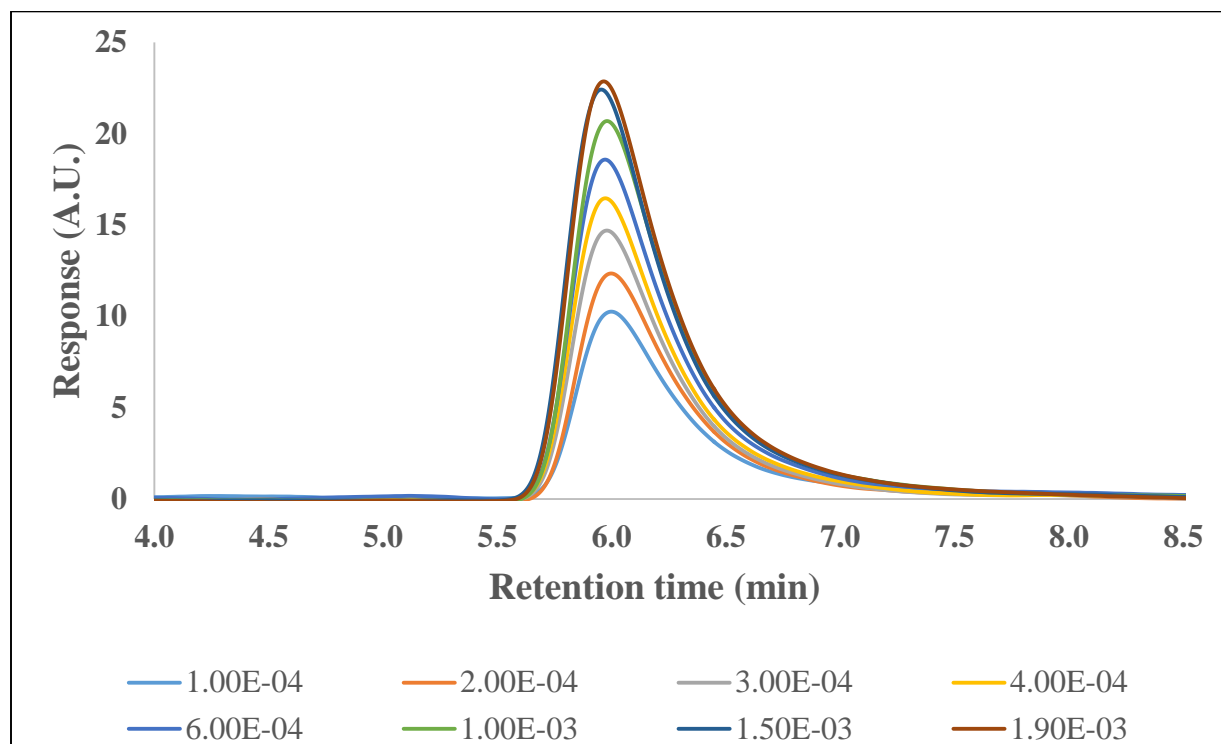


Figure 54: Levo chromatogram for the loading experiment.

Percent Removal Study:

The results of this study are presented on Figure 55. The sulfadiazine drug seems to be less affected by the nanoparticles. The percent of removal for this drug was 14.80%. Meanwhile when the sample matrix is more complicated and other factors like the presences of dissolved material, organic matter among other factors are present, the percent of removal is less than 1%. The fluoroquinolones behavior on a contrary is more consistent independent of the complex the matrix could be. For the laboratory sample the Levo removal was a 50.46%. In the surface water sample the Levo almost remain constant with a 49.89%. The Cipro is experience a change in its behavior when it is exposed to surface waters matrix, this time the removal decreased from 53.48% to 44.31%. This can be justified by the presence of suspended material like the case mentioned on the total suspended solids.

The results for this study confirm the effective use of CeO₂ nanoparticles as a remediation agent for the remediation of Pharmaceutical Agents in laboratory and surface waters samples. This findings supports the development of new strategies that could focus in the use of several transition metals nanoparticles for this remediation process. One of these new strategies is discussed on the following section.

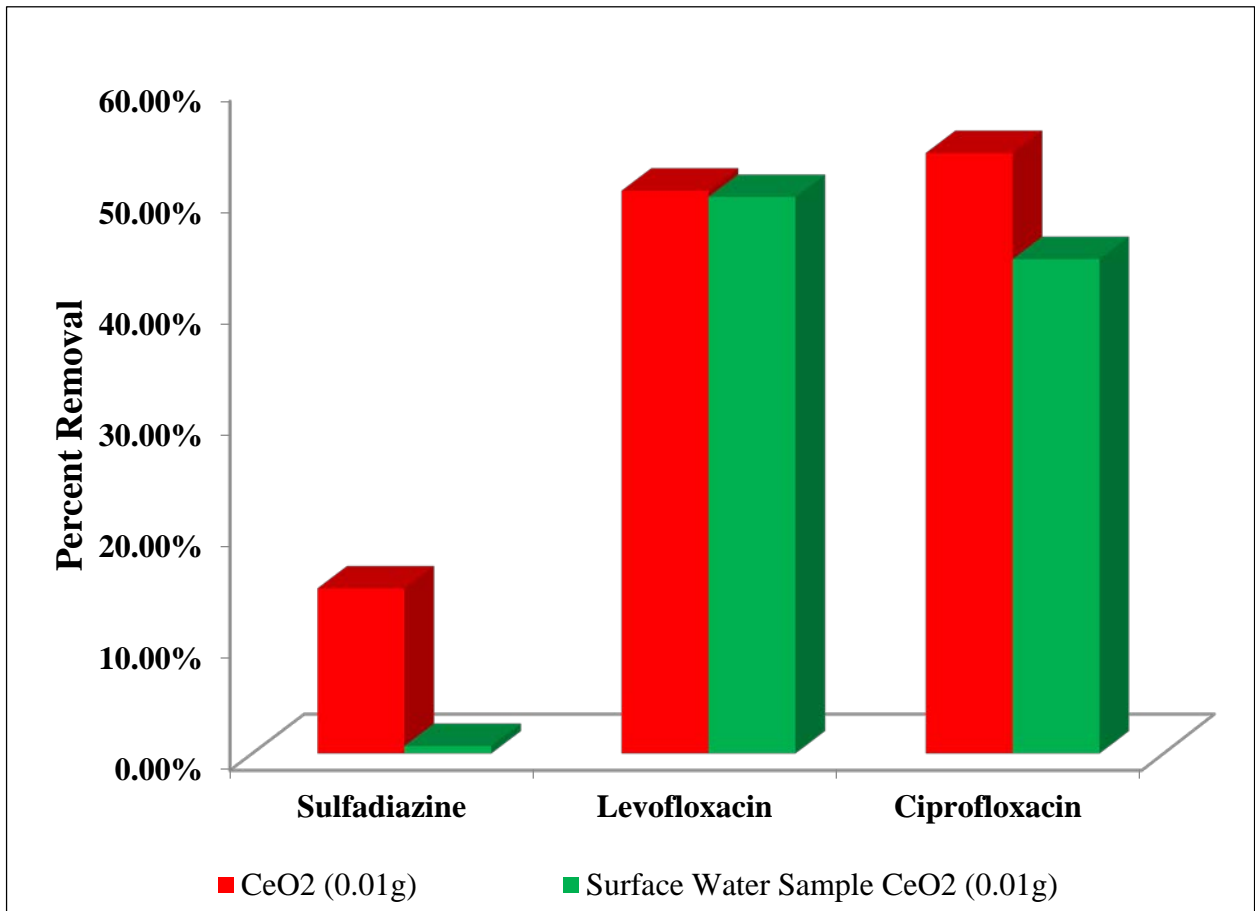


Figure 55: CeO₂ filter removal effect against laboratory and surface water samples.

5.6. New economical alternative for a nanoparticle synthesis

The coordination between metals and pharmaceutical agents is a process that had been studied for several years.¹⁵⁹ For this reason the development of new methodology that ensure fabrication of potential materials that can be used on any of the remediation process is more demanding. Nonetheless some of this materials can be purchased commercially the cost of them make more attractive the idea of in-site fabrication. Specially to reduce cost or to avoid unnecessary expenses on materials that at the end will no work for the intended use. This section describes the fabrication of a zinc sulfide nanoparticles using a simple method that use the light source and materials commonly found on a research laboratory.

There is empirical evidence of the binding preference of zinc nanoparticles to several fluoroquinolones.¹⁶⁰⁻¹⁶¹ The results strongly suggest, that the use of zinc sulfide nanoparticles could be more efficient to the removal of the studied pharmaceutical products. Also previous studies suggest the same behavior for the sulfonamides compounds.¹⁶² Photocatalytic activities of the Zinc Sulfide nanoparticles had been presented as an alternative for the degradation of some dyes.¹⁶³ The number of research studies performed gives a clear direction that the use of Zinc Sulfide nanoparticles could be successfully applied to the remediation and removal of several pharmaceutical products. The section is an extract of the publication and had been reproduced with the author's permission. Please refer to the Disclaimer note at the beginning of this chapter.

5.6.1. Introduction

Recently, we have devised an entirely new IR assisted controlled method for the synthesis of CdS nanoparticles by means of a kinetic approach using the well-known Stokes' law for a free body falling in a quiescent fluid.¹⁶⁴ The reaction is controlled by means of IR heating only at the surface of the reactants and the successive synthesis of nanoparticles was governed by Stokes' law. The detailed description of the method is given elsewhere.¹⁶⁵

A survey reveals that a large number of techniques for preparing ZnS nanoparticles have been applied by different workers such as solid state reaction¹⁶⁵, chemical methods¹⁶⁶⁻¹⁷², ball milling¹⁷³, sol-gel method, reverse micelle method¹⁷⁴, microwave assisted method¹⁷⁵⁻¹⁷⁸, and laser assisted method.^{175, 179} Infrared-assisted eco-friendly green chemistry based methods have been employed in organic chemistry¹⁸⁰⁻¹⁸³ but the infrared- assisted synthesis of inorganic nanoparticles has not been unveiled. Inspired from this, recently, we have synthesized IR assisted CdS nanoparticles by means of a kinetic approach using the well-known Stokes' law without using any surfactant, capping agent, or stirring.¹⁸⁴ In this present research work, we have synthesized ZnS nanoparticles by a simple controlled chemical co-precipitation method using IR radiation heating by means of a kinetic approach using the well-known Stokes' law for a free body falling in a quiescent and viscous fluid without using any surfactant or stirring during the reaction.

5.6.2. Materials and Experimental

ZnS nanoparticles were prepared through an experiment designed in accordance with Stokes' law for a free body falling in a quiescent fluid using IR radiation lamp as a heating source. The experiment mainly consists of a long beaker (~30 cm) for free falling of particles, IR radiation lamp (commercial) for heating the upper surface of the solution, and burette to add the anion (sulfur ions) solution to the cation (zinc ions) solution in a controlled manner. All the chemicals are of analytic grade and used without further purification. The entire process is carried out in distilled water for its inherent benefit of being straightforward and environmentally friendly. Nanoparticles of ZnS were made by controlled reaction through a chemical precipitation method using an aqueous solution of zinc nitrate ($\text{Zn}(\text{NO}_3)_2 \cdot 4\text{H}_2\text{O}$) and thioacetamide (CH_3CSNH_2). The reaction was controlled with the help of a drop-by-drop addition of the aqueous solution of thioacetamide (CH_3CSNH_2) into the aqueous solution of zinc nitrate ($\text{Zn}(\text{NO}_3)_2 \cdot 4\text{H}_2\text{O}$) in the presence of continuous IR lamp heating on the top as shown in schematic diagram figure 56. Firstly, the stock aqueous solutions of zinc nitrate ($\text{Zn}(\text{NO}_3)_2 \cdot 4\text{H}_2\text{O}$) (0.2M) and thioacetamide (CH_3CSNH_2) (0.2M) were made. The stock solution of zinc nitrate and thioacetamide was transferred to a long beaker (~30 cm) and a micro burette respectively. The aqueous solution of thioacetamide was added in a controlled manner to the solution of zinc nitrate using a burette drop-by-drop on a beaker wall in the presence of continuous IR lamp heating on the top of the beaker as illustrated in figure 56. A controlled precipitation reaction occurs on the top contact layer of solutions when the cation and an anion aqueous solutions react on the upper surface (top layer) in the presence of IR radiation¹⁸⁴ to form an insoluble ZnS solid as a precipitate in the solution. As a result, the

nanoparticles of ZnS float down to the bottom of the long beaker following Stokes' law. The process is continuous as synthesis starts at the top and moves downward under gravity in the quiescent and viscous solution according to Stokes' law. The rate of reaction is very slow so the process of formation of nanoparticles takes a few days and after completing the process the nanoparticles accumulate at the bottom of beaker in the form of a precipitate. Finally, the precipitate was decanted and dried so as to have a final product for further characterization.

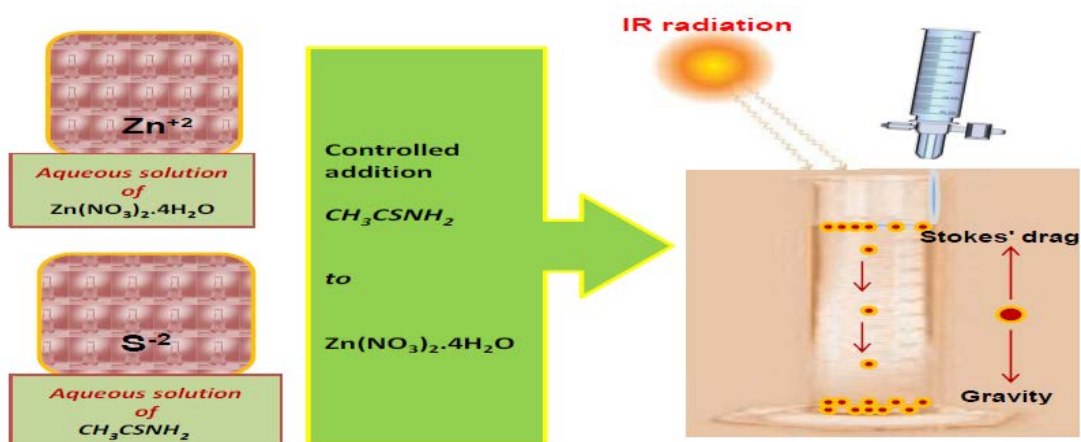


Figure 56: Schematic illustration of controlled IR assisted chemical precipitation method based on Stokes' law for a free body falling in a quiescent and viscous fluid as used for synthesis of ZnS nanoparticles.

5.6.3. Optical Properties:

Semiconductors behave very differently, in comparison with bulk, when their crystal sizes are reduced down to the order of a few nanometers. One of the most significant characteristic in these materials is the variation of the band gap when the sizes of nanocrystal decrease below the Bohr exciton radius (a_B). The optical absorption spectroscopic technique is used to study the electronic band structure of semiconductors and metals for determination of their optical properties. Optical absorption spectrum of ZnS samples were measured at room temperature using a HITACHI-U 3400 UV-Vis Spectrophotometer. The as-prepared ZnS nano powder that was suspended in glycerol using a magnetic stirrer and the optical absorption spectra was recorded at room temperature in the wavelength range 300-500 nm as shown in Fig.57.

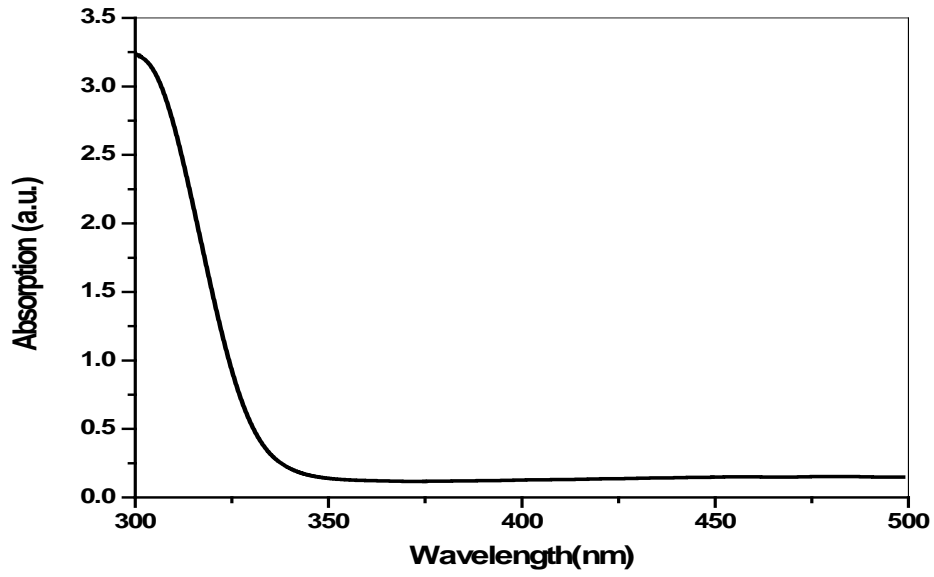


Figure 57: Absorption spectra of as-prepared ZnS nanocrystals.

The absorption spectra shows the optical absorption coefficient increases sharply at lower wavelength, which is a sign of the narrower size distribution of the ZnS nanoparticles. Blue shifting of the absorption peak (absorption edge at about 325 nm) is due to quantum confinement of the excitons present in the sample resulting in a more discrete energy of the spectrum of individual nanoparticles. Optical excitation of electrons across the band gap is a strongly allowed transition, and this causes a sharp increase in the absorbance at the wavelength corresponding to the optical energy band gap.

5.6.4. X-Ray Analysis:

Figure 58, shows the XRD pattern of ZnS nanoparticles at room temperature. From this figure, it is clear that as-prepared ZnS nanoparticles have a high degree of crystallographic orientation. The peak broadening in the XRD pattern of ZnS clearly indicates the formation of ZnS nanocrystals of small size. The higher intensity peaks at around 28.95° , 48.29° and 57.15° reveals a cubic (zinc blende) lattice structure of ZnS, which were consistent with the literature data of JCPDS card No. 05-0566. These peaks could be easily assigned to the planes (111), (220) and (311) respectively of the cubic phase.¹⁸⁵ Two low intensity peaks at 70.62° and 77.55° are also the characteristics of cubic (400) and (311) planes respectively. From the XRD patterns, it is clear that the ZnS nanoparticles are polycrystalline in nature having a cubic (zinc blende) lattice structure. The d_{hkl} values (distances between successive lattice planes) of the as-prepared ZnS nanocrystals were calculated from well-known Bragg relation:

$$2d_{hkl} \sin\theta = n\lambda, \quad (11)$$

where λ is the wavelength of X-ray radiation source, θ is the Bragg's angle of incidence and the integer n is the order of the corresponding reflection. The lattice constant 'a' of the ZnS crystallites was determined from the XRD patterns (Figure 58) using the following formula:

$$d_{hkl} = \frac{a}{\sqrt{h^2+k^2+l^2}} \quad (12)$$

Lattice constants of as-prepared ZnS nanocrystals are given in Table 15. The value of lattice constant 'a' of as-prepared ZnS nanocrystals is in good agreement with the standard value for ZnS cubic (zinc blende) lattice structure phase ($a = 5.398 \text{ \AA}$).

Table 15: Lattice constants as-prepared ZnS nanocrystals

S.No.	Plane (hkl)	$d_{hkl} (\text{Å}^\circ)$	a (Å $^\circ$)	$a_{\text{average}} (\text{Å}^\circ)$
1.	(111)	3.08	5.33	5.33
2.	(220)	1.88	5.32	
3.	(311)	1.61	5.33	
4.	(400)	1.33	5.32	
5.	(331)	1.23	5.36	

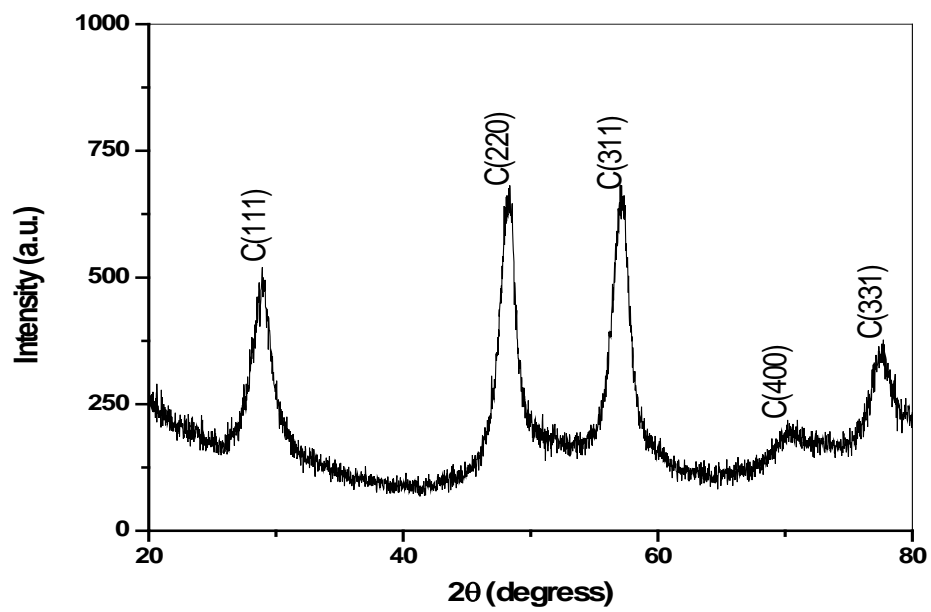


Fig.58: XRD pattern of as-prepared ZnS nanoparticles.

Chapter #6: Concluding Remarks and Future Works

The use of SERS as an identification technique had proven to be successful over the years. Based on the generation of Surface Resonance Plasmon it has overcome the major drawbacks of their parent technique Raman. The need to design and development new plasmonic substrates with new features that bring better performance and more sensitive and reproducible signals are more demanding these days.

Bio Inspired materials offer a unique group of characteristics that are the result of years of continuous evolution over the years. For that reason, the development of SERS substrates with these characteristics is possible. In combination with lithographic techniques the fabrication of arrays with specific morphologies, aspects ratios gap and height are possible. In addition, the capacity of cloning these structures into large areas of significant enhancement. Chapter #3 presented the fabrication and plasmonic evaluation of nine bio inspired arrays. Most of the Bio-Inspired nano composites were successfully fabricated ensuring high effectiveness of the EBL technique in the fabrication of nano complex arrangements. The optical capabilities of these substrates were also evaluated. Analysis of the nine proposed arrays demonstrated better performance when the 632 nm laser source was used. Acacia leaf, asian liliun sunflower and orchid substrates resulted on the most prominent substrates with EF that are in the 8.0×10^7 to 4.5×10^9 range. The optimum pillar height for most of the bio-inspired nano composites were in the 159-195 nm range. In addition sunflower and orchid patterns demonstrated to be the most promising substrates for laboratory-controlled analysis. In addition both substrates showed an acceptable analytical response to less energy laser sources. This proves the tuning capability that

these substrates can have and their use with chemical species that may be thermally unstable, thus allowing their detection by SERS.

These research also provided the fabrication of a new generation of substrates that were characterized in terms of their morphology, height and gap ready to evaluate their plasmonics properties. This also provides a new tool for the identification of PPCPs. The complete characterization of this new generation particles is described on the appendix 1. The evaluation of these new arrays with the different antimicrobial drugs could be an interesting area of future research for this type of substrate.

In addition to lithographic Substrates, a series of fabrication tools are available for the development of less expensive substrates but with the capacity of generate good Raman signal. The substrates fabricated with PDMS have the drawbacks of being affected by thermal degradation for the use with high energy sources. Also, the possible photolytic destruction of the analyte by the continuous irradiation lead to irreproducible measurements that reduce the use of SERS as an analytical tool for the quantitation of several compounds.

Chapter #4 presented a new group of strategies to develop a new methodology translational/rotational device and a new protocol for the quantitation of two fluoroquinolones and a sulfonamide. The design and fabrication of a Portable USB-DC Sample Translational Device was successfully tested to the detection of Antimicrobial drugs. Adsorption time, pH and speed results demonstrate the suitable conditions for the analysis of those compounds. Precision results demonstrate acceptable results for the use of portable device. Quantitative model was developed using Partial Least Squares treatment.

The continuous need for new remediation alternatives to remove environmental pollutants creates

a constant demand for new approaches that can contribute to the solution. To provide an alternative to this problematic. Chapter #5 presents the application of Cerium Oxide nanoparticles for the effective elimination of the Ciprofloxacin, Levofloxacin and Sulfadiazine. The results demonstrate the capability of these nanoparticles to remove near the 50% of the initial concentration of the different fluoroquinolones. Future research projects could consider to make an adsorption study for these particles in order to determine the mechanisms of action and their capability of being effective in the removal of other drugs.

ZnS nanoparticles were effectively synthesized by an infrared (IR) radiation assisted and Stokes' law based new controlled bottom-up approach without using any capping agent or stirring. The structural and optical characterization of the as-prepared ZnS nanoparticles confirms the nanosize formation. The initial results of this study show the importance of their synthesis approach and further work to expose the control of size, shape and orientation of the nanoparticles by optimizing the process parameters is in progress. The use of this nanoparticles in the removal of the antimicrobial drugs should be explored.

Lastly, a new chromatographic method for the simultaneous determination of four compounds was successfully developed and validated. A new dimension of this method using a variable wavelength was also developed and the validation results presented on Appendix II. This new method analyzes each group of drugs at the maximum wavelength of intensity using a variable wavelength detector. The method that was not tested due to problems with the unstable baseline. The addition of a fifth drug is still possible because there is a gap between the last sulfonamide and the first fluoroquinolones to elute.

References

1. Furtak, T.; Chang, R., Surface Enhanced Raman Scattering Plenum Press. *New York* **1981**.
2. Katrin, K.; Harald, K.; Irving, I.; Ramachandra, R. D.; Michael, S. F., Surface-enhanced Raman scattering and biophysics. *J. Phys.: Condens. Matter* **2002**, *14* (18), R597.
3. Vo-Dinh, T., Surface-enhanced Raman spectroscopy using metallic nanostructures. *TrAC, Trends Anal. Chem.* **1998**, *17* (8–9), 557-582.
4. Olavarría-Fullerton, J. Development Of Plasmonic Nanostructures As Raman Sensors For The Detection Of Arsenic Antimicrobials. University of Puerto Rico, Mayagüez, 2013.
5. Campion, A.; Kambhampati, P., Surface-enhanced Raman scattering. *Chem. Soc. Rev.* **1998**, *27* (4), 241-250.
6. Fleischmann, M.; Hendra, P. J.; McQuillan, A. J., Raman spectra of pyridine adsorbed at a silver electrode. *Chem. Phys. Lett.* **1974**, *26* (2), 163-166.
7. Jeanmaire, D. L.; Van Duyne, R. P., Surface Raman spectroelectrochemistry: Part I. Heterocyclic, aromatic, and aliphatic amines adsorbed on the anodized silver electrode. *J. Electroanal. Chem. Interfacial Electrochem.* **1977**, *84* (1), 1-20.
8. Albrecht, M. G.; Creighton, J. A., Anomalous intense Raman spectra of pyridine at a silver electrode. *J. Am. Chem. Soc.* **1977**, *99* (15), 5215-5217.
9. Sharma, B.; Frontiera, R. R.; Henry, A.-I.; Ringe, E.; Van Duyne, R. P., SERS: materials, applications, and the future. *Mater. Today* **2012**, *15* (1), 16-25.
10. Alvarez-Puebla, R.; Liz-Marzan, L., Environmental applications of plasmon assisted Raman scattering. *Energy & Environmental Science* **2010**, *3* (8), 1011-1017.
11. Izake, E. L., Forensic and homeland security applications of modern portable Raman spectroscopy. *Forensic Sci. Int.* **2010**, *202* (1), 1-8.
12. Stoddart, P.; White, D., Optical fibre SERS sensors. *Anal. Bioanal. Chem.* **2009**, *394* (7), 1761-1774.
13. Kneipp, K.; Dasari, R. R.; Wang, Y., Near-infrared surface-enhanced Raman scattering (NIR SERS) on colloidal silver and gold. *Appl. Spectrosc.* **1994**, *48* (8), 951-955.
14. Lee, P. C.; Meisel, D., Adsorption and surface-enhanced Raman of dyes on silver and gold sols. *J. Phys. Chem.* **1982**, *86* (17), 3391-3395.
15. Hutter, E.; Fendler, J. H.; Roy, D., Surface Plasmon Resonance Studies of Gold and Silver Nanoparticles Linked to Gold and Silver Substrates by 2-Aminoethanethiol and 1,6-Hexanedithiol. *J. Phys. Chem. B* **2001**, *105* (45), 11159-11168.
16. Li, L.; Hutter, T.; Finnemore, A. S.; Huang, F. M.; Baumberg, J. J.; Elliott, S. R.; Steiner, U.; Mahajan, S., Metal oxide nanoparticle mediated enhanced Raman scattering and its use in direct monitoring of interfacial chemical reactions. *Nano Lett.* **2012**, *12* (8), 4242-4246.
17. McNay, G.; Eustace, D.; Smith, W. E.; Faulds, K.; Graham, D., Surface-enhanced Raman scattering (SERS) and surface-enhanced resonance Raman scattering (SERRS): a review of applications. *Appl. Spectrosc.* **2011**, *65* (8), 825-837.
18. Cao, Y.; Zhang, J.; Yang, Y.; Huang, Z.; Long, N. V.; Fu, C., Engineering of SERS substrates based on noble metal nanomaterials for chemical and biomedical applications. *Appl. Spectrosc. Rev.* **2015**, *50* (6), 499-525.

19. Creighton, J., Surface Raman electromagnetic enhancement factors for molecules at the surface of small isolated metal spheres: The determination of adsorbate orientation from SERS relative intensities. *Surf. Sci.* **1983**, *124* (1), 209-219.
20. Campion, A.; Ivanecy III, J.; Child, C.; Foster, M., On the mechanism of chemical enhancement in surface-enhanced Raman scattering. *J. Am. Chem. Soc.* **1995**, *117* (47), 11807-11808.
21. Fateixa, S.; Nogueira, H. I.; Trindade, T., Hybrid nanostructures for SERS: materials development and chemical detection. *Phys. Chem. Chem. Phys.* **2015**, *17* (33), 21046-21071.
22. Jensen, L.; Aikens, C. M.; Schatz, G. C., Electronic structure methods for studying surface-enhanced Raman scattering. *Chem. Soc. Rev.* **2008**, *37* (5), 1061-1073.
23. Olavarría-Fullerton, J.; Velez, R. A.; Wells, S.; Sepaniak, M. J.; Hernández-Rivera, S. P.; De Jesús, M. A., Design and Characterization of Hybrid Morphology Nanoarrays as Plasmonic Raman Probes for Antimicrobial Detection. *Appl. Spectrosc.* **2013**, *67* (11), 1315-1322.
24. Le Ru, E.; Etchegoin, P., Principles of surface enhanced Raman scattering and related plasmonic effects. Elsevier, Amsterdam: 2009.
25. Zeng, J.; Jia, H.; An, J.; Han, X.; Xu, W.; Zhao, B.; Ozaki, Y., Preparation and SERS study of triangular silver nanoparticle self-assembled films. *J. Raman Spectrosc.* **2008**, *39* (11), 1673-1678.
26. Zoppi, A.; Lofrumento, C.; Castellucci, E. M.; Sciau, P., Al-for-Fe substitution in hematite: the effect of low Al concentrations in the Raman spectrum of Fe₂O₃. *J. Raman Spectrosc.* **2008**, *39* (1), 40-46.
27. Fan, M.; Brolo, A. G., Silver nanoparticles self assembly as SERS substrates with near single molecule detection limit. *Phys. Chem. Chem. Phys.* **2009**, *11* (34), 7381-7389.
28. Ratner, B. D.; Hoffman, A. S.; Schoen, F. J.; Lemons, J. E., *Biomaterials science: an introduction to materials in medicine*. Academic press: 2004.
29. Mattox, D. M., *Handbook of physical vapor deposition (PVD) processing*. William Andrew: 2010.
30. Guillot, N.; de la Chapelle, M. L., Lithographed nanostructures as nanosensors. *J. Nanophotonics* **2012**, *6* (1), 064506-1-064506-28.
31. Yoshiiwa, M.; Kageyama, H.; Shirota, Y.; Wakaya, F.; Gamo, K.; Takai, M., Novel class of low molecular-weight organic resists for nanometer lithography. *Appl. Phys. Lett.* **1996**, *69*, 2605.
32. Fujita, J.; Watanabe, H.; Ochiai, Y.; Manako, S.; Tsai, J. S.; Matsui, S., Sub-10 nm lithography and development properties of inorganic resist by scanning electron beam. *Appl. Phys. Lett.* **1995**, *66*, 3064.
33. Robinson, A. P. G.; Palmer, R. E.; Tada, T.; Kanayama, T.; Preece, J. A., A Fullerene derivative as an electron beam resist for nanolithography. *Appl. Phys. Lett.* **1998**, *72*, 1302.
34. Robinson, A.; Palmer, R. E.; Tada, T.; Allen; Allen, M. T.; Preece, J. A.; Harris, K., 10 nm scale electron beam lithography using a triphenylene derivative as a negative/positive tone resist. *J. Phys. D: Appl. Phys.* **1999**, *32*.
35. Grigorescu, A. E.; Hagen, C. W., Resists for sub-20-nm electron beam lithography with a focus on HSQ: state of the art. *Nanotechnology* **2009**, *V20*, 29, 292001-292032.

36. Wilkinson, C. D. W.; Rhaman, M., *Dry etching and sputtering*. Department of Electronics and Electrical Engineering and Department of Physics and Astronomy: University of Glasgow, 2003.
37. Appelbaum, P. C.; Hunter, P. A., The fluoroquinolone antibacterials: past, present and future perspectives. *Int. J. Antimicrob. Agents* **2000**, *16* (1), 5-15.
38. Shen, Q.; Jin, R.; Xue, J.; Lu, Y.; Dai, Z., Analysis of trace levels of sulfonamides in fish tissue using micro-scale pipette tip-matrix solid-phase dispersion and fast liquid chromatography tandem mass spectrometry. *Food Chem.* **2016**, *194*, 508-515.
39. Croisier, D.; Etienne, M.; Bergoin, E.; Charles, P.-E.; Lequeu, C.; Piroth, L.; Portier, H.; Chavanet, P., Mutant Selection Window in Levofloxacin and Moxifloxacin Treatments of Experimental Pneumococcal Pneumonia in a Rabbit Model of Human Therapy. *Antimicrob. Agents Chemother.* **2004**, *48* (5), 1699-1707.
40. Wagenlehner, F. M. E.; Münch, F.; Pilatz, A.; Bärman, B.; Weidner, W.; Wagenlehner, C. M.; Straubinger, M.; Blenk, H.; Pfister, W.; Kresken, M.; Naber, K. G., Urinary Concentrations and Antibacterial Activities of Nitroxoline at 250 Milligrams versus Trimethoprim at 200 Milligrams against Uropathogens in Healthy Volunteers. *Antimicrob. Agents Chemother.* **2014**, *58* (2), 713-721.
41. Radi, A.; El-Sherif, Z., Determination of levofloxacin in human urine by adsorptive square-wave anodic stripping voltammetry on a glassy carbon electrode. *Talanta* **2002**, *58* (2), 319-324.
42. Cribb, A. E.; Lee, B. L.; Trepanier, L. A.; Spielberg, S., Adverse reactions to sulphonamide and sulphonamide-trimethoprim antimicrobials. *Adverse Drug React. Toxicol. Rev.* **1996**, *15* (1), 9.
43. Woo, T. M.; Robinson, M. V., *Pharmacotherapeutics for Advanced Practice Nurse Prescribers*. F. A. Davis Company: 2015.
44. Liu, F.-F.; Zhao, J.; Wang, S.; Xing, B., Adsorption of sulfonamides on reduced graphene oxides as affected by pH and dissolved organic matter. *Environ. Pollut.* **2016**, *210*, 85-93.
45. Supuran, C. T.; Scozzafava, A.; Conway, J., *Carbonic anhydrase: its inhibitors and activators*. CRC Press: 2004; Vol. 1.
46. Finland, M.; Strauss, E.; Peterson, O. L., Sulfadiazine: therapeutic evaluation and toxic effects on four hundred and forty-six patients. *Jama* **1984**, *251* (11), 1467-1474.
47. Heuer, H.; Smalla, K., Manure and sulfadiazine synergistically increased bacterial antibiotic resistance in soil over at least two months. *Environ. Microbiol.* **2007**, *9* (3), 657-666.
48. Sukul, P.; Lamshöft, M.; Zühlke, S.; Spiteller, M., Sorption and desorption of sulfadiazine in soil and soil-manure systems. *Chemosphere* **2008**, *73* (8), 1344-1350.
49. Dowling, A. P., Development of nanotechnologies. *Mater. Today* **2004**, *7* (12), 30-35.
50. Wilson, B. A.; Smith, V. H.; deNoyelles, F.; Larive, C. K., Effects of Three Pharmaceutical and Personal Care Products on Natural Freshwater Algal Assemblages. *Environ. Sci. Technol.* **2003**, *37* (9), 1713-1719.
51. Ferguson, P. J.; Bernot, M. J.; Doll, J. C.; Lauer, T. E., Detection of pharmaceuticals and personal care products (PPCPs) in near-shore habitats of southern Lake Michigan. *Sci. Total Environ.* **2013**, *458-460*, 187-196.

52. Blair, B. D.; Crago, J. P.; Hedman, C. J.; Klaper, R. D., Pharmaceuticals and personal care products found in the Great Lakes above concentrations of environmental concern. *Chemosphere* **2013**, *93* (9), 2116-2123.
53. Mutiyar, P. K.; Mittal, A. K., Pharmaceuticals and Personal Care Products (PPCPs) Residues in Water Environment of India: A Neglected but Sensitive Issue.
54. Peng, X.; Tan, J.; Tang, C.; Yu, Y.; Wang, Z., Multiresidue determination of fluoroquinolone, sulfonamide, trimethoprim, and chloramphenicol antibiotics in urban waters in China. *Environ. Toxicol. Chem.* **2008**, *27* (1), 73-79.
55. Oulton, R. L.; Kohn, T.; Cwiertny, D. M., Pharmaceuticals and personal care products in effluent matrices: a survey of transformation and removal during wastewater treatment and implications for wastewater management. *J. Environ. Monit.* **2010**, *12* (11), 1956-1978.
56. Reif, R.; Santos, A.; Judd, S. J.; Lema, J. M.; Omil, F., Occurrence and fate of pharmaceutical and personal care products in a sewage treatment works. *J. Environ. Monit.* **2011**, *13* (1), 137-144.
57. Tratnyek, P. G.; Johnson, R. L., Nanotechnologies for environmental cleanup. *Nano Today* **2006**, *1* (2), 44-48.
58. Verlicchi, P.; Al Aukidy, M.; Zambello, E., Occurrence of pharmaceutical compounds in urban wastewater: Removal, mass load and environmental risk after a secondary treatment—A review. *Sci. Total Environ.* **2012**, *429*, 123-155.
59. Ratola, N.; Cincinelli, A.; Alves, A.; Katsoyiannis, A., Occurrence of organic microcontaminants in the wastewater treatment process. A mini review. *J. Hazard. Mater.* **2012**, *239-240*, 1-18.
60. Li, X.; Zheng, W.; Kelly, W. R., Occurrence and removal of pharmaceutical and hormone contaminants in rural wastewater treatment lagoons. *Sci. Total Environ.* **2013**, *445*, 22-28.
61. Cortinas, I.; Field, J. A.; Kopplin, M.; Garbarino, J. R.; Gandolfi, A. J.; Sierra-Alvarez, R., Anaerobic biotransformation of roxarsone and related N-substituted phenylarsonic acids. *Environ. Sci. Technol.* **2006**, *40* (9), 2951-2957.
62. Jackson, B. P.; Bertsch, P. M., Determination of arsenic speciation in poultry wastes by IC-ICP-MS. *Environ. Sci. Technol.* **2001**, *35* (24), 4868-4873.
63. Luo, S.-C.; Sivashanmugan, K.; Liao, J.-D.; Yao, C.-K.; Peng, H.-C., Nanofabricated SERS-active substrates for single-molecule to virus detection in vitro: A review. *Biosens. Bioelectron.* **2014**, *61*, 232-240.
64. Xu, X.; Kim, K.; Liu, C.; Fan, D., Fabrication and Robotization of Ultrasensitive Plasmonic Nanosensors for Molecule Detection with Raman Scattering. *Sensors* **2015**, *15* (5), 10422.
65. Shiohara, A.; Wang, Y.; Liz-Marzán, L. M., Recent approaches toward creation of hot spots for SERS detection. *J. Photochem. Photobiol., C* **2014**, *21*, 2-25.
66. Crozier, K. B.; Zhu, W.; Chu, Y.; Wang, D.; Banaee, M., Lithographically-Fabricated SERS Substrates: Double Resonances, Nanogaps, and Beamed Emission. In *Frontiers of Surface-Enhanced Raman Scattering*, John Wiley & Sons, Ltd: 2014; pp 219-241.
67. Sharma, B.; Fernanda Cardinal, M.; Kleinman, S. L.; Greeneltch, N. G.; Frontiera, R. R.; Blaber, M. G.; Schatz, G. C.; Van Duyne, R. P., High-performance SERS substrates: Advances and challenges. *MRS Bulletin* **2013**, *38* (08), 615-624.

68. Ringe, E.; Langille, M. R.; Sohn, K.; Zhang, J.; Huang, J.; Mirkin, C. A.; Van Duyne, R. P.; Marks, L. D., Plasmon Length: A Universal Parameter to Describe Size Effects in Gold Nanoparticles. *J. Phys. Chem. Lett.* **2012**, *3* (11), 1479-1483.
69. Gu, Y.; Li, H.; Xu, S.; Liu, Y.; Xu, W., Evanescent field excited plasmonic nano-antenna for improving SERS signal. *Phys. Chem. Chem. Phys.* **2013**, *15* (37), 15494-15498.
70. Wells, S. M.; Retterer, S. D.; Oran, J. M.; Sepaniak, M. J., Controllable Nanofabrication of Aggregate-like Nanoparticle Substrates and Evaluation for Surface-Enhanced Raman Spectroscopy. *ACS Nano* **2009**, *3* (12), 3845-3853.
71. Judith, L.; Sergey, M. N.; Luis, M. L.-M., Sensing using plasmonic nanostructures and nanoparticles. *Nanotechnology* **2015**, *26* (32), 322001.
72. Enzo Di Fabrizio, F. G., Michela Perrone Donnorso, Manohar Chirumamilla Chowdary, Ermanno Miele, Maria Laura Coluccio, Rosanna La Rocca, Rosaria Brescia, Roman Krahné, Gobind Das, Francesco De Angelis, Carlo Liberale, Andrea Toma, Luca Razzari, Liberato Manna and Remo Proietti Zaccaria, Nanoparticles and Nanostructures for Biophotonic Applications. In *The Delivery of Nanoparticles*, Dr. Abbass A. Hashim (Ed.), r. A. A. H. E., Ed. InTech: 2012; pp 293-316.
73. Petryayeva, E.; Krull, U. J., Localized surface plasmon resonance: Nanostructures, bioassays and biosensing—A review. *Anal. Chim. Acta* **2011**, *706* (1), 8-24.
74. Kang, G.; Matikainen, A.; Stenberg, P.; Färm, E.; Li, P.; Ritala, M.; Vahimaa, P.; Honkanen, S.; Tan, X., High Aspect-Ratio Iridium-Coated Nanopillars for Highly Reproducible Surface-Enhanced Raman Scattering (SERS). *ACS Appl. Mater. Interfaces* **2015**, *7* (21), 11452-11459.
75. Yang, J.; Li, J. B.; Gong, Q. H.; Teng, J. H.; Hong, M. H., High aspect ratio SiNW arrays with Ag nanoparticles decoration for strong SERS detection. *Nanotechnology* **2014**, *25* (46), 465707.
76. Sepúlveda, B.; Angelomé, P. C.; Lechuga, L. M.; Liz-Marzán, L. M., LSPR-based nanobiosensors. *Nano Today* **2009**, *4* (3), 244-251.
77. Toma, A.; Chiappe, D.; Massabò, D.; Boragno, C.; Buatier de Mongeot, F., Self-organized metal nanowire arrays with tunable optical anisotropy. *Appl. Phys. Lett.* **2008**, *93* (16), 163104.
78. Schmidt, M. S.; Hübner, J.; Boisen, A., Large Area Fabrication of Leaning Silicon Nanopillars for Surface Enhanced Raman Spectroscopy. *Adv. Opt. Mater.* **2012**, *24* (10), OP11-OP18.
79. Wells, S. M.; Polemi, A.; Lavrik, N. V.; Shuford, K. L.; Sepaniak, M. J., Efficient disc on pillar substrates for surface enhanced Raman spectroscopy. *Chem. Commun.* **2011**, *47* (13), 3814-3816.
80. Li, J.; Chen, C.; Jans, H.; Xu, X.; Verellen, N.; Vos, I.; Okumura, Y.; Moshchalkov, V. V.; Lagae, L.; Van Dorpe, P., 300 nm Wafer-level, ultra-dense arrays of Au-capped nanopillars with sub-10 nm gaps as reliable SERS substrates. *Nanoscale* **2014**, *6* (21), 12391-12396.
81. Gartia, M. R.; Xu, Z.; Behymer, E.; Nguyen, H.; Britten, J. A.; Larson, C.; Miles, R.; Bora, M.; Chang, A. S.; Bond, T.; Liu, G. L., Rigorous Surface Enhanced Raman Spectral Characterization of Large-Area High-Uniformity Silver-Coated Tapered Silica Nanopillar Arrays. *Nanotechnology* **2010**, *vol. 21* (N/A), pp. 395701-9.

82. Abu Hatab, N. A.; Oran, J. M.; Sepaniak, M. J., Surface-Enhanced Raman Spectroscopy Substrates Created via Electron Beam Lithography and Nanotransfer Printing. *ACS Nano* **2008**, *2* (2), 377-385.
83. Jain, K. P.; El-Sayed, M. A., Surface Plasmon Coupling and Its Universal Size Scaling in Metal Nanostructures of Complex Geometry: Elongated Particle Pairs and Nanosphere Trimers. *J. Phys. Chem. C* **2008**, *112*, 4954-4960.
84. Kneipp, K., Raman Spectroscopy of Single Molecules. *Single Mol.* **2001**, *2* (4), 291-292.
85. Rivas, L.; Sanchez-Cortes, S.; Garcia-Ramos, J. V.; Morcillo, G., Growth of silver colloidal particles obtained by citrate reduction to increase the Raman enhancement factor. *Langmuir* **2001**, *17* (3), 574-577.
86. Moody, R. L.; Vo-Dinh, T.; Fletcher, W. H., Investigation of Experimental Parameters for Surface-Enhanced Raman Scattering (SERS) Using Silver-Coated Microsphere Substrates. *Appl. Spectrosc.* **1987**, *41* (6), 966-970.
87. De Jesús, M. A.; Giesfeldt, K. S.; Sepaniak, M. J., Improving the analytical figures of merit of SERS for the analysis of model environmental pollutants. *J. Raman Spectrosc.* **2004**, *35* (10), 895-904.
88. De Jesús, M. A.; Giesfeldt, K. S.; Oran, J. M.; Abu-Hatab, N. A.; Lavrik, N. V.; Sepaniak, M. J., Nanofabrication of Densely Packed Metal-Polymer Arrays for Surface-Enhanced Raman Spectrometry. *Appl. Spectrosc.* **2005**, *59* (12), 1501-1508.
89. Jensen, T. R.; Malinsky, M. D.; Haynes, C. L.; Van Duyne, R. P., Nanosphere Lithography: Tunable Localized Surface Plasmon Resonance Spectra of Silver Nanoparticles. *J. Phys. Chem. B* **2000**, *104* (45), 10549-10556.
90. Chang, T.; Thomson, M.; Kratschmer, E.; Kim, H.; Yu, M.; Lee, K.; Rishton, S.; Hussey, B.; Zolgharnain, S., Electron-beam microcolumns for lithography and related applications. *J. Vac. Sci. Technol., B* **1996**, *14* (6), 3774-3781.
91. Coyle, S.; Holmgren, D.; Chen, X.; Thomas, T.; Sagle, A.; Maldonado, J.; Shamoun, B.; Allen, P.; Gesley, M., Prototype raster multibeam lithography tool. *Journal of Vacuum Science & Technology B* **2002**, *20* (6), 2657-2661.
92. Coyle, S.; Shamoun, B.; Yu, M.; Maldonado, J.; Thomas, T.; Holmgren, D.; Chen, X.; Scheinfein, M.; DeVore, B.; Gesley, M., Progress toward a raster multibeam lithography tool. *J. Vac. Sci. Technol., B* **2004**, *22* (2), 501-505.
93. Lin, T.-W.; Wu, H.-Y.; Tasi, T.-T.; Lai, Y.-H.; Shen, H.-H., Surface-enhanced Raman spectroscopy for DNA detection by the self-assembly of Ag nanoparticles onto Ag nanoparticle-graphene oxide nanocomposites. *Phys. Chem. Chem. Phys.* **2015**, *17* (28), 18443-18448.
94. Ozhikandathil, J.; Badilescu, S.; Packirisamy, M., Plasmonic Gold Decorated MWCNT Nanocomposite for Localized Plasmon Resonance Sensing. *Sci. Rep.* **2015**, *5*, 13181.
95. Shankaran, D. R.; Gobi, K. V.; Miura, N., Recent advancements in surface plasmon resonance immunosensors for detection of small molecules of biomedical, food and environmental interest. *Sens. Actuators, B* **2007**, *121* (1), 158-177.
96. Iancu, V.; Baia, L.; Tarcea, N.; Popp, J.; Baia, M., Towards TiO₂Ag porous nanocomposites based SERS sensors for chemical pollutant detection. *J. Mol. Struct.* **2014**, *1073*, 51-57.

97. Ren, W.; Zhou, Z.; Irudayaraj, J. M. K., Trichloroethylene sensing in water based on SERS with multifunctional Au/TiO₂ core-shell nanocomposites. *Analyst* **2015**, *140* (19), 6625-6630.
98. Abalde-Cela, S.; Auguie, B.; Fischlechner, M.; Huck, W. T. S.; Alvarez-Puebla, R. A.; Liz-Marzan, L. M.; Abell, C., Microdroplet fabrication of silver-agarose nanocomposite beads for SERS optical accumulation. *Soft Matter* **2011**, *7* (4), 1321-1325.
99. Santos, E. d. B.; Lima, E. C. N. L.; Oliveira, C. S. d.; Sigoli, F. A.; Mazali, I. O., Fast detection of paracetamol on a gold nanoparticle-chitosan substrate by SERS. *Anal. Methods* **2014**, *6* (11), 3564-3568.
100. Dong, C.; Yan, Z.; Kokx, J.; Chrisey, D. B.; Dinu, C. Z., Antibacterial and surface-enhanced Raman scattering (SERS) activities of AgCl cubes synthesized by pulsed laser ablation in liquid. *Appl. Surf. Sci.* **2012**, *258* (23), 9218-9222.
101. Ray, P. C.; Khan, S. A.; Singh, A. K.; Senapati, D.; Fan, Z., Nanomaterials for targeted detection and photothermal killing of bacteria. *Chem. Soc. Rev.* **2012**, *41* (8), 3193-3209.
102. Wang, Y.; Wang, F., Janus Nanostructures and Their Bio-medical Applications. In *Bio-Inspired Nanomaterials and Applications*, WORLD SCIENTIFIC: 2014; pp 111-133.
103. Bhattacharya, P.; Du, D.; Lin, Y., Bioinspired nanoscale materials for biomedical and energy applications. *J. R. Soc., Interface* **2014**, *11* (95), 20131067.
104. Wen, H.; Li, Y.; Zhao, X., Redox-Sensitive Polymeric Nanoparticles for Intracellular Drug Delivery. In *Bio-Inspired Nanomaterials and Applications*, WORLD SCIENTIFIC: 2014; pp 21-48.
105. Yang, J., Nanomaterial-Based Sensors for Environmental Monitoring. In *Bio-Inspired Nanomaterials and Applications*, WORLD SCIENTIFIC: 2014; pp 91-110.
106. Lee, K. G.; Lee, S.; Chang, S. J.; Choi, B. G.; Seo, J.; Sangalang, A.; Kim, D. H.; Park, T. J.; Lee, M. K.; Lee, S. J., Bio-inspired Hierarchical Nanowebs for Green Catalysis. *Small* **2015**, *11* (34), 4292-4297.
107. Forestiere, C.; Walsh, G. F.; Miano, G.; Dal Negro, L., Nanoplasmonics of prime number arrays. *Opt. Express* **2009**, *17* (26), 24288-24303.
108. Gupta, S. D.; Ray, D. S., Optical multistability in a nonlinear Fibonacci multilayer. *Phys. Rev. B: Condens. Matter Mater. Phys.* **1988**, *38* (5), 3628-3631.
109. Huang, X. Q.; Jiang, S. S.; Peng, R. W.; Hu, A., Perfect transmission and self-similar optical transmission spectra in symmetric Fibonacci-class multilayers. *Phys. Rev. B: Condens. Matter Mater. Phys.* **2001**, *63* (24), 245104.
110. Kohmoto, M.; Sutherland, B.; Iguchi, K., Localization of optics: Quasiperiodic media. *Phys. Rev. Lett.* **1987**, *58* (23), 2436-2438.
111. Jiang, W.; Wang, L.; Liu, H.; Ma, H.; Tian, H.; Chen, B.; Shi, Y.; Yin, L.; Ding, Y., Bio-inspired directional high-aspect-ratio nanopillars: fabrication and actuation. *RSC Adv.* **2014**, *4* (79), 42002-42008.
112. Amarandei, G.; O'Dwyer, C.; Arshak, A.; Corcoran, D., Fractal Patterning of Nanoparticles on Polymer Films and Their SERS Capabilities. *ACS Appl. Mater. Interfaces* **2013**, *5* (17), 8655-8662.
113. Dal Negro, L.; Feng, N.-N., Spectral gaps and mode localization in Fibonacci chains of metal nanoparticles. *Opt. Express* **2007**, *15* (22), 14396-14403.

114. Dallapiccola, R.; Gopinath, A.; Stellacci, F.; Dal Negro, L., Quasi-periodic distribution of plasmon modes in two-dimensional Fibonacci arrays of metal nanoparticles. *Opt. Express* **2008**, *16* (8), 5544-5555.
115. Gopinath, A.; Boriskina, S. V.; Feng, N.-N.; Reinhard, B. r. M.; Negro, L. D., Photonic-plasmonic scattering resonances in deterministic aperiodic structures. *Nano Lett.* **2008**, *8* (8), 2423-2431.
116. Le Ru, E. C.; Etchegoin, P. G., Chapter 3 - Introduction to plasmons and plasmonics. In *Principles of Surface-Enhanced Raman Spectroscopy*, Ru, E. C. L.; Etchegoin, P. G., Eds. Elsevier: Amsterdam, 2009; pp 121-183.
117. Atanasov, P.; Nedyalkov, N.; Dikovska, A. O.; Nikov, R.; Amoruso, S.; Wang, X.; Bruzzese, R.; Hirano, K.; Shimizu, H.; Terakawa, M., Noble metallic nanostructures: preparation, properties, applications. *J. Phys.: Conf. Ser.* **2014**, *514* (1), 012024.
118. Duan, S.; Wang, R., Bimetallic nanostructures with magnetic and noble metals and their physicochemical applications. *Progress in Natural Science: Materials International* **2013**, *23* (2), 113-126.
119. De Jesús, M. A.; Giesfeldt, K. S.; Sepaniak, M. J., Use of a Sample Translation Technique to Minimize Adverse Effects of Laser Irradiation in Surface-Enhanced Raman Spectrometry. *Appl. Spectrosc.* **2003**, *57* (4), 428-438.
120. Jain, P. K.; El-Sayed, M. A., Plasmonic coupling in noble metal nanostructures. *Chem. Phys. Lett.* **2010**, *487* (4-6), 153-164.
121. Olavarria-Fullerton, J.; Wells, S.; Ortiz-Rivera, W.; Sepaniak, M. J.; Jesus, M. A. d., Surface-Enhanced Raman Scattering (SERS) Characterization of Trace Organoarsenic Antimicrobials Using Silver/Polydimethylsiloxane Nanocomposites. *Appl. Spectrosc.* **2011**, *65* (4), 423-428.
122. Jackson, M. J., *Microfabrication and nanomanufacturing*. CRC Press: 2005.
123. Tolfree, D. W.; Jackson, M. J., 2 Microfabrication Using X-Ray Lithography. *Microfabrication and Nanomanufacturing* **2005**, 33.
124. Suresh, V.; Huang, M. S.; Srinivasan, M.; Guan, C.; Fan, H. J.; Krishnamoorthy, S., Robust, high-density zinc oxide nanoarrays by nanoimprint lithography-assisted area-selective atomic layer deposition. *J. Phys. Chem. C* **2012**, *116* (44), 23729-23734.
125. W., C. J. E-beam Process for ZEP- 520A to be used for Metal Liftoff and RIE. <http://snf.stanford.edu/Process/Lithography/EBResist/ZEP520-Anisole.pdf> (accessed 11-21-13).
126. Stratakis, E.; Ranella, A.; Fotakis, C., *Biomimetic micro/nanostructured functional surfaces for microfluidic and tissue engineering applications*. AIP: Vol. 5, p 013411.
127. Han, S. W.; Lee, S. J.; Kim, K., Self-Assembled Monolayers of Aromatic Thiol and Selenol on Silver: Comparative Study of Adsorptivity and Stability. *Langmuir* **2001**, *17* (22), 6981-6987.
128. Shalabaeva, V.; La Rocca, R.; Miele, E.; Dipalo, M.; Messina, G. C.; Perrone, M.; Maidecchi, G.; Gentile, F.; De Angelis, F., Plasmonic microholes for SERS study of biomolecules in liquid. *Microelectronic Engineering* **2016**, *158*, 59-63.
129. Zvatora, P.; Režanka, P.; Prokopec, V.; Siegel, J.; Svorcik, V.; Kral, V., Polytetrafluorethylene-Au as a substrate for surface-enhanced Raman spectroscopy. *Nanoscale Res Lett* **2011**, *6*.

130. Chu, M.-W.; Myroshnychenko, V.; Chen, C. H.; Deng, J.-P.; Mou, C.-Y.; García de Abajo, F. J., Probing Bright and Dark Surface-Plasmon Modes in Individual and Coupled Noble Metal Nanoparticles Using an Electron Beam. *Nano Lett.* **2008**, *9* (1), 399-404.
131. Liu, G. L.; Choi, Y.-K.; Kwon, S.; Lee, L. P. In *Nanopillar Substrate for SERS*, Proceedings of the 7th International Conference on Miniaturized Chemical and Biochemical Analysis Systems, 2003; pp 705-708.
132. Li, W.-D.; Ding, F.; Hu, J.; Chou, S. Y., Three-dimensional cavity nanoantenna coupled plasmonic nanodots for ultrahigh and uniform surface-enhanced Raman scattering over large area. *Opt. Express* **2011**, *19* (5), 3925-3936.
133. Chamuah, N.; Nath, P., Periodically Varying Height in Metal Nano-pillars for Enhanced Generation of Localized Surface Plasmon Field. *Plasmonics* **2015**, *10* (6), 1-6.
134. Aherne, G.; English, J.; Marks, V., The role of immunoassay in the analysis of microcontaminants in water samples. *Ecotoxicol. Environ. Saf.* **1985**, *9* (1), 79-83.
135. Ternes, T. A., Occurrence of drugs in German sewage treatment plants and rivers. *Water Res.* **1998**, *32* (11), 3245-3260.
136. Jobling, S.; Nolan, M.; Tyler, C. R.; Brighty, G.; Sumpter, J. P., Widespread sexual disruption in wild fish. *Environ. Sci. Technol.* **1998**, *32* (17), 2498-2506.
137. Batt, A. L.; Kostich, M. S.; Lazorchak, J. M., Analysis of ecologically relevant pharmaceuticals in wastewater and surface water using selective solid-phase extraction and UPLC–MS/MS. *Anal. Chem.* **2008**, *80* (13), 5021-5030.
138. Kasprzyk-Hordern, B.; Dinsdale, R. M.; Guwy, A. J., The occurrence of pharmaceuticals, personal care products, endocrine disruptors and illicit drugs in surface water in South Wales, UK. *Water Res.* **2008**, *42* (13), 3498-3518.
139. Teo, T. L.; Coleman, H. M.; Khan, S. J., Occurrence and daily variability of pharmaceuticals and personal care products in swimming pools. *Environmental Science and Pollution Research* **2016**, *23* (7), 6972-6981.
140. Oaks, J. L.; Gilbert, M.; Virani, M., Z., ; Watson, R. T.; Meteyer, C. U.; Rideout, B. A.; Shivaprasad, H. L.; Ahmed, S.; Chaudhry, M.; Arshad, M.; Mahmood, S.; All, A.; Khan, A. A., Diclofenac in residues as the cause of vulture population decline in Pakistan. *Nature* **2004**, *427* 630–633.
141. Sumpter, J., *Green and sustainable pharmacy*. Springer-Verlag: Berlin Heidelberg, 2010.
142. Wang, Y.; Yu, K.; Wang, S., Vibrational spectra study on quinolones antibiotics. *Spectrochim. Acta, Part A* **2006**, *65* (1), 159-163.
143. Liu, S.; Huang, J.; Chen, Z.; Chen, N.; Pang, F.; Wang, T.; Hu, L., Raman spectroscopy measurement of levofloxacin lactate in blood using an optical fiber nano-probe. *J. Raman Spectrosc.* **2015**, *46* (2), 197-201.
144. Neugebauer, U.; Szeghalmi, A.; Schmitt, M.; Kiefer, W.; Popp, J.; Holzgrabe, U., Vibrational spectroscopic characterization of fluoroquinolones. *Spectrochim. Acta, Part A* **2005**, *61* (7), 1505-1517.
145. Sahoo, S.; Chakraborti, C. K.; Mishra, S. C.; Nanda, U. N.; Naik, S., Raman Spectroscopy as an Analytical Tool for Characterization of Fluoroquinolones. **2011**.

146. Abell, J.; Driskell, J.; Dluhy, R.; Tripp, R.; Zhao, Y.-P., Fabrication and characterization of a multiwell array SERS chip with biological applications. *Biosens. Bioelectron.* **2009**, *24* (12), 3663-3670.
147. Yang, L.; Qin, X.; Jiang, X.; Gong, M.; Yin, D.; Zhang, Y.; Zhao, B., SERS investigation of ciprofloxacin drug molecules on TiO₂ nanoparticles. *Phys. Chem. Chem. Phys.* **2015**, *17* (27), 17809-17815.
148. Papapanagiotou, E.; Iossifidou, E.; Psomas, I.; Photis, G., Simultaneous HPLC determination of sulfadiazine and trimethoprim in cultured gilthead sea bream (*Sparus aurata*, L.) tissues. **2000**.
149. González, J. A. O.; Callejón Mochón, M.; de la Rosa, F. J. B., Spectrofluorimetric determination of levofloxacin in tablets, human urine and serum. *Talanta* **2000**, *52* (6), 1149-1156.
150. Babić, S.; Horvat, A. J.; Pavlović, D. M.; Kaštelan-Macan, M., Determination of pK_a values of active pharmaceutical ingredients. *TrAC, Trends Anal. Chem.* **2007**, *26* (11), 1043-1061.
151. Hirst, S. M.; Karakoti, A. S.; Tyler, R. D.; Sriranganathan, N.; Seal, S.; Reilly, C. M., Anti-inflammatory Properties of Cerium Oxide Nanoparticles. *Small* **2009**, *5* (24), 2848-2856.
152. Asati, A.; Santra, S.; Kaittanis, C.; Perez, J. M., Surface-charge-dependent cell localization and cytotoxicity of cerium oxide nanoparticles. *ACS Nano* **2010**, *4* (9), 5321-5331.
153. Schubert, D.; Dargusch, R.; Raitano, J.; Chan, S.-W., Cerium and yttrium oxide nanoparticles are neuroprotective. *Biochem. Biophys. Res. Commun.* **2006**, *342* (1), 86-91.
154. Celardo, I.; Pedersen, J. Z.; Traversa, E.; Ghibelli, L., Pharmacological potential of cerium oxide nanoparticles. *Nanoscale* **2011**, *3* (4), 1411-1420.
155. Li, H.; Wang, G.; Zhang, F.; Cai, Y.; Wang, Y.; Djerdj, I., Surfactant-assisted synthesis of CeO₂ nanoparticles and their application in wastewater treatment. *RSC Adv.* **2012**, *2* (32), 12413-12423.
156. Li, R.; Li, Q.; Gao, S.; Shang, J. K., Exceptional arsenic adsorption performance of hydrous cerium oxide nanoparticles: Part A. Adsorption capacity and mechanism. *Chem. Eng. J.* **2012**, *185*, 127-135.
157. Alhooshani, K. R., Adsorption of chlorinated organic compounds from water with cerium oxide-activated carbon composite. *Arabian J. Chem.* **2015**.
158. Hoecke, K. V.; Quik, J. T.; Mankiewicz-Boczek, J.; Schamphelaere, K. A. D.; Elsaesser, A.; Meeren, P. V. d.; Barnes, C.; McKerr, G.; Howard, C. V.; Meent, D. V. D., Fate and effects of CeO₂ nanoparticles in aquatic ecotoxicity tests. *Environ. Sci. Technol.* **2009**, *43* (12), 4537-4546.
159. Turel, I., The interactions of metal ions with quinolone antibacterial agents. *Coord. Chem. Rev.* **2002**, *232* (1), 27-47.
160. Efthimiadou, E. K.; Psomas, G.; Sanakis, Y.; Katsaros, N.; Karaliota, A., Metal complexes with the quinolone antibacterial agent N-propyl-norfloxacin: Synthesis, structure and bioactivity. *J. Inorg. Biochem.* **2007**, *101* (3), 525-535.
161. Tarushi, A.; Kljun, J.; Turel, I.; Pantazaki, A. A.; Psomas, G.; Kessissoglou, D. P., Zinc (II) complexes with the quinolone antibacterial drug flumequine: structure, DNA- and albumin-binding. *New J. Chem.* **2013**, *37* (2), 342-355.
162. Arafat, Y.; Ali, S.; Shahzadi, S.; Shahid, M., Preparation, characterization, and antimicrobial activities of bimetallic complexes of sarcosine with Zn (II) and Sn (IV). *Bioinorg. Chem. Appl.* **2013**, *2013*.

163. Hoa, T. T. Q.; Canh, T. D.; Long, N. N. In *Preparation of ZnS nanoparticles by hydrothermal method*, Journal of Physics: Conference Series, IOP Publishing: 2009; p 012081.
164. Singh, B. P.; Tyagi, S.; Kumar, R., Gradation of nanoparticle size by stokes' law: a new approach for synthesis of CdS nanoparticles. *International Journal of Advanced Applied Physics Research* **2015**, 2 (1), 31-36.
165. Wang, L.; Hong, G., A new preparation of zinc sulfide nanoparticles by solid-state method at low temperature. *Mater. Res. Bull.* **2000**, 35 (5), 695-701.
166. Chandrakar, R. K.; Baghel, R.; Chandra, V.; Chandra, B., Synthesis, characterization and photoluminescence studies of undoped ZnS nanoparticles. *Superlattices Microstruct.* **2015**, 84, 132-143.
167. Kaur, J.; Sharma, M.; Pandey, O., Photoluminescence and photocatalytic studies of metal ions (Mn and Ni) doped ZnS nanoparticles. *Opt. Mater.* **2015**, 47, 7-17.
168. Lu, S. W.; Lee, B. I.; Wang, Z. L.; Tong, W.; Wagner, B. K.; Park, W.; Summers, C. J., Synthesis and photoluminescence enhancement of Mn 2+-doped ZnS nanocrystals. *J. Lumin.* **2000**, 92 (1), 73-78.
169. Pathak, C.; Mishra, D.; Agarwala, V.; Mandal, M., Blue light emission from barium doped zinc sulfide nanoparticles. *Ceram. Int.* **2012**, 38 (7), 5497-5500.
170. Singh, B. P.; Singh, S. P.; Vishnoi, S.; Kumar, R., Synthesis and optical properties of aggregated nanospheres of ZnS nanoparticles. *Journal of Optoelectronics and Biomedical Materials Vol* **2012**, 4 (2), 29-33.
171. Wageh, S.; Ling, Z. S.; Xu-Rong, X., Growth and optical properties of colloidal ZnS nanoparticles. *J. Cryst. Growth* **2003**, 255 (3), 332-337.
172. Yang, P.; Lü, M.; Xü, D.; Yuan, D.; Chang, J.; Zhou, G.; Pan, M., Strong green luminescence of Ni²⁺-doped ZnS nanocrystals. *Appl. Phys. A: Mater. Sci. Process.* **2002**, 74 (2), 257-259.
173. Pathak, C.; Mishra, D.; Agarwala, V.; Mandal, M., Optical properties of ZnS nanoparticles prepared by high energy ball milling. *Mater. Sci. Semicond. Process.* **2013**, 16 (2), 525-529.
174. Cao, L.; Zhang, J.; Ren, S.; Huang, S., Luminescence enhancement of core-shell ZnS: Mn/ZnS nanoparticles. *Appl. Phys. Lett.* **2002**, 80 (23), 4300-4302.
175. Zhang, J.; Chen, Q.; Zhang, W.; Mei, S.; He, L.; Zhu, J.; Chen, G.; Guo, R., Microwave-assisted aqueous synthesis of transition metal ions doped ZnSe/ZnS core/shell quantum dots with tunable white-light emission. *Appl. Surf. Sci.* **2015**, 351, 655-661.
176. Yan, X.; Michael, E.; Komarneni, S.; Brownson, J. R.; Yan, Z.-F., Microwave-and conventional-hydrothermal synthesis of CuS, SnS and ZnS: optical properties. *Ceram. Int.* **2013**, 39 (5), 4757-4763.
177. Zhao, Y.; Hong, J.-M.; Zhu, J.-J., Microwave-assisted self-assembled ZnS nanoballs. *J. Cryst. Growth* **2004**, 270 (3), 438-445.
178. La Porta, F. A.; Ferrer, M. M.; De Santana, Y. V.; Raubach, C. W.; Longo, V. M.; Sambrano, J. R.; Longo, E.; Andrés, J.; Li, M. S.; Varela, J. A., Synthesis of wurtzite ZnS nanoparticles using the microwave assisted solvothermal method. *J. Alloys Compd.* **2013**, 556, 153-159.

179. Onwudiwe, D. C.; Krüger, T. P.; Jordaan, A.; Strydom, C. A., Laser-assisted synthesis, and structural and thermal properties of ZnS nanoparticles stabilised in polyvinylpyrrolidone. *Appl. Surf. Sci.* **2014**, *321*, 197-204.
180. Penieres-Carrillo, G.; García-Estrada, J. G.; Gutiérrez-Ramírez, J. L.; Alvarez-Toledano, C., Infrared-assisted eco-friendly selective synthesis of diindolylmethanes. *Green Chem.* **2003**, *5* (3), 337-339.
181. Polshettiwar, V.; Varma, R. S., Green chemistry by nano-catalysis. *Green Chem.* **2010**, *12* (5), 743-754.
182. Wang, D.; Li, Y., Bimetallic nanocrystals: liquid-phase synthesis and catalytic applications. *Adv. Mater.* **2011**, *23* (9), 1044-1060.
183. Noguez, M. O.; Marcelino, V.; Rodríguez, H.; Martín, O.; Martínez, J. O.; Arroyo, G. A.; Pérez, F. J.; Suárez, M.; Miranda, R., Infrared assisted production of 3, 4-Dihydro-2 (1H)-pyridones in solvent-free conditions. *Int. J. Mol. Sci.* **2011**, *12* (4), 2641-2649.
184. Singh, B. P.; Tyagi, S.; Kumar, R., Gradation of Nanoparticle Size by Stokes' Law: A New Approach for Synthesis of CdS Nanoparticles.
185. Sahraei, R.; Aval, G. M.; Baghizadeh, A.; Lamahi-Rachti, M.; Goudarzi, A.; Ara, M. M., Investigation of the effect of temperature on growth mechanism of nanocrystalline ZnS thin films. *Mater. Lett.* **2008**, *62* (28), 4345-4347.

Appendix 1

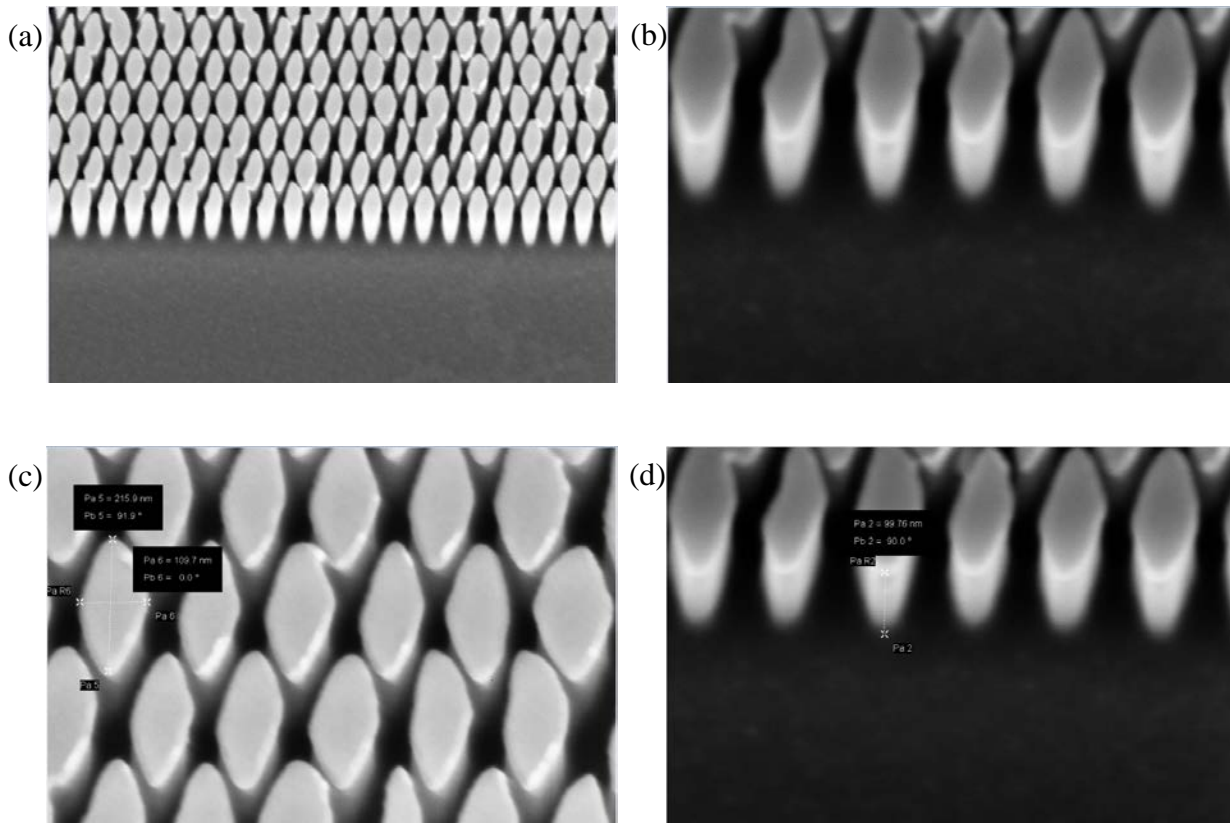


Figure 58: Diamond Micrograph

Table 16: Diamond particles dimension characterization

Pattern	Length (nm)	Width (nm)	Altitude (nm)	Gap (nm)	Aspect Ratio
	218.0(±3.7)	106.6 (±3.7)	93.7 (±6.4)	44.0(±2.4)	2.0
Diamond	Length 1	Length 2	Length 3	Average	SD
	222.2	215.8	215.9	217.96	3.66
	Width 1	Width 2	Width 3		
	102.5	107.6	109.7	106.6	3.70
	Altitude 1	Altitude 2	Altitude 3		
94.31	87.06	99.76	93.71	6.37	
Gap 1	Gap 2	Gap 3			
41.4	46.2	44.5	44.03	2.43	

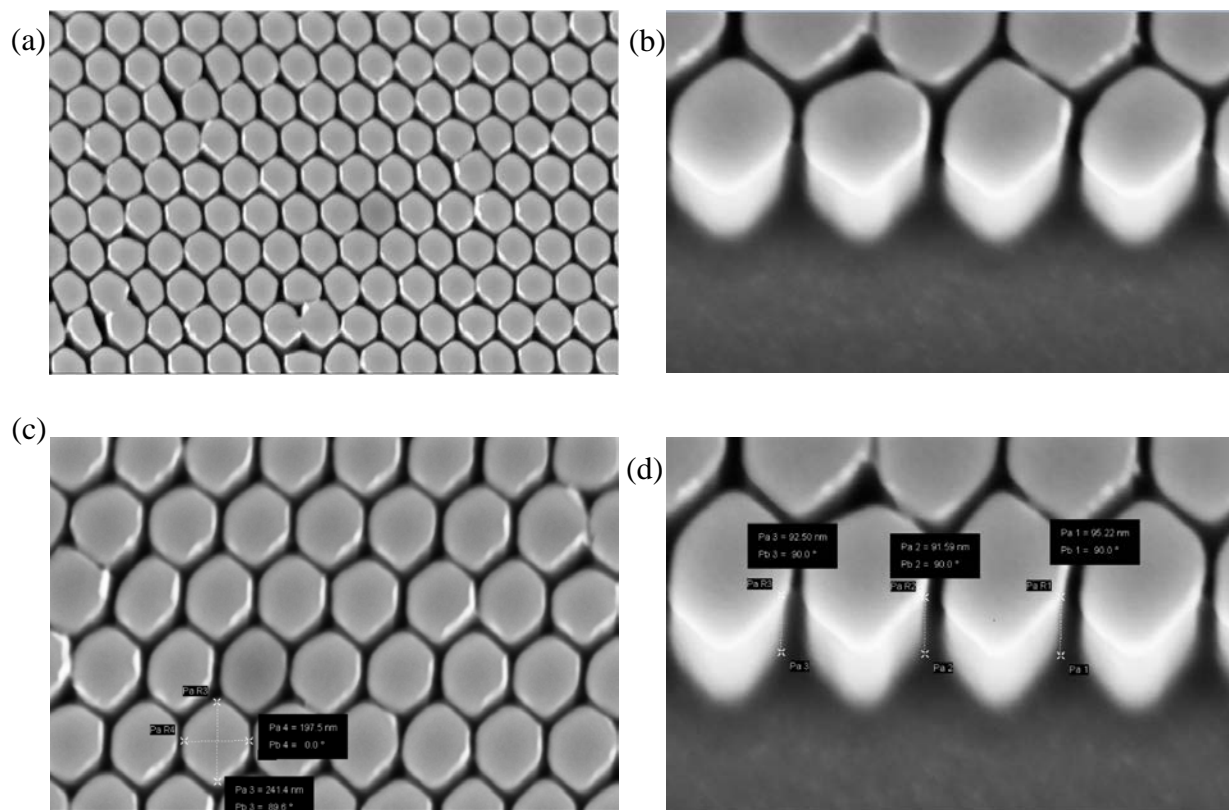


Figure 59: Honeycombs Micrograph

Table 17: New Honeycombs particles dimensions characterization

Pattern	Avg. Length (nm)	Width (nm)	Altitude (nm)	Gap (nm)	Aspect Ratio
New Honeycomb	234.1(±3.7)	187.4(±8.9)	93.1(±1.9)	27.2(±6.4)	1.2
	Length 1	Length 2	Length 3	Average	SD
	229.6	241.4	231.2	234.1	6.40
	Width 1	Width 2	Width 3		
	180.6	197.5	184	187.4	8.94
	Altitude 1	Altitude 2	Altitude 3		
	95.22	91.59	92.5	93.1	1.89
Gap 1	Gap 2	Gap 3			
31.74	29.94	19.95	27.21	6.35	

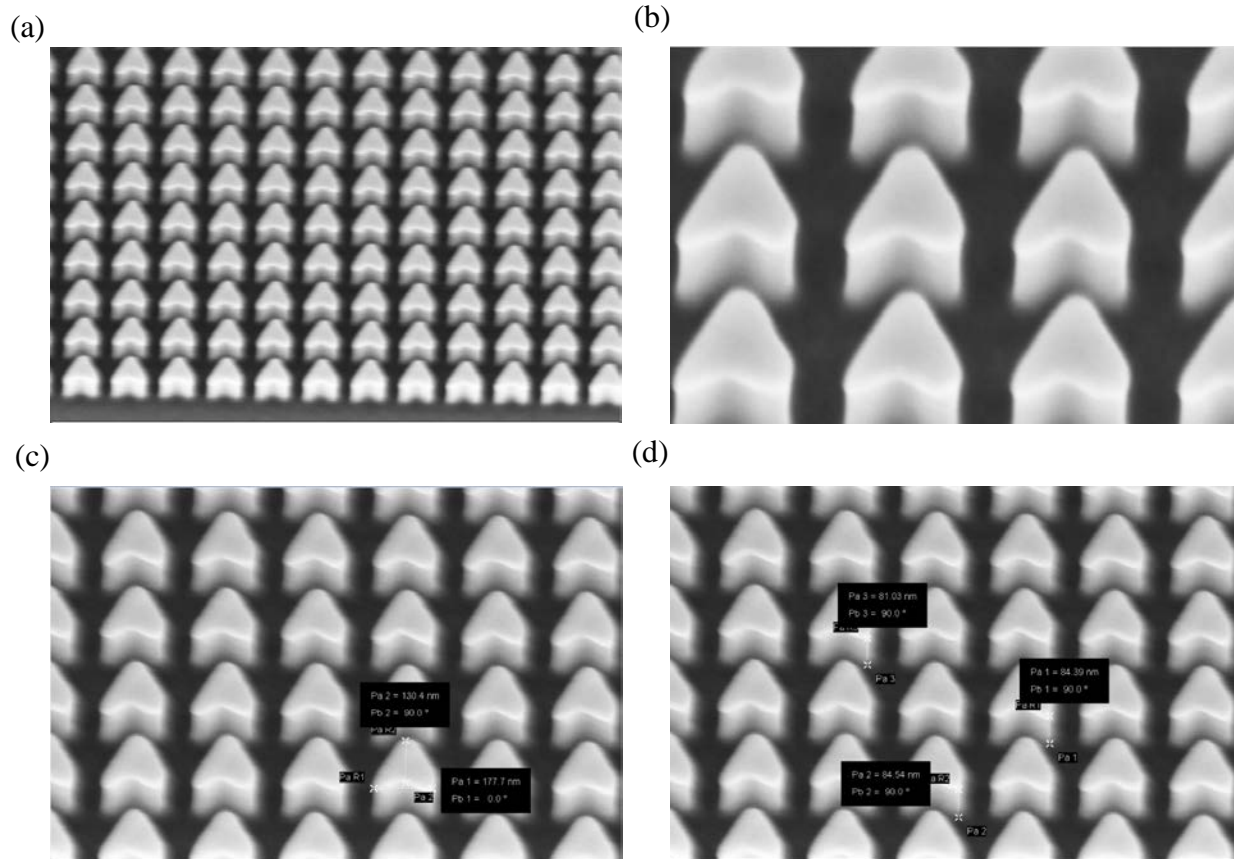


Figure 60: Wings Micrograph

Table 18: Wings particles dimensions Characterization

Pattern	Length (nm)	Width (nm)	Altitude (nm)	Gap (nm)	Aspect Ratio
Wings	129.1(\pm 1.4)	176.6(\pm 1.2)	83(\pm 2)	83.7(\pm 0.5)	0.7
	Length 1	Length 2	Length 3	Average	SD
	130.4	129.3	127.7	129.13	1.36
	Width 1	Width 2	Width 3		
	177.7	175.4	177	176.70	1.18
	Altitude 1	Altitude 2	Altitude 3		
84.39	84.54	81.03	83.32	1.98	
Gap 1	Gap 2	Gap 3			
83.43	84.34	83.43	83.73	0.53	

Appendix 2

Table 19: Resolutions results for the HPLC Analysis

Samples	Resolution Averages		
	Carboxy/Sulfa	Sulfa/Levo	Levo/Cipro
STD 1	2.21	7.46	2.75
STD 2	2.46	7.56	2.74
STD 3	2.46	7.52	2.74
STD 4	2.46	7.53	2.75
STD 5	2.45	7.55	2.78
STD 6	2.44	7.74	2.85
QC1	1.64	6.90	2.71
QC2	1.64	7.10	2.80

Table 20: Results of the Validation process for HPLC Analysis for 4-Carboxy

Samples	4-CarboxyBenzenesulfonamide		
	N _{Ave}	K' _{Ave}	%RSD _{Area}
STD 1	3370	23.43	0.4596
STD 2	3403	23.36	1.3047
STD 3	3394	23.33	0.5444
STD 4	3436	23.33	1.4532
STD 5	3404	23.36	1.7357
STD 6	3393	23.32	1.8781
QC1	3656	23.44	0.7431
QC2	3657	23.44	0.5576

Table 21: Results of the Validation process for HPLC Analysis for Sulfadiazine

Sulfadiazine			
Samples	N_{Ave}	K'_{Ave}	%RSD_{Area}
STD 1	3822	27.33	1.7098
STD 2	3760	27.72	1.3077
STD 3	3766	27.68	1.9043
STD 4	3738	27.68	1.8959
STD 5	3749	27.72	0.7901
STD 6	3658	27.68	1.9500
QC1	3884	26.20	1.6142
QC2	3914	26.20	0.4174

Table 22: Results of the Validation process for HPLC Analysis for Levofloxacin

Levofloxacin			
Samples	N_{Ave}	K'_{Ave}	%RSD_{Area}
STD 1	1018	65.39	0.5829
STD 2	988.5	68.04	4.0693
STD 3	971	68.07	0.2037
STD 4	973.5	68.17	1.4864
STD 5	983	68.18	6.5910
STD 6	1048	68.10	15.1362
QC1	950	59.30	2.9652
QC2	1025	59.10	1.1917

Table 23: Results of the Validation process for HPLC Analysis for Ciprofloxacin

Ciprofloxacin			
Samples	N_{Ave}	K'_{Ave}	%RSD_{Area}
STD 1	2401	86.71	2.3650
STD 2	2369	90.33	3.0022
STD 3	2427	90.41	0.6080
STD 4	2433	90.54	0.6696
STD 5	2521	90.61	5.9348
STD 6	2578	90.59	9.6721
QC1	2763	78.13	1.5010
QC2	2805	78.00	0.8195

Table 24: Results of the Regression Analysis

Samples	m	b	R²
4-CarboxyBe	19.0702	2.6968	1.0000
Sulfadiazine	12.7152	0.6542	1.0000
Levofloxacin	26.9984	-18.3950	0.9999
Ciprofloxacin	33.3279	-11.3800	0.9999